



UNIVERSITÀ
DEGLI STUDI
DI PADOVA

Università degli Studi di Padova

Dipartimento dei Beni Culturali: Archeologia,
Storia dell'Arte, del Cinema e della Musica

Master Degree in
ARCHAEOLOGICAL SCIENCES

Curriculum in
APPLIED SCIENCES TO CULTURAL HERITAGE MATERIALS AND SITES

Characterization of wall paintings from the site of
Teotihuacan, Mexico: pigment and plaster analyses

Supervisor:

Prof. Michele Secco

Co-supervisor:

Prof. Domenico Miriello

Candidate: Chloe Kelly

Matricola: 2071817

ACADEMIC YEAR 2023/2024

Acknowledgments

I would like to express my deepest gratitude for my supervisor, Professor Michele Secco, for his continued guidance and support throughout each step of this project.

The completion of this thesis would not have been possible without the help and patience of University of Padova staff and professors. I would like to extend my thanks to Leonardo Tauro for his assistance and kindness in sample preparation, Giulia Ricci for her time and contribution to micro-FTIR results, Caterina Canovaro for her explanations and patience with optical microscopy, Lisa Santello for her guidance and knowledge of micro-Raman, and Federico Zorzi for his expertise with SEM-EDS. I would also like to thank Professor Domenico Miriello for providing the samples used in this study, and his previous work in this research area.

Finally, I would like to thank my parents, my grandparents, and my sister for their endless support and encouragement.

Ringraziamenti

Vorrei esprimere la mia più profonda gratitudine al mio supervisore, il professor Michele Secco, per la sua continua guida e supporto durante ogni fase di questo progetto.

Il completamento di questa tesi non sarebbe stato possibile senza l'aiuto e la pazienza del personale e dei professori dell'Università di Padova. Vorrei estendere i miei ringraziamenti a Leonardo Tauro per la sua assistenza e gentilezza nella preparazione dei campioni, Giulia Ricci per il suo tempo e il suo contributo ai risultati micro-FTIR, Caterina Canovaro per le sue spiegazioni e pazienza con la microscopia ottica, Lisa Santello per la sua guida e conoscenza di micro-Raman e Federico Zorzi per la sua esperienza con SEM-EDS. Desidero inoltre ringraziare il Professor Domenico Miriello per aver fornito i campioni utilizzati in questo studio e per il suo precedente lavoro in quest'area di ricerca.

Infine, vorrei ringraziare i miei genitori, i miei nonni e mia sorella per il loro infinito sostegno e incoraggiamento.

Table of Contents

| | |
|--|----|
| Acknowledgments..... | 2 |
| Ringraziamenti..... | 2 |
| List of Figures..... | 4 |
| List of Tables..... | 8 |
| Abstract..... | 9 |
| Sommario..... | 11 |
| 1. Introduction..... | 13 |
| 1.2 History of Mesoamerican Wall Painting..... | 14 |
| 1.3 Wall Paintings of Teotihuacan..... | 15 |
| 1.4 Archaeological Site of Teotihuacan..... | 16 |
| 2. Sample Description..... | 19 |
| 3. Experimental methods..... | 21 |
| 3.1 X-Ray Diffraction – X-Ray Powder Diffraction (XRD-XRPD)..... | 21 |
| 3.2 Fourier Transform Infrared Spectroscopy (FTIR)..... | 23 |
| 3.3 Optical Microscopy..... | 24 |
| 3.4 micro-Raman Spectroscopy..... | 25 |
| 3.5 micro-FTIR Spectroscopy..... | 26 |
| 3.6 Scanning Electron Microscopy – Energy Dispersive X-Ray Spectroscopy..... | 27 |
| 4. Results..... | 28 |
| 4.1 X-Ray Diffraction – X-ray Powder Diffraction (XRD – XRPD)..... | 28 |
| 4.2 Fourier Transform Infrared Spectroscopy (FTIR)..... | 36 |
| 4.3 Optical microscopy – Polarized light microscopy (PLM)..... | 37 |
| 4.4 micro-Raman..... | 44 |
| 4.5 Scanning Electron Microscopy – Energy Dispersive X-Ray Spectroscopy (SEM-EDS)..... | 54 |
| 4.6 micro-FTIR..... | 61 |
| 5. Discussion..... | 65 |
| 6. Conclusions..... | 69 |
| References..... | 72 |

List of Figures

| | |
|---|----|
| Figure 1: Map of Mexico indicating the location of Teotihuacan (Encyclopedia Britannica, 2024). | 16 |
| Figure 2: Map of Teotihuacan, with the Techinantitla building complex indicated in red (Ruvalcaba- Sil et al, 2021). | 17 |
| Figure 3: Example of a wall painting from the Techinantitla apartment complex, 500–550 CE, located at the Metropolitan Museum of Art (MET, 2024). | 18 |
| Figure 4: Map of Techinantitla compound displaying the retrieval locations of samples studied in this work (courtesy of Margarita Muñoz). | 19 |
| Figure 5: Cross-section of sample 8Pi displaying red paint layer, intermediate white intonaco layer, and lower brown plaster layer. | 21 |
| Figure 6: Samples 2Pi, 6Pi1, 6Pi2, 7Pi1, 7Pi2, and 8Pi (not pictured) mounted to supports with pigment surfaces face-up. | 22 |
| Figure 7: Sample preparation for XRPD. a) small mortar and pestle used to grind sample. b) finely ground sample. c) Powder samples mounted to zero-background sample holders. | 22 |
| Figure 8: a) Detail view of the Malvern PANalytical X' Pert Pro diffractometer at the Department of Geosciences, University of Padova. b) Distance view of the diffractometer. | 23 |
| Figure 9:a) Bruker Alpha-P compact FTIR spectrophotometer. b) Detail view of sample under probe. | 24 |
| Figure 10: a) Plastic containers with samples being filled with epoxy resin. b) Sample containers in oven..... | 24 |
| Figure 11: Left: unpolished samples embedded in resin. Right: Struers polisher..... | 25 |
| Figure 12: Left: Nikon Eclipse ME600 microscope equipped with camera. Right: close-up of sample on stage. | 25 |
| Figure 13: WITec Raman microscope alpha300 at Department of Geosciences, Padova. | 26 |
| Figure 14: Bruker Hyperion II FTIR microscope located at the University of Padova, Department of Geosciences. | 27 |
| Figure 15: a) Coxem EM-30AX scanning electron microscope. b) Quorum Q150R coater. | 27 |
| Figure 16: XRPD results of sample 2I. | 29 |
| Figure 17: XRPD results of sample 8I. | 30 |
| Figure 18: XRPD results of sample 2P. | 31 |
| Figure 19: XRD results of sample 2Pi. | 31 |
| Figure 20: XRD results of sample 6Pi1. | 32 |
| Figure 21: XRD results of sample 6Pi2. | 33 |
| Figure 22: XRD results of sample 7Pi1. | 33 |
| Figure 23: XRD results of sample 7Pi2. | 34 |
| Figure 24: XRD results of sample 8Pi. | 34 |
| Figure 25: Quantitative results of samples a) 2I and b) 8I..... | 35 |
| Figure 26: Quantitative results of samples a) 2P, b) 5P, and c) 8P..... | 35 |
| Figure 27:FTIR spectra for samples 2Pi, 6Pi2, 7Pi2, and 8Pi. Samples 6Pi2 and 7Pi2 did not produce meaningful signals, where both 2Pi and 8Pi demonstrate signals corresponding to wood ash. | 36 |

| | |
|--|----|
| Figure 28: Darkfield micrograph in reflected light of sample 6Pi1 in cross-section, indicating the pigment, intonaco, and base plaster layers..... | 38 |
| Figure 29: Micrographs of the interface between pigment and intonaco of a) sample 2Pi (secco technique) b) sample 6Pi2 (fresco) c) sample 6Pi1 (fresco) d) sample 8Pi (fresco)..... | 38 |
| Figure 30: a) Micrograph of sample 2Pi with dotted line indicating the distinction in pigment layer, b) micrograph of sample 2Pi displaying entire cross-section view..... | 39 |
| Figure 31: Micrograph of sample 6Pi1 indicating specular hematite and/or magnetite particles in blue circles. | 40 |
| Figure 32: a) Micrograph of sample 7Pi2, b) micrograph of sample 7Pi1, c) micrograph of sample 6Pi1, and d) micrograph of sample 6Pi2. | 40 |
| Figure 33: Volcanic glass fragments in the intonaco and pigment layers of sample 7Pi1..... | 41 |
| Figure 34: a) Brightfield micrograph in reflected light of sample 2Pi, b) sample 6Pi2, and c) sample 8Pi..... | 42 |
| Figure 35: a) Darkfield micrograph of sample 2P, b) brightfield micrograph of sample 2P with tezontle fragments indicated in red. | 43 |
| Figure 36: a) Raman spectra of three sampled points in the pigment layer of sample 7Pi2, b) micrograph of samples 7Pi2 indicating sampling locations. | 45 |
| Figure 37: a) Raman spectra of sampled points in the pigment layers of sample 2Pi, indicating the presence of calcite, hematite, and carbon, b) micrograph indicating sampling locations..... | 46 |
| Figure 38: a) Raman spectra of sampled points in samples 2Pi, 6Pi1, 6Pi2, and 8Pi showing signals of hematite, b) micrograph indicating sampled location in sample 2Pi, c) in sample 6Pi1, d) in sample 6Pi, and e) in sample 8Pi..... | 46 |
| Figure 39: Raman spectrum of sampled point in 8Pi showing peaks of hematite. | 47 |
| Figure 40: a) Raman spectrum of sampled point in 6Pi2 showing peaks of quartz, b) micrograph of sample 6Pi2 indicating sampled location. | 47 |
| Figure 41: a) Raman spectra of three sampled points in the intonaco layer of 6Pi1, b) micrograph of sample 6Pi1 showing sampled locations. | 48 |
| Figure 42: a) Raman spectra of two sampled points in the intonaco layer of 7Pi1, b) micrograph of sample 7Pi1 indicating sampled locations..... | 48 |
| Figure 43: a) Raman spectrum of sampled point in the intonaco layer of sample 7Pi2, showing peaks of carbon and apatite, b) micrograph of sample 7Pi2 indicating sampled location..... | 49 |
| Figure 44: a) Raman spectra of three sampled points in the intonaco layer of sample 6Pi2, b) micrograph of sample 6Pi2 indicating sampled locations. | 49 |
| Figure 45: a) Raman spectra of two sampled points in the aggregate of the intonaco layer of sample 8Pi, b) micrograph sample 8Pi indicating sampled locations..... | 50 |
| Figure 46: a) Raman spectra of four sampled points in the matrix of the base plaster layer of sample 6Pi1, b) micrograph of sample 6Pi1 showing sampled locations. | 51 |
| Figure 47: a) Raman spectrum of sampled point in the base plaster layer of sample 7Pi2 showing peaks of carbon and anatase, b) micrograph of sample 7Pi2 showing sampled location. | 51 |
| Figure 48: a) Raman spectra of three sampled points in the aggregate of sample 6Pi2 showing peaks of plagioclase feldspar, b) micrograph of sample 6Pi2 indicating sampled locations..... | 52 |
| Figure 49: a) Raman spectra of five sampled points in the aggregate of sample 7Pi1 showing peaks of plagioclase feldspar, b) micrograph of sample 7Pi1 indicating sampled locations..... | 52 |

| | |
|--|----|
| Figure 50: Raman spectrum of sampled point in the aggregate of the base plaster layer of sample 6Pi2 showing peaks of forsterite, b) micrograph of sample 6Pi2 indicating sampled location.... | 53 |
| Figure 51: a) Raman spectra of two sampled points sample 7Pi1 showing peaks of hornblende, b) micrograph of sample 7Pi1 indicating sampled locations. | 53 |
| Figure 52: Microchemical maps of the interface between pigment and intonaco layers of a) sample 6Pi1 b) sample 6Pi2, c) sample 7Pi1, and d) sample 7Pi2. White dotted line marks the approximate interface boundary..... | 54 |
| Figure 53: Microchemical map of sample 2Pi pigment and intonaco interface. White dotted lines display interface boundaries. | 55 |
| Figure 54: a) Microchemical maps of the interface between intonaco and plaster layer of a) sample 6Pi2, b) sample 7Pi1, c) sample 7Pi2, and d) microchemical map of base plaster layer of sample 6Pi1 featuring tezontle and matrix..... | 55 |
| Figure 55: Microchemical maps displaying the presence of carbon (teal) in the intonaco and pigment layers of a) sample 6Pi1, b) sample 6Pi2, and c) sample 7Pi2. | 56 |
| Figure 56: BSE image of sample 6Pi1 indicating three points sampled with EDS, and the resulting spectra. | 57 |
| Figure 57: BSE image of sample 2Pi indicating two points sampled with EDS, and the resulting spectra. | 57 |
| Figure 58: BSE image of sample 8Pi indicating two points sampled with EDS, and the resulting spectra | 58 |
| Figure 59: BSE image of sample 7Pi1 indicating two points sampled with EDS, and the resulting spectra. | 58 |
| Figure 60: a) BSE image of sample 8Pi indicating point sampled with EDS, and the resulting spectrum, b) BSE image of sample 7Pi2 indicating point sampled with EDS, and the resulting spectrum..... | 59 |
| Figure 61: a) BSE image of intonaco /tezontle in sample 6Pi1 indicating point sampled with EDS, and the resulting spectrum showing elements consistent with ilmenite, b) BSE image of base plaster layer in sample 6Pi1 indicating point sampled with EDS, and the resulting spectrum showing elements consistent with ilmenite..... | 60 |
| Figure 62: BSE image of sample 7Pi2 indicating point sampled with EDS, and the resulting spectrum showing elements consistent with apatite. | 60 |
| Figure 63: FTIR spectra of three representative points in the matrix and aggregate of the intonaco and base plaster, and integration map of the main peaks related to silicates, sample 7Pi2 (provided by Giulia Ricci). | 61 |
| Figure 64: a) FTIR spectra of three sampled points, and integration map of peak of silicates in the range 1300-1080 cm^{-1} , (“silicate 1”), sample 7Pi2. b) FTIR spectra of three sampled points and integration map of peak of silicates in the range 1080-800 cm^{-1} , (“silicate 2”), sample 7Pi2 (provided by Giulia Ricci). | 62 |
| Figure 65: FTIR spectra of three sampled points and integration map of the main peak related to calcite, sample 7Pi2 (provided by Giulia Ricci). | 62 |
| Figure 66: FTIR spectra of four sampled points, and integration map of the main peak related to calcite, sample 6Pi2 (provided by Giulia Ricci). | 63 |

Figure 67: FTIR spectra of four sampled points, and integration map of the main peak related to silicates, sample 6Pi2 (provided by Giulia Ricci)..... 64

List of Tables

| | |
|---|----|
| Table 1: Chronology of Teotihuacan phases and developments in wall paintings. Table adapted from (Argote et al, 2020; Clayton, 2015; Magaloni, 1996). | 15 |
| Table 2: Sample description and images. | 20 |
| Table 3: Sample list and applied analytical techniques..... | 21 |
| Table 4: Summary of XRD results for pigment surfaces displaying sample names and minerals detected. | 28 |
| Table 5: Summary of XRD results for plaster and intonaco samples. | 28 |
| Table 6: Stratified samples and determined features. | 37 |
| Table 7: Samples analyzed by micro-Raman, with the layers of sampling locations indicated. .. | 44 |
| Table 8: Summary of minerals identified using micro-Raman. | 44 |

Abstract

This study details the characterization of wall painting fragments from the ancient Mesoamerican site of Teotihuacan, located in present-day Mexico. Analyses of pigments, plasters, and sample microstratigraphy were performed with the aim of providing insights into their production methodology and variations in technological style. To achieve this, several analytical techniques were employed, namely: X-Ray Diffraction (XRD), Fourier-transform infrared spectroscopy (FTIR), polarized light microscopy (PLM), micro-Raman spectroscopy, micro-FTIR spectroscopy, and scanning electron microscopy paired with energy dispersive X-ray spectroscopy (SEM-EDS).

Samples were first prepared for XRD analysis to determine their mineralogical composition. Plaster samples were prepared in powder form for X-ray Powder Diffraction (XRPD), whereas the preparation of pigment surfaces was achieved non-invasively. The results of XRD-XRPD were sufficient to provide a starting point for characterization of pigment and plaster components, including pigment identification, pigment additives, and variations in plaster composition.

To provide information about potential organic components included in the pigment surfaces or pigment matrices, FTIR spectroscopy was employed. The pigment surfaces of four samples were selected for analysis, however some technical difficulties with the apparatus allowed for meaningful results of only two samples. To supplement these results, the question of organic components was considered in subsequent methods.

It was then necessary to prepare the samples in cross sections for analyses via optical microscopy, micro-Raman spectroscopy, micro-FTIR spectroscopy, and SEM-EDS. This involved embedding the samples in epoxy resin, curing in an oven, and finally polishing the surfaces. Imaging of all samples was then performed with an optical microscope equipped with a camera, and micrograph maps were generated by image-stitching in Photoshop. These images provided information on the microstratigraphy of the samples, revealing the interactions between pigment, *intonaco*, and base plaster layers.

To complement results obtained from XRD, FTIR, and optical microscopy, micro-Raman spectroscopy was subsequently performed. This enabled confirmation of the presence of mineral phases identified by XRD, as well as providing additional information concerning the nature of the mixture of components incorporated in the pigment layers.

Continuing, the samples were analyzed using SEM-EDS. Images of the samples at varying magnifications were taken, and specific regions of the samples were selected for EDS point analyses. Microchemical mapping was then performed at the interfaces of the stratified samples, allowing for a more comprehensive understanding of interactions between and within layers. These findings again confirmed hypotheses suggested from previous methods as well as contributed new information about the production technology of plaster layers and the chemical interaction of phases.

Finally, micro-FTIR analyses and integration mapping were performed on the microstratigraphy of two samples to further understand the interactions between the matrix and aggregate of plaster

and pigment layers. FTIR maps were used to determine the distribution of calcite and silicates in these layers, and provided useful comparison with SEM-EDS chemical maps.

Ultimately, the results of these complementary methods contribute to a more comprehensive understanding of the techniques employed in creating the wall paintings of Teotihuacan. Through uncovering the material composition of pigments and plaster, technological advancements, and production methods used at the site, we come closer to interpreting the society behind the paintings.

Sommario

Questo studio descrive in dettaglio la caratterizzazione di frammenti di pittura murale dell'antico sito mesoamericano di Teotihuacan, situato nell'attuale Messico. Sono state eseguite analisi di pigmenti, intonaci e microstratigrafie dei campioni allo scopo di fornire informazioni sulla loro metodologia di produzione e sulle variazioni nello stile tecnologico. Per raggiungere questo obiettivo, sono state impiegate diverse tecniche analitiche: diffrazione ai raggi X (XRD), spettroscopia infrarossa a trasformata di Fourier (FTIR), microscopia a luce polarizzata (PLM), spettroscopia micro-Raman, micro-FTIR e microscopia elettronica a scansione abbinata a spettroscopia a raggi X a dispersione di energia (SEM-EDS).

I campioni sono stati prima preparati per l'analisi XRD al fine di determinare la loro composizione mineralogica. I campioni di *intonaco* sono stati preparati in polvere per la diffrazione ai raggi X delle polveri (XRPD), mentre la preparazione delle superfici dei pigmenti è stata ottenuta in modo non invasivo. I risultati di XRD-XRPD sono stati sufficienti a fornire un punto di partenza per la caratterizzazione dei componenti di pigmenti e strati preparatori, tra cui l'identificazione dei pigmenti, gli additivi dei pigmenti e le variazioni nella composizione degli strati di *intonaco*.

Per fornire informazioni sui potenziali componenti organici inclusi nelle superfici dei pigmenti o nelle matrici dei pigmenti, è stata impiegata la spettroscopia FTIR. Le superfici dei pigmenti di quattro campioni sono state selezionate per l'analisi, tuttavia alcune difficoltà tecniche con lo strumento hanno consentito di ottenere risultati significativi solo per due campioni. Per integrare questi risultati, la questione dei componenti organici è stata presa in considerazione nelle analisi successive.

È stato quindi necessario preparare i campioni in sezioni trasversali per le analisi tramite microscopia ottica, spettroscopia micro-Raman, spettroscopia micro-FTIR e SEM-EDS. Ciò ha comportato l'inclusione dei campioni in resina epossidica, la polimerizzazione in un forno e infine la lucidatura delle superfici. L'imaging di tutti i campioni è stato quindi eseguito con un microscopio ottico dotato di una fotocamera e le mappe micrografiche sono state generate tramite l'unione delle immagini in Photoshop. Queste immagini hanno fornito informazioni sulla microstratigrafia dei campioni, rivelando le interazioni tra pigmento, *intonaco* e strati di *intonaco* di base.

Per integrare i risultati ottenuti da XRD, FTIR e microscopia ottica, è stata successivamente eseguita la spettroscopia micro-Raman. Ciò ha consentito di confermare la presenza di fasi minerali identificate tramite XRD, oltre a fornire informazioni aggiuntive sulla natura della miscela di componenti incorporati negli strati di pigmento.

Proseguendo, i campioni sono stati analizzati utilizzando SEM-EDS. Sono state acquisite micrografie dei campioni a diversi ingrandimenti e sono state selezionate regioni specifiche dei campioni per l'analisi elementare EDS. Successivamente è stata eseguita una mappatura chimica alle interfacce dei campioni stratificati, consentendo una comprensione più completa delle interazioni tra e all'interno degli strati.

Infine, sono state eseguite analisi e mappature micro-FTIR sulla microstratigrafia di due campioni per comprendere ulteriormente le interazioni tra la matrice e l'aggregato di *intonaco* e strati di pigmento. Sono state utilizzate mappe FTIR per determinare la distribuzione di calcite e silicati in questi strati e hanno fornito un utile confronto con le mappe chimiche SEM-EDS.

Questi risultati hanno confermato nuovamente le ipotesi suggerite dai metodi precedenti e hanno anche fornito nuove informazioni sulla tecnologia di produzione degli strati di *intonaco* e sull'interazione chimica delle fasi. In definitiva, i risultati di questi metodi complementari contribuiscono a una comprensione più completa delle tecniche impiegate nella creazione delle pitture murali di Teotihuacan. Attraverso la scoperta della composizione materiale dei pigmenti e degli intonaci, dei progressi tecnologici e dei metodi di produzione utilizzati nel sito, ci avviciniamo all'interpretazione della società che ha prodotto i suddetti dipinti.

1. Introduction

Wall painting is one of the most ancient forms of artistic expression. It is a powerful medium, capable of storytelling, of conveying cultural values and beliefs, and communicating the human experience. The study of these paintings allows researchers to investigate crucial aspects of the societies that created them, from production methods to technological advancements to trade and resource availability.

In pre-Columbian Mesoamerican societies, wall paintings were key tools in asserting political authority and mythological ideals (Pasztory, 1997). From early Olmec cave paintings, through the wall paintings of the Maya and Teotihuacanos, to the accomplishments of the Aztecs until the Spanish conquest, murals were reflections of life (Miller, 2012). Especially relevant in the case where written records are undeciphered or not present, artistic depictions act as a vital torch in a dark tunnel. Early research in this area was mostly iconographic in nature, but an increase in archeomaterial study starting in the mid-20th century has continued to allow for novel findings concerning the materials and methods used by ancient artists to produce these works (Kubler, 1967; Domingo et al, 2021).

This study is centered on investigating wall painting fragments from one of the most extensively decorated and highly influential cities of the Mesoamerica: Teotihuacan. As the first complex state in the Mexican plateau, and largest city in the western hemisphere during its height, Teotihuacan stands alone as a unique example of a dominant power in pre-Columbian Mexico (López-Puértolas et al, 2023; Cowgill, 2015). Among accomplishments in manufacturing, pyramid building, and trade, Teotihuacan was known to be a vibrantly decorated city (Magaloni, 1996). Not only civic buildings and residences of the upper class, but virtually all structures throughout the city were adorned with colorful wall paintings depicting scenes of deities and naturalistic imagery (Magaloni, 1996).

The objective of this work is to characterize the pigments and plasters of wall painting samples obtained from the Techinantitla building complex, located in the Amanalco neighborhood of Teotihuacan. Situated near the civic-ceremonial center of the city, this neighborhood is known for its high-quality mural paintings. Unfortunately, the area underwent severe looting in the 1960s, and study of the remains has been limited (Ruvalcaba- Sil et al, 2021).

This study employs X-Ray Diffraction (XRD), Fourier transform infrared spectroscopy (FTIR), optical microscopy, micro-Raman spectroscopy, micro-FTIR spectroscopy, and SEM-EDS to analyze pigment and plaster samples from Techinantitla. Accompanying characterization, the results are compared with those of previous studies to gain new understanding of plaster and pigment production technology and its role in Teotihuacan society.

1.2 History of Mesoamerican Wall Painting

The study of Mesoamerican wall painting reflects an extensive art historical and scientific tradition, inseparable from history of the region's cultural and religious practices. These artworks, found in sites like Bonampak, Oxtotitlan Cave, and Teotihuacan provide valuable insights into the technological advancements and artistic practices of pre-Columbian societies (Magaloni et al, 2011; Grove, 1970; Pasztory, 1997). They were often created on the surfaces of monumental architecture, such as temples, palaces, and residential complexes, with themes ranging from religious and mythological scenes to depictions of daily life and historical events (Pasztory, 1997).

The process began with preparation of the wall, which usually involved application of a mud-based plaster followed by a thin lime-based plaster combined with sand, volcanic glass, or other aggregates (Magaloni, 1996). Lime mortar is produced through the heating of calcium carbonate rocks, such as limestone, to produce calcium oxide, or quicklime. Water is then added to quicklime to create slaked lime (calcium hydroxide), at which point aggregate can be added, resulting in a resistant mixture after carbonation and hardening (Rodríguez-Navarro, 2012). This mortar, known as stucco, *intonaco*, or *enlucido*, served as the ground for the paintings and was smoothed and sometimes burnished to achieve a polished finish (Magaloni, 1996). In some cases, multiple layers of plaster were applied, with the final, thinnest layer serving as the painting surface.

The first use of lime mortar for architectural purposes dates to 10,000-12,000 BCE, corresponding to the origin of pyrotechnology in the Levant (Kingery et al, 1988; Rodríguez-Navarro et al, 2023). It has been used extensively in ancient civilizations such as Egypt, Greece, and Rome to produce some of the world's most enduring and significant monuments and architecture. In Mesoamerica, pyrotechnology was developed independently with first instances of architectural use of lime dating approximately 1100 BCE (Hansen et al, 2000; Rodríguez-Navarro et al, 2023). Lime mortars produced in Mesoamerica demonstrate excellent durability despite a general lack of evidenced hydraulicity, often attributed to the addition of organic additives (Rodríguez-Navarro et al, 2023).

Pigments used in Mesoamerican wall paintings were derived from various inorganic and organic natural sources. Minerals such as hematite, cinnabar, limonite, malachite, azurite, and calcite were primary inorganic sources used for generating red, yellow, green, blue, and white colors. Organic colorants like indigo and charcoal were also used to create varied blue and black shades (Ruvalcaba-Sil, 2021). Pigments and organic colorants were often mixed with filler material such as carbon, calcite, and other additives to produce various effects in the finished murals.

The application of the pigments was typically executed using the *fresco* technique, in which the pigment is combined with a lime binder and applied to wet plaster (Argote et al, 2020). This allows the pigments to become incorporated into the wall as the plaster dries, ensuring the durability of pictorial layer over time (Magaloni, 1996). However, there is also evidence of Mesoamerican wall paintings created using the *secco* technique, where pigments are applied to dry plaster.

1.3 Wall Paintings of Teotihuacan

Although wall painting was part of the artistic landscape of many ancient Mesoamerican societies, Teotihuacan represents a unique case of an extensively painted city. To understand the progress of wall painting technology developed by Teotihuacano artisans over the rise of the city's influence, it is useful to refer to the chronology established by Diana Magaloni in her seminal 1996 work on Teotihuacan color theory (Magaloni, 1996). Through analyses via optical microscopy, XRD, and SEM-EDS of over 800 samples from various periods across the site, Magaloni identified four technical phases of wall painting development in Teotihuacan (Magaloni, 1996; Argote et al, 2020).

Table 1 displays the chronology of Teotihuacan phases alongside the general chronology for Mesoamerica, accompanied by brief descriptions of the technical phases of mural painting at the site.

Table 1: Chronology of Teotihuacan phases and developments in wall paintings. Table adapted from (Argote et al, 2020; Clayton, 2015; Magaloni, 1996).

| General Chronology | Teotihuacan Phases | Approximate Years | Technical Developments in Wall Painting |
|-----------------------------------|---------------------------|-------------------|---|
| Postclassic period | Atlatongo | 950-1150 CE | |
| | Mazapan | 850-950 CE | |
| Late classic period | Coyotlatelco | 650-850 CE | |
| | Metepec | 550-650 CE | Fourth technical phase: Last technical phase, continued development of lime plaster with equal ratios binder to aggregate |
| Early classic | Xolalpan | 350-550 CE | Third technical phase: Expansion of pictorial palette, introduction of mica and specular hematite in pigment to produce sparkling effect. Improvement of lime plaster technology |
| | Tlamimilolpa | 200-350 CE | Second technical phase: characteristic Teotihuacan red shade emerges. <i>Intonaco</i> comprised of lime and volcanic glass, a technical development that persists through all phases of mural painting |
| Terminal Preclassic/ Formative | Tzacualli-Micaotli | 1-200 CE | First technical phase: two shades of red, <i>intonaco</i> comprised of lime mortar and sand aggregate |
| | Patlachique | 150 BCE-1 CE | |

It must also be noted that more recent studies have placed the widespread introduction of volcanic glass shards in the Xolalpan phase (350-550 CE), and not the Tlamimilolpa (200-350 CE) as postulated by Magaloni (Murakami, 2010; Pecci et al, 2018).

The color used most frequently throughout Teotihuacan mural paintings is red, produced primarily from red ochre, a naturally occurring clay earth pigment comprised of hematite, clays, and silicates. Its earliest use dates to the Paleolithic, making it one of the first pigments used by humankind; its

popularity as a pigment prevailed throughout ancient cultures across the world, and is still used as a source for red pigments in the modern era.

Technical developments are centered around the improvement in the formula for lime-based plasters, as well as the introduction of additives to pigments to produce various effects, such as the addition of specular hematite to create a sparkling painted surface. Developments also include expansion of the palette and standardization of manufacturing. It could be argued that the height of wall painting technology was reached during the Late Xolalpan, after which political struggles and unrest resulted in a decrease in standardization of *intonaco* production processes (Murakami, 2010).

1.4 Archaeological Site of Teotihuacan

The archaeological site of Teotihuacan is located 40 km outside of present-day Mexico City, indicated in Figure 1. At its height during the Classic period, approximately 200 BCE–650 CE, it was a flourishing metropolis with estimated population of 125,000, exerting extensive cultural and economic influence throughout Mesoamerica (Cowgill, 2015).



Figure 1: Map of Mexico indicating the location of Teotihuacan (Encyclopedia Britannica, 2024).

The city was organized on a grid pattern around the central Avenue of the Dead, with surrounding apartment compounds and monumental architecture. The three most significant structures are pyramids of the site, the Pyramid of the Sun, the Pyramid of the Moon, and the Temple of Quetzalcoatl, also referred to as the Pyramid of the Feathered Serpent.

In estimated 600/650 CE, many of Teotihuacan's monuments were destroyed by fire, after which there was a significant population decline (Cowgill, 2015). Without a deciphered written record, little is known about the cause of this violent event, but scholars are inclined towards a theory of civic unrest and a rejection of the governing elites.

Figure 2 displays the layout of the city, with the Techinantitla compound indicated in red. The Techinantitla complex is a single large building structure, approximately 75 x 95 m in area located in the Amanalco neighborhood of the city (Miriello, 2021). As one of the largest

recognized complexes in Teotihuacan, its function has been speculated to be partially public and partially residential (Manzanilla, 2009; Millon, 1973).

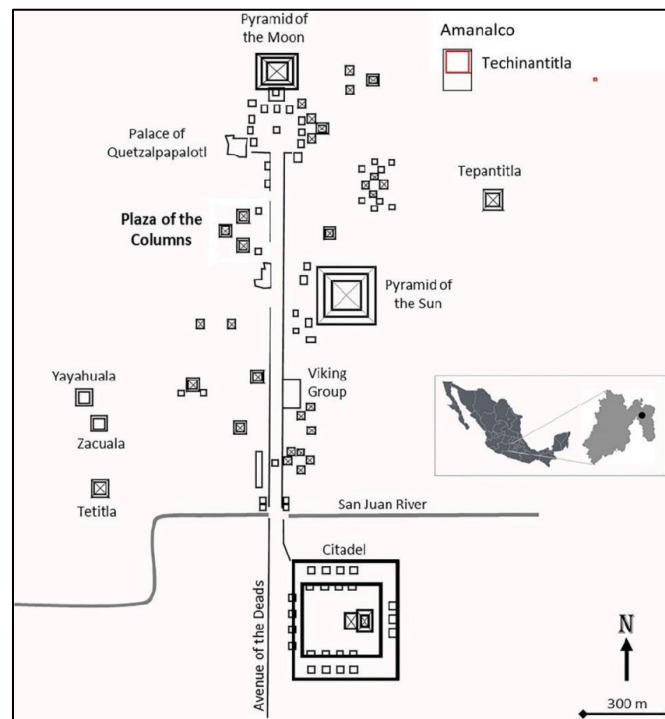


Figure 2: Map of Teotihuacan, with the Techinantitla building complex indicated in red (Ruvalcaba-Sil et al, 2021).

Official archaeological excavations at Teotihuacan began in the early 20th century, with the Mexican government taking ownership of the site in 1906 (Millon et al, 1973). Early work focused on excavation and restoration of the Pyramid of the Sun, with the intention of creating a symbol in celebration of the anniversary of the Mexican War of Independence. Excavations continued throughout the 20th century, notably at Temple of Quetzalcoatl, the Avenue of the Dead, and the Palace of Quetzalpapalotl, continuing to unveil new aspects of the expansive site.

The first full-coverage surface survey of the city was achieved with the Teotihuacan Mapping Project (TMP), began in 1962 and led by René Millon, mapping over 5000 individual structures (Millon et al, 1973). More recent excavations have led to discoveries such as mass sacrificial burials in the foundations of the Temple of Quetzalcoatl, and the detection of cavities beneath the major pyramids of the site (Taube, 1992; Argote et al, 2020). These findings, combined with modern techniques and archaeometric research, continue to uncover details about Teotihuacan's religious practices, daily life, and interactions with other Mesoamerican civilizations. Despite these advances, information concerning the city's rulers and political system remains a mystery.

The site is known for its extensive wall painting. Temples, palaces, and residential compounds were covered in detailed scenes, most commonly of spiritual subject matter (Magaloni, 1996). Defining features of the style include vibrant colour, complex iconography, and the technical skill of the artisans who completed the works. Figure 3 displays an example of a fresco found in the Techinantitla compound, likely of a deity or possibly an undeciphered glyph (The Met, 2024).



Figure 3: Example of a wall painting from the Techinantitla apartment complex, 500–550 CE, located at the Metropolitan Museum of Art (MET, 2024).

Excavations at the Techinantitla complex have revealed the presence of murals executed with a high degree of technical proficiency, depicting representations of religious figures and mythological scenes. The subject matter and quality of these works suggests its identity as a place of social status, likely housing elites as well as providing a semi-public function (López-Puértolas et al, 2021). One of thirteen complexes in the Amanalco neighborhood, its layout features a courtyard and several large rooms surrounding a temple. Continued excavations of the compound provide valuable insights into the social, economic, and religious life of Teotihuacan's elite residents (López-Puértolas et al, 2021).

2. Sample Description

This study is centered around five samples obtained from the Techinantitla building complex of Teotihuacan. Figure 4 displays the location of collection of each sample positioned in the map of Techinantitla.

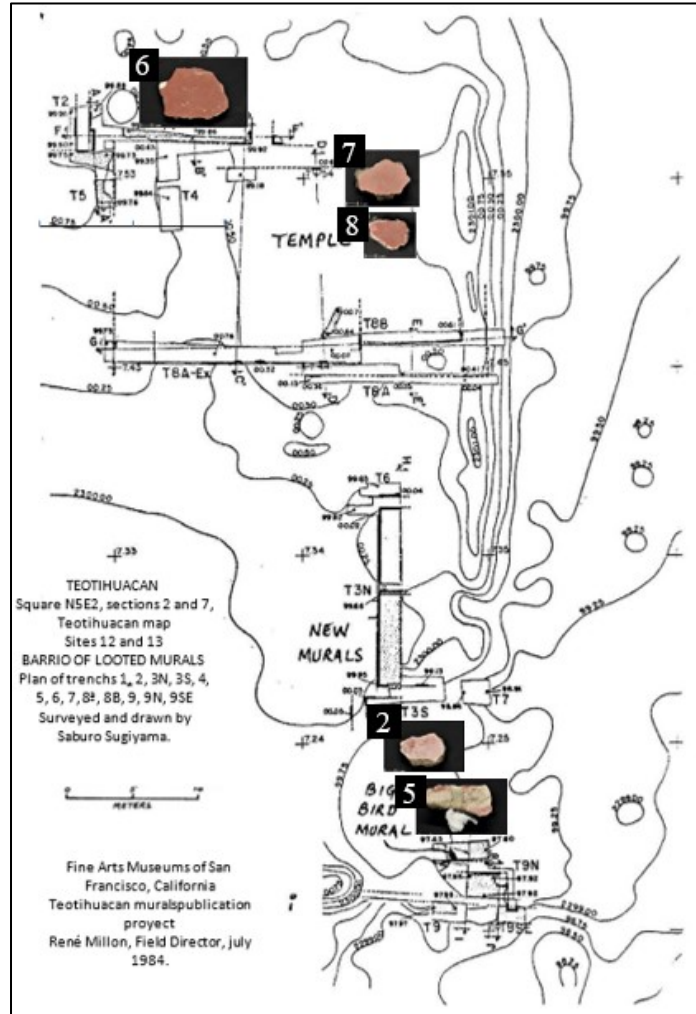














Figure 4: Map of Techinantitla compound displaying the retrieval locations of samples studied in this work (courtesy of Margarita Muñoz).

Four of the samples (2, 6, 7, and 8) are comprised of a pictorial layer and supporting plaster, while sample 5 is a plaster sample with no pictorial layer. Note that for locations marked 6 and 7, two separate stratified samples were studied per location, labeled 6Pi1, 6Pi2, 7Pi1, and 7Pi2. The pigment surfaces consist of red, black, and pink; with two pink samples, two red samples, one black sample, and one sample displaying both black and red.

Sample descriptions and images can be found in Table 1.

Table 2: Sample description and images.

| Sample Number | Image | Cross-section view | Description |
|---------------|---|--|--|
| 2Pi |  |  | Pink pigment surface, <i>intonaco</i> , base plaster* |
| 5P |  | No image | Base plaster |
| 6Pi1 |  |  | Red pigment surface, <i>intonaco</i> , base plaster |
| 6Pi2 |  |  | Black and red polychromy, <i>intonaco</i> , base plaster |
| 7Pi1 |  |  | Pink pigment surface, <i>intonaco</i> , base plaster |
| 7Pi2 |  | No image | Black pigment surface with visible red underpainting, <i>intonaco</i> , base plaster |
| 8Pi |  |  | Red pigment surface, <i>intonaco</i> , base plaster* |

*Samples 2Pi and 8Pi were further segmented to obtain samples exclusively of base plaster (P) and *intonaco* (I); these are referred to as 2P, 2I, 8P, and 8I.

The term plaster or base plaster is used here to define the underlying support layer, where *intonaco* is used to describe the thinner white layer between base plaster and pigment. These layers are also referred to in literature by their Spanish names, *firme* and *enlucido* respectively. Figure 5 depicts these layers in sample 8Pi.

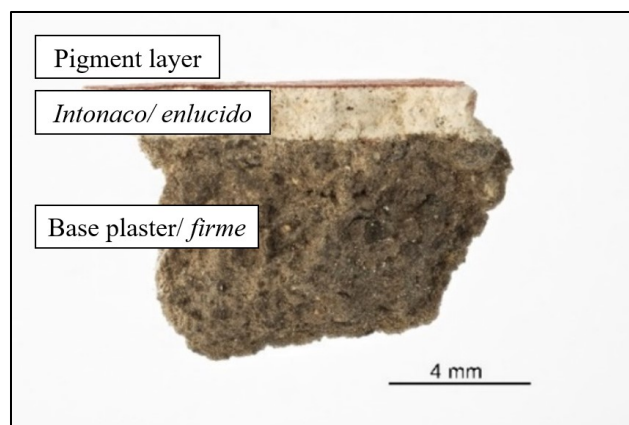


Figure 5: Cross-section of sample 8Pi displaying red paint layer, intermediate white intonaco layer, and lower brown plaster layer.

3. Experimental methods

Several analytical methods were applied in the study of this sample set, namely: X-Ray Diffraction – X-Ray Powder Diffraction (XRD-XRPD), Fourier transform infrared spectroscopy (FTIR), polarized light microscopy (PLM), micro-Raman, micro-FTIR, and SEM-EDS. Table 3 displays the list of samples along with the techniques performed for each sample.

Table 3: Sample list and applied analytical techniques.

| Sample | XRD-XRPD | FTIR | SEM-EDS | PLM | micro-Raman | micro-FTIR |
|--------|----------|------|---------|-----|-------------|------------|
| 2P | x | | | x | | |
| 5P | x | | | x | | |
| 8P | x | | | | | |
| 2I | x | | | | | |
| 8I | x | | | | | |
| 2Pi | x | x | x | x | x | |
| 6Pi1 | x | | x | x | x | |
| 6Pi2 | x | x | x | x | x | x |
| 7Pi1 | x | | x | x | x | |
| 7Pi2 | x | x | x | x | x | x |
| 8Pi | x | x | x | x | x | |

3.1 X-Ray Diffraction – X-Ray Powder Diffraction (XRD-XRPD)

X-Ray Diffraction (XRD) is an analytical technique used to identify and quantify crystalline phases of materials (Artioli, 2012). Commonly used in cultural heritage applications such as conservation science and archaeometry, it is a micro-destructive to non-invasive method to characterize the mineralogical composition of samples (Artioli, 2012). In this study, the pigment surfaces of samples 2Pi, 6Pi1, 6Pi2, 7Pi1, 7Pi2, and 8Pi were prepared for XRD analysis via mounting with plasticine onto supports, pictured in Figure 6.



Figure 6: Samples 2Pi, 6Pi1, 6Pi2, 7Pi1, 7Pi2, and 8Pi (not pictured) mounted to supports with pigment surfaces face-up.

A small piece of plasticine was placed onto the support in a cone shape, and the samples were placed atop the plasticine. A piece of glass was then used to slowly and carefully compress the sample until it was level with the surrounding rim of the support. It was important that the sample surfaces were level, as an oblique orientation would affect the outcome of the XRD measurements.

For the plaster and *intonaco* layers, samples 2P, 5P, 8P, 2I and 8I, X-Ray Powder Diffraction (XRPD) was employed. XRPD requires the samples to be in a fine powder form for analysis. The samples were first ground using a mortar and pestle, and a 20 wt% zinc oxide standard was added. This internal standard allows for the quantification of amorphous phases present in the sample, as well as enables the detection of instrumental errors such as a shift in the resultant peaks. Figure 7 displays the preparation process for these samples.

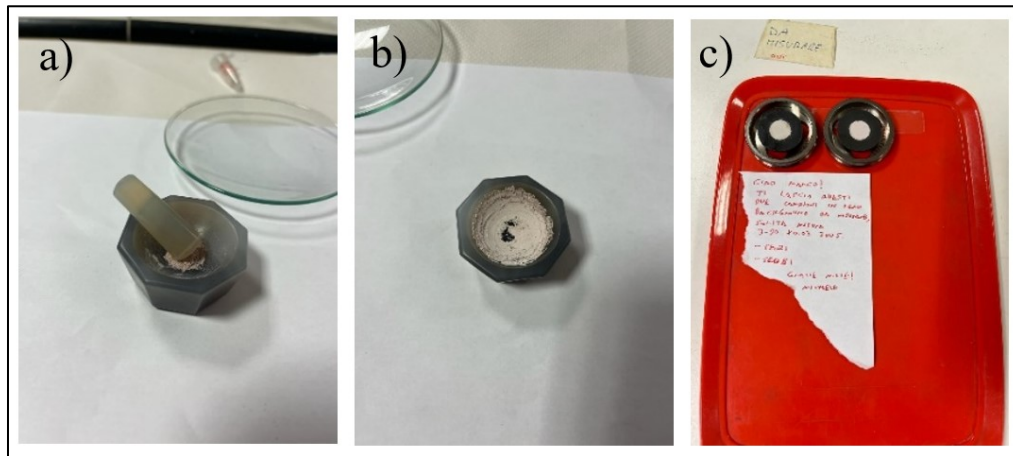


Figure 7: Sample preparation for XRPD. a) small mortar and pestle used to grind sample. b) finely ground sample. c) Powder samples mounted to zero-background sample holders.

Following sample preparation, the analysis was performed using the Malvern PANalytical X'Pert Pro diffractometer in Bragg-Brentano geometry at the University of Padova Department of Geosciences, pictured in Figure 8, using a continuous scan in the range 3-90° 2 θ , a step size of 0.03° and 300 s counts per step.

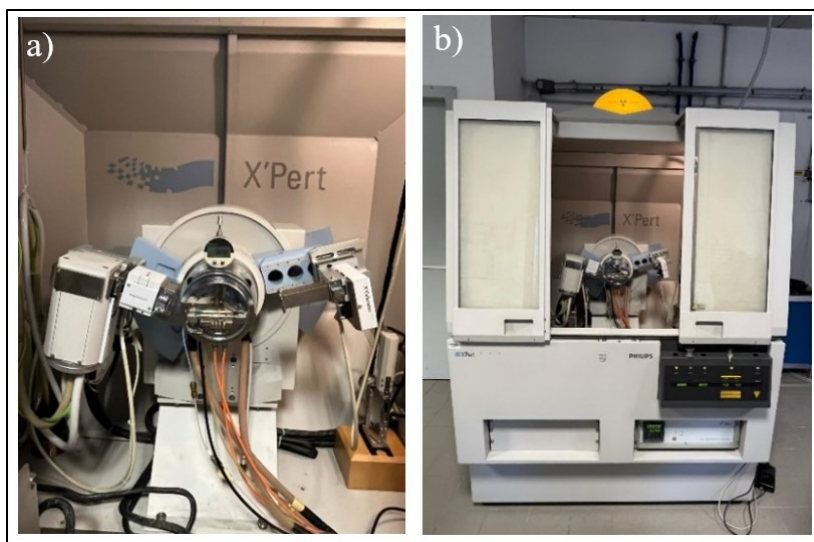


Figure 8: a) Detail view of the Malvern PANalytical X'Pert Pro diffractometer at the Department of Geosciences, University of Padova. b) Distance view of the diffractometer.

Data analysis was subsequently performed using X'Pert HighScore Plus equipped with the International Centre for Diffraction Data (ICDD) database, (Inorganic Crystal Structure Database) ICSD, and Crystallography Open Database (COD). Further quantitative analysis was performed using Rietveld refinement in Topas software.

3.2 Fourier Transform Infrared Spectroscopy (FTIR)

Fourier Transform Infrared Spectroscopy (FTIR) is a spectroscopic method used to identify materials by their infrared spectra (Poliszuk, 2014). An established analytical technique used in cultural heritage applications, it is especially suitable for the identification of organic substances, as well as degradation products (Poliszuk, 2014). No sample preparation was required for these analyses, the pigment surfaces of samples were simply placed atop the attenuated total reflection (ATR) crystal of the Bruker Alpha-P compact FTIR spectrophotometer seen in Figure 9, and contact between the sample surface and sensor maintained via the arm of the device.

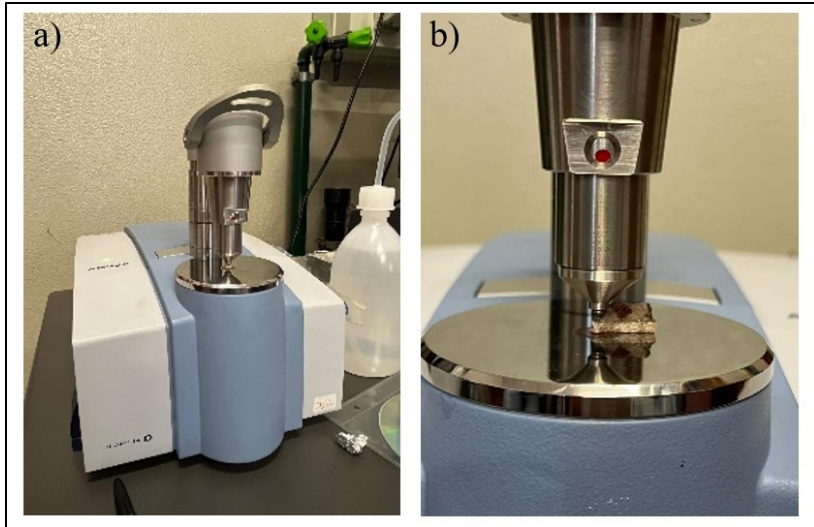


Figure 9: a) Bruker Alpha-P compact FTIR spectrophotometer. b) Detail view of sample under probe.

Plotting and analysis of FTIR data was performed using Spectragryph software with use of the Kimmel Center IR Spectra Library database.

3.3 Optical Microscopy

Optical microscopy, otherwise known as light microscopy, is a form of microscopy that uses visible light and a series of lenses to generate magnified images of objects. It is a key tool for examining the microstratigraphy of wall painting samples, allowing for the determination of method of application of pigment layers, i.e. *fresco* versus *secco* application, size and distribution of aggregate materials, and identification of additives.

For optical microscopy, micro-Raman spectroscopy, micro-FTIR, and SEM-EDS analyses samples were prepared as cross sections. The samples were first placed in cylindrical plastic molds that were subsequently filled with epoxy resin, as seen in Figure 10. They were then exposed to vacuum conditions for a few minutes to remove pores, and left to cure in an oven at 40 °C for 24 hours.



Figure 10: a) Plastic containers with samples being filled with epoxy resin. b) Sample containers in oven.

Upon removal from the containers, their surfaces were ground using increasingly fine grit paper to achieve optimally polished surfaces using a Struers grinding and polishing system, seen in Figure 11.



Figure 11: Left: unpolished samples embedded in resin. Right: Struers polisher.

Optical microscopy analysis was performed using a Nikon Eclipse ME600 microscope equipped with a Canon EOS Rebel T3i DSLR camera, seen in Figure 12.

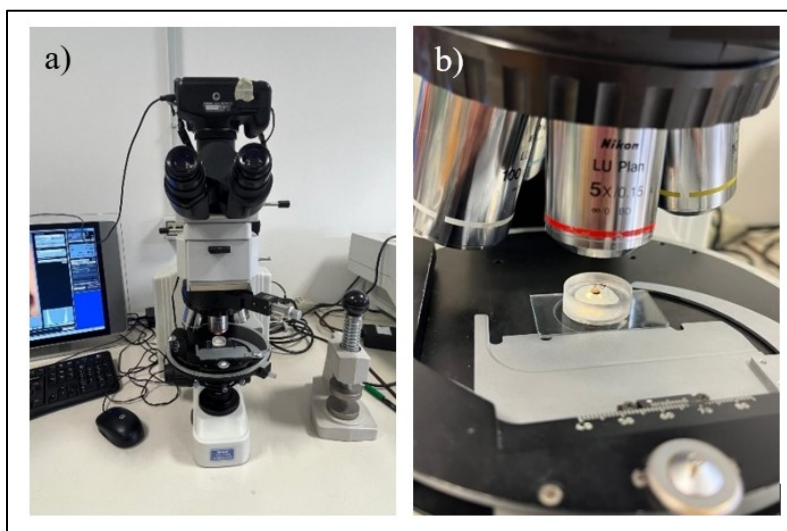


Figure 12: Left: Nikon Eclipse ME600 microscope equipped with camera. Right: close-up of sample on stage.

3.4 micro-Raman Spectroscopy

Raman spectroscopy is an analytical technique that enables the detection of vibrational modes of molecules, thereby allowing identification of molecular components of a sample. The working principle is based on the inelastic scattering of photons when interacting with matter, called Raman scattering. The difference in the energy of incoming and outgoing photons directed at a sample allows for the identification of vibrational modes, and by extension molecular species. Micro-

Raman spectroscopy is a technique that combines Raman spectroscopy with microscopy allowing for precise sampling areas, down to the micron scale. Figure 13 displays the Raman microscope used in this study, the WITec Raman microscope alpha300 present at the University of Padova, Department of Geosciences.

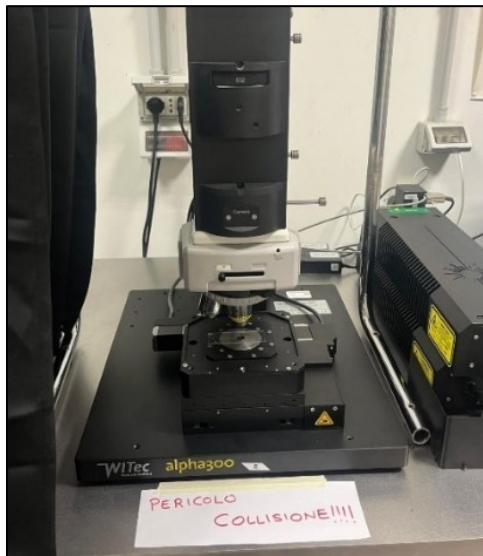


Figure 13: WITec Raman microscope alpha300 at Department of Geosciences, Padova.

Measurements were obtained using a 532 nm laser, at a power of 3 or 5 mW, over a Raman shift range of 50 - 3850 cm^{-1} . Analysis of micro-Raman data was completed with Omnic software, using RRUFF Raman Minerals database.

3.5 micro-FTIR Spectroscopy

Similar to micro-Raman spectroscopy, micro-FTIR combines the principles of FTIR spectroscopy with microscopy. Paired together, it is possible to obtain FTIR spectra of areas as small as 10 μm allowing for precise and targeted data acquisition, as well as FTIR integration mapping. Micro-FTIR analyses were performed using a Bruker Hyperion II FTIR microscope in reflection mode, pictured in Figure 14. Each spectrum was obtained in the IR wavelength range of 4000 cm^{-1} - 400 cm^{-1} , and mapping was performed using 32 scans per spectrum, with an analyzed area of 50 x 50 μm for each point, and spectral resolution of 4 cm^{-1} . Data was acquired and analyzed using OPUS software.



Figure 14: Bruker Hyperion II FTIR microscope located at the University of Padova, Department of Geosciences.

3.6 Scanning Electron Microscopy – Energy Dispersive X-Ray Spectroscopy

Scanning electron microscopy (SEM) is a variation of microscopy which uses a beam of electrons to scan sample surfaces and produce magnified images. Interactions between the electrons and atoms of the sample generate characteristic signals that can be used to image sample morphology and to determine elemental composition. Imaging was performed using the Coxem EM-30AX scanning electron microscope present at the CEASC laboratories of the University of Padova, pictured in Figure 15. To prevent charge accumulation, the samples were first sputter coated in gold using a Quorum Q150R rotary pumped coater, also shown in Figure 15. Elemental characterization and mapping of sample surfaces was made possible via an energy dispersive X-ray detector, EDAX Element-C2B, used in conjunction with SEM.

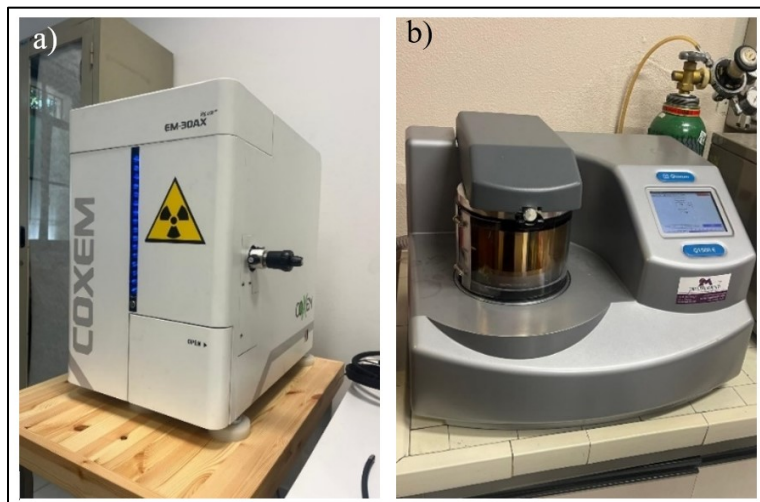


Figure 15: a) Coxem EM-30AX scanning electron microscope. b) Quorum Q150R coater.

4. Results

4.1 X-Ray Diffraction – X-ray Powder Diffraction (XRD – XRPD)

In total, 11 sample segments were prepared for XRD/XRPD. As mentioned in section 3.1, samples 2I, 8I, 2P, 5P, and 8P were prepared in powder form with the addition of a 20 wt % internal standard of zincite for X-Ray Powder Diffraction (XRPD), and samples 2Pi, 6Pi1, 6Pi2, 7Pi1, 7Pi2, and 8Pi were prepared for non-invasive measurement via mounting onto supports for XRD analysis. The qualitative results for the pigment samples are summarized in Table 4, and the results of the plaster and *intonaco* samples are seen in Table 5.

Table 4: Summary of XRD results for pigment surfaces displaying sample names and minerals detected.

| Sample | Chromophore | Pigment accessory phases | | | | | | | Alteration products | | | | |
|--------|-------------|--------------------------|-----|-----|------|-----|------|-----|---------------------|------|-----|-----|------|
| | Hem | Cal | Qtz | Kln | Musc | And | Dias | Mag | Gyp | Bass | Wed | Vat | Trid |
| 2Pi | x | x | x | x | | | | x | | | x | | |
| 6Pi1 | x | x | x | x | x | x | | | x | x | | | |
| 6Pi2 | x | x | x | x | x | x | | | | x | | x | |
| 7Pi1 | x | x | x | x | | x | | | | | | | |
| 7Pi2 | x | x | x | x | | x | x | | | | | | |
| 8Pi | x | x | x | x | | x | | x | | | | | x |

*Hem: hematite, Mag: magnetite, Cal: calcite, Qtz: quartz, Kln: kaolinite, Musc: muscovite, And: andesine, Dias: diaspore, Gyp: gypsum, Bass: bassanite, Wed: weddellite, Vat: vaterite, Tri: tridymite.

Table 5: Summary of XRD results for plaster and *intonaco* samples.

| Sample | Lime binder | Inclusions/ Aggregate | | | | | | | | | |
|--------|-------------|-----------------------|-----|-------|------|------|-----|-----|-----|------|--|
| | Cal | Qtz | And | Forst | Diop | Horn | Hem | Mag | Kln | Musc | |
| 2I | x | x | x | | x | x | | | | | |
| 8I | x | x | x | | | x | x | x | x | x | |
| 2P | | x | x | x | x | x | | | | | |
| 5P | | x | x | x | x | x | | | | | |
| 8P | | x | x | x | x | x | | | | | |

*Cal: calcite, Qtz: quartz, And: andesine, Forst: forsterite, Diop: diopside, Horn: hornblende, Hem: hematite, Mag: magnetite, Kln: kaolinite, Musc: muscovite

The pigment surfaces (2Pi, 6Pi1, 6Pi2, 7Pi1, 7Pi2, 8Pi) revealed common minerals of hematite, calcite, quartz, and kaolinite. The combination of kaolinite and hematite indicates the presence of red ochre, the pigment used most abundantly to produce Teotihuacan red and pink colors (López-Puértolas et al., 2020). Red ochre is a pigment used from prehistory, and is composed of iron oxides and silicate minerals such as quartz, clays, and feldspars (Secco et al, 2021). Hematite (α -Fe₂O₃) is the chromophore responsible for producing the red color, present both as a component of red ochre, and added intentionally by Teotihuacan artists in the form of specular hematite to produce a sparkling effect (López-Puértolas, et al., 2023). Quartz and muscovite have also been identified as additives used for this purpose, however they could also be present as accessory components of red ochre (López-Puértolas, et al., 2023; Argote et al, 2020).

The presence of calcite is indicative of the carbonate binder used to apply the wall paintings in *fresco* and *secco* technique. It is also a known filler added to the pigments, and was used in varying ratios to generate pink hues.

The *intonaco* samples 2I and 8I produced similar results, with calcite, quartz, andesine, and hornblende being identified in both. Diopside was also detected in 2I, as well as in all the plaster layer samples (2P, 5P, and 8P). The composition of the base plaster samples proved to be identical, with quartz, andesine, hornblende, diopside, and forsterite identified in all.

Figure 16 displays the XRPD results of sample 2I, revealing peaks of calcite, quartz, andesine, hornblende, and diopside. These findings are in accordance with previous studies performed on Teotihuacan plaster which identified plagioclase, quartz, calcite, pyroxene, and amphibole as the most abundant minerals in the *intonaco* layer of Teotihuacan plaster samples (Miriello et al, 2021; Barca et al, 2019). This layer is known to be a mixture of lime-based mortar with rhyolitic volcanic glass shard aggregate, therefore the prevalence of calcite in samples 2I and 8I is to be expected (Miriello et al, 2021).

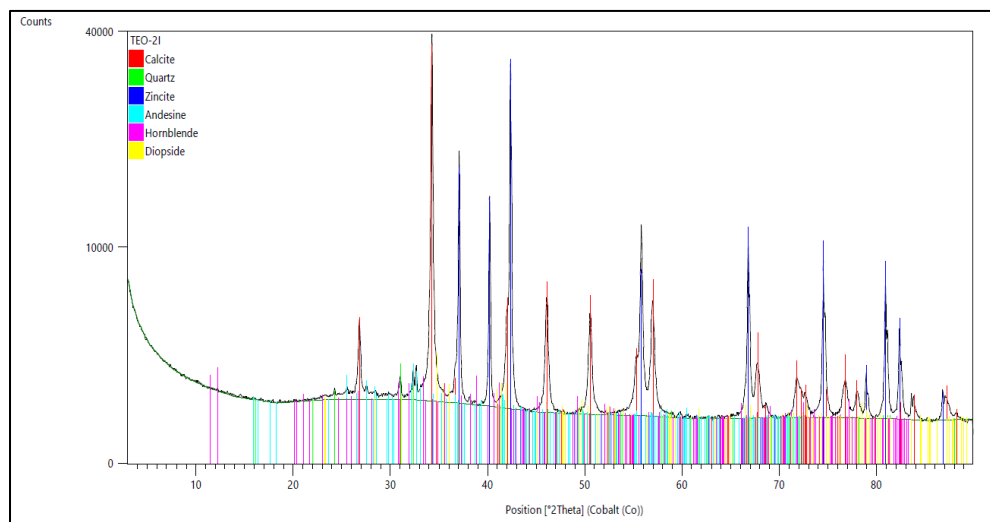


Figure 16: XRPD results of sample 2I.

Quartz, andesine, hornblende, and diopside are all silicate minerals, indicative of the expected aggregate, rhyolitic volcanic glass shards. Andesine is a framework silicate and member of the plagioclase feldspar series, where hornblende and diopside are inosilicates, or chain silicate minerals.

Sample 8I revealed XRD peaks of calcite, quartz, andesine, and hornblende consistent with the other *intonaco* sample tested, 2I. Additionally, hematite, kaolinite, magnetite, and muscovite were also identified in this sample. These minerals may be the result of inclusions in the lime binder, or possibly the result of intermixing with the pigment layer.

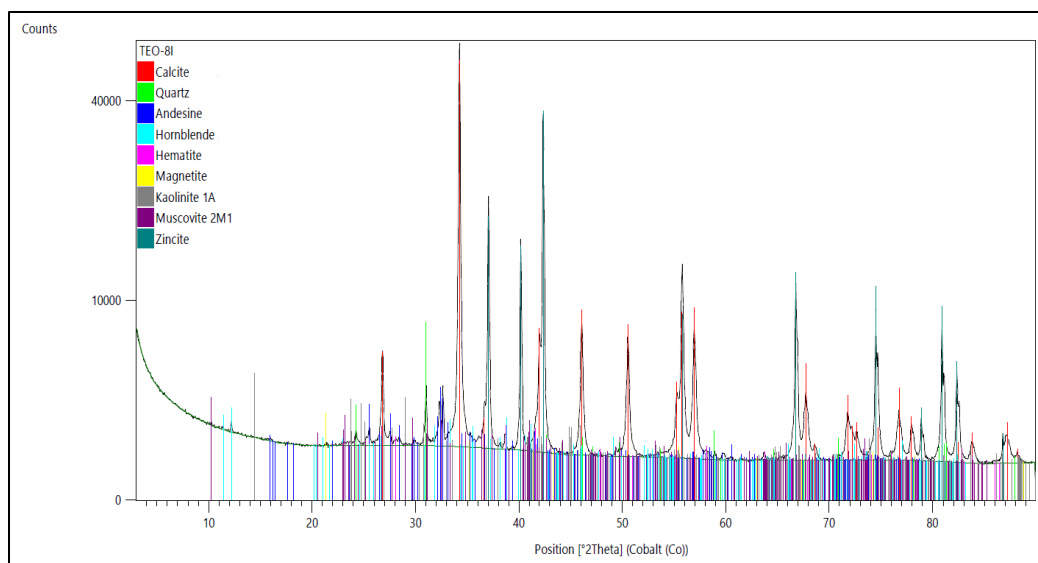


Figure 17: XRPD results of sample 8I.

Magnetite (Fe_3O_4) is a ferrimagnetic iron oxide mineral often occurring together with hematite. It has been identified in the pigment of wall paintings from the Mesoamerican sites of Cacaxtla, Cholula, and Templo Mayor, in which the remnant magnetization of murals was determined via the presence of magnetite and to a lesser extent hematite (Goguitchaichvili, et al, 2004). However, recent studies of pigments at Teotihuacan do not report the occurrence of magnetite (Argote et al, 2020; López-Puértolas et al, 2023; López-Puértolas et al, 2020; Ruvalcaba-Sil et al, 2021). As mentioned, magnetite often occurs with hematite so it is possible that it is an accessory mineral of red ochre. However, the possibility of the intentional addition of magnetite cannot be excluded based on XRD results alone; further analysis via micro-Raman and SEM-EDS can provide more insights in this area.

The XRPD spectra of plaster sample 2P, displayed in Figure 18 showed consistency with the other plaster samples 5P and 8P, with quartz, andesine, hornblende, diopside, and forsterite were identified among all samples. Forsterite, another silicate mineral part of the olivine solid solution series, is only identified in the base plaster samples where the other silicate minerals identified (quartz, andesine, hornblende, diopside) are identified in both the *intonaco* and base plaster layers. The consistency of silicate minerals present in both the *intonaco* and base plaster layers is a potential indication of a standardized production process and aggregate acquisition from the same source (Barca et al, 2019).

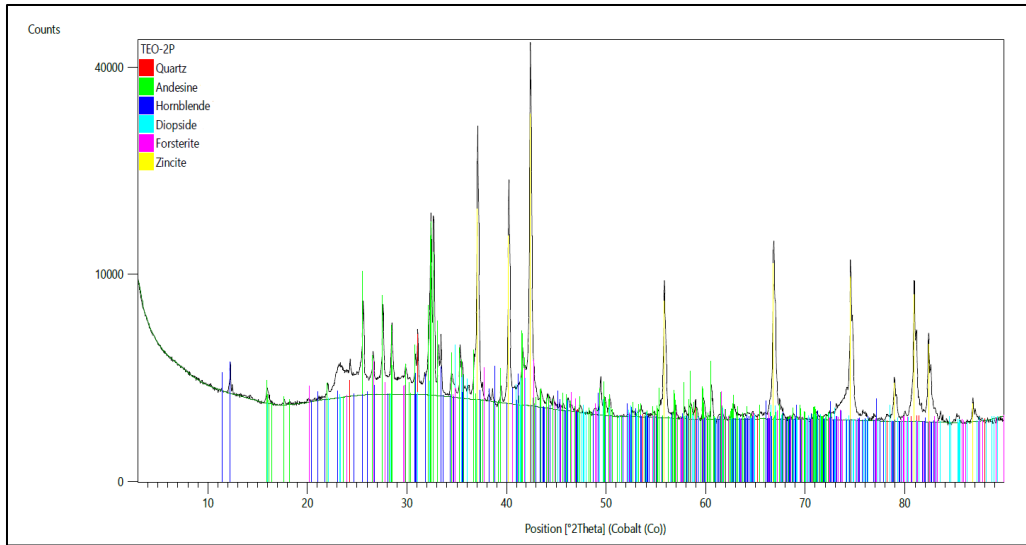


Figure 18: XRPD results of sample 2P.

The results of pigment sample 2Pi, shown in Figure 19 reveal the presence of calcite, quartz, andesine, hematite, magnetite, kaolinite, and weddellite. Again, magnetite is identified here; either detected as an iron oxide present in the red ochre pigment, or intentionally added as in the case of specular hematite to produce a glittering effect. Weddellite is a mineral form of calcium oxalate, and has been studied in the field of cultural heritage as an alteration product of calcium carbonate, known to form patinas on carbonate rocks through the action of evaporating fluids (Secco et al, 2021; González-Gómez et al, 2018).

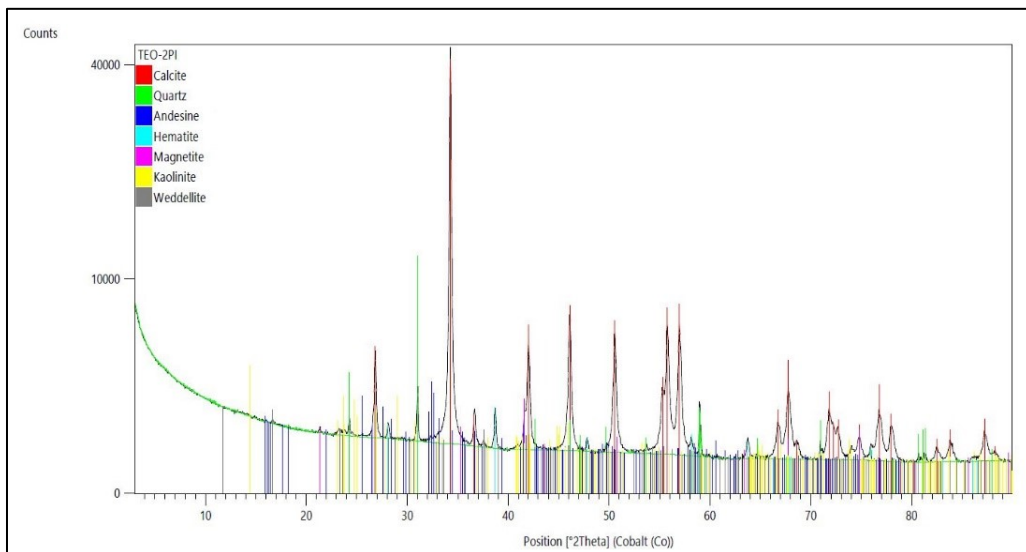


Figure 19: XRD results of sample 2Pi.

In addition to the expected combination of calcite, quartz, hematite, kaolinite, and andesine, sample 6Pi1 uncovers the presence of muscovite, gypsum, and bassanite, seen in Figure 20. Gypsum is a mineral of calcium sulphate, and was identified in iron oxide-based pigments from the Late Xolalpan phase (450–550 CE), as well as in white pigments from the Techinantitla

building complex (Magaloni, 1996; Luis Ruvalcaba-Sil, 2021). Similar to weddellite, gypsum is also known to be a superficial alteration product of carbonate minerals, and bassanite is a further alteration product of gypsum (Secco et al, 2021; McGee et al, 1992). The presence of both gypsum and bassanite here are likely indicative of alteration of *intonaco* layer, as opposed to intentional addition by Teotihuacan artisans to the pigment.

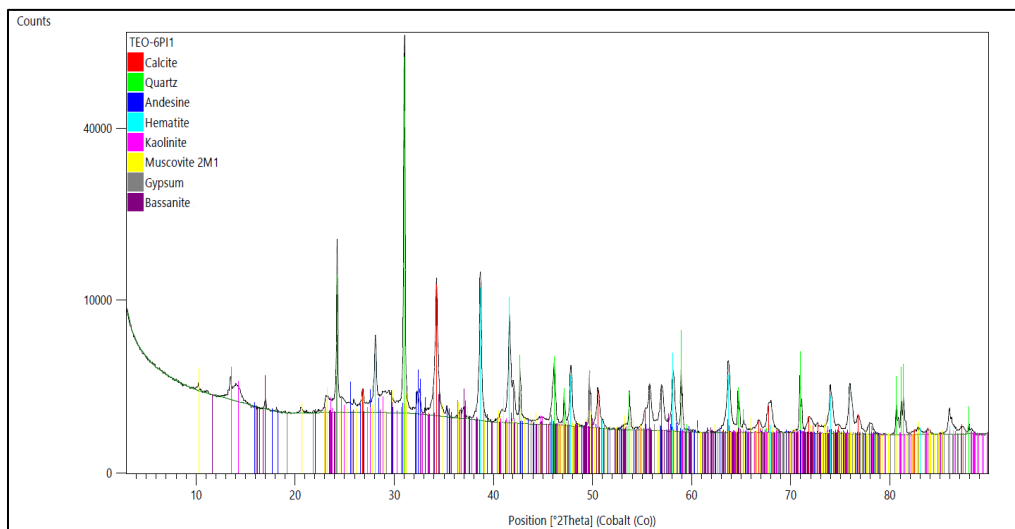


Figure 20: XRD results of sample 6Pi1.

Sample 6Pi2 shows strong similarity to that of 6Pi1, with only the exclusion of gypsum and the addition of vaterite. Again, bassanite exists here as evidence of the alteration of gypsum. Vaterite is a metastable polymorph of calcium carbonate, having a hexagonal crystal system compared to calcite's trigonal system. It has been recognized as an intermediate product preceding the formation of stable calcite in the carbonation process of lime-based mortars, however its identification even in historical mortars remains perplexing (Rodríguez-Navarro et al, 2023). A possible explanation is that the presence of organic additives in the mortar composition allows for the production and stabilization of vaterite (Rodríguez-Navarro et al, 2023; Fiori et al, 2009; Thirumalini et al, 2018). This is one indication of the potential addition of organic matter to the *intonaco* layer of Teotihuacan plasters, possibly contributing to its strength and durability despite uncertain hydraulic properties.

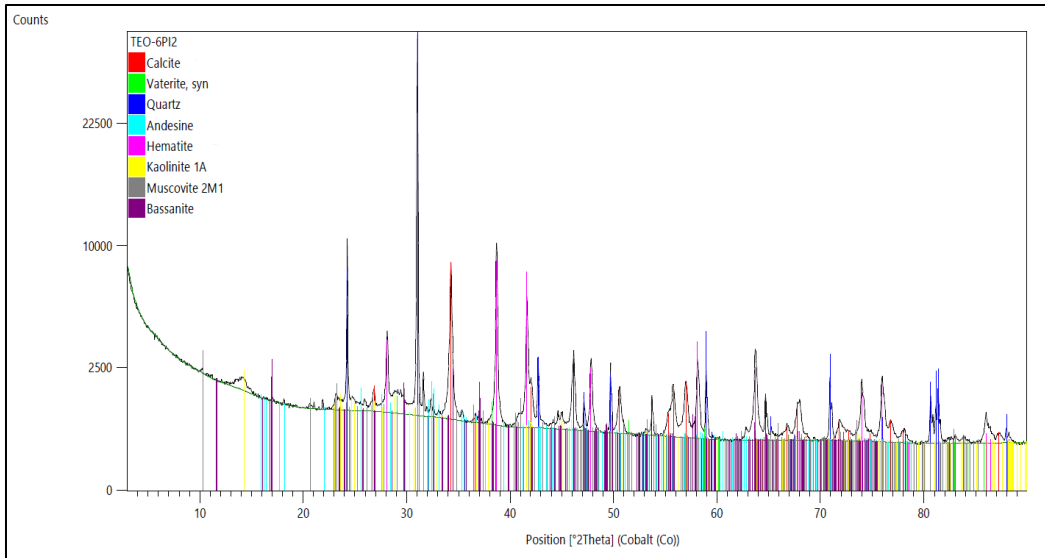


Figure 21: XRD results of sample 6Pi2.

The results of sample 7Pi1, displayed in Figure 22, reveal the standard minerals found in all pigment samples: calcite, quartz, andesine, hematite, and kaolinite, with no evidence of alteration products.

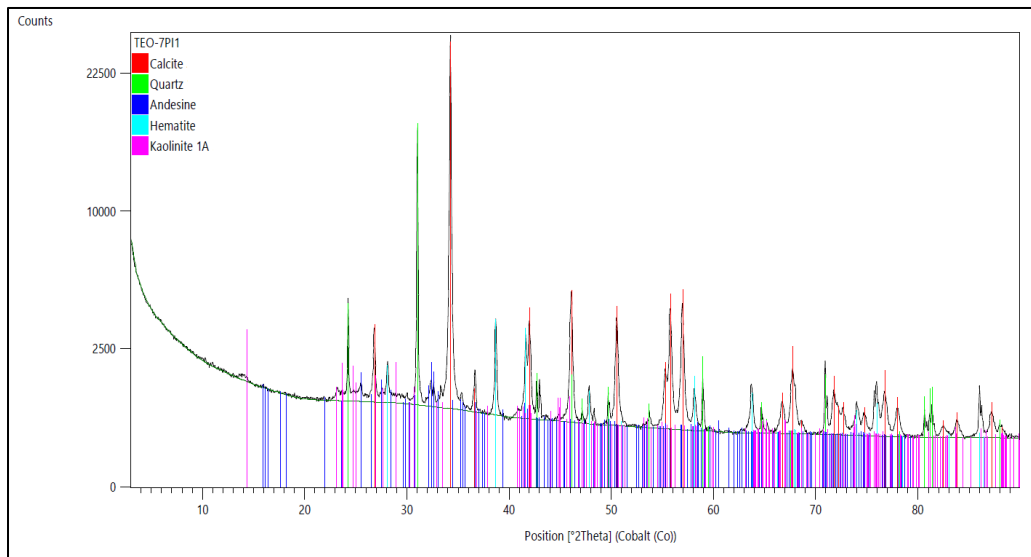


Figure 22: XRD results of sample 7Pi1.

The diffractogram of sample 7Pi2, shown in Figure 23 is consistent with that of 7Pi1 with only the addition of diaspre (α -AlO(OH)) an aluminium hydroxide oxide mineral with a pearly lustre. This is the only indication of diaspre among all samples studied. There is no mention of diaspre identified among wall painting samples from Teotihuacan, however there was the discovery of a diaspre mineral at Tzompantli, a stone platform of skulls, at the site of Chichen Itza, Mexico (González-Gómez et al, 2018).

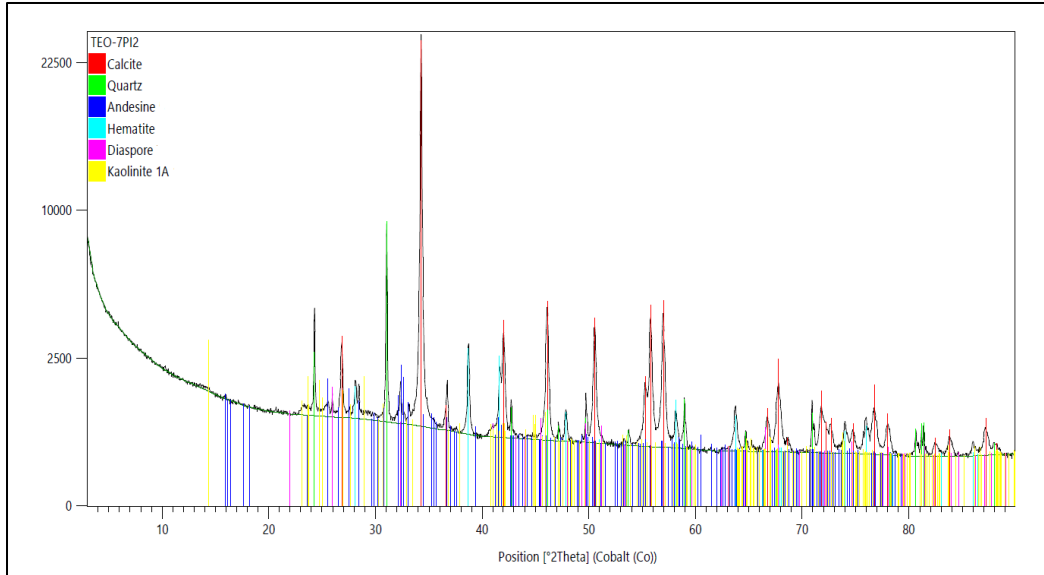


Figure 23: XRD results of sample 7Pi2.

Figure 24 displays the XRD results of sample 8Pi. It shares the same basic minerals as the other pigment samples, with the addition of magnetite and tridymite. Tridymite is a high-temperature polymorph of silica, commonly found in volcanic material such as tuffs (Gutiérrez-Castorena et al, 2010). It has been identified in a sample from the Xalla complex of Teotihuacan in addition to cristobalite and quartz; its inclusion either indicating it as an accessory mineral to natural red ochre, or intentional addition (as with quartz) to create iridescent effects (López-Puértolas et al, 2019).

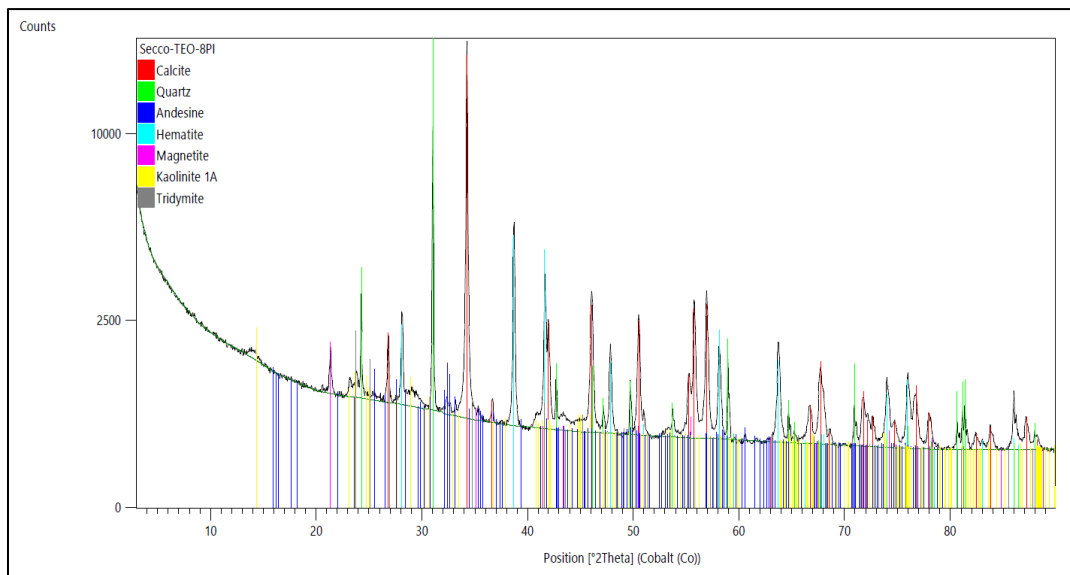


Figure 24: XRD results of sample 8Pi.

Following qualitative analysis of the samples in HighScore Plus, quantitative analysis of samples 2I, 8I, 2P, 5P, and 8P were performed using Rietveld refinement in Topas software. Only the *intonaco* and plaster samples were eligible for quantitative analysis as they were prepared in powder form with the addition of 20 wt% zincite internal standard. Figure 25 displays the results for the *intonaco* samples, 2I and 8I.

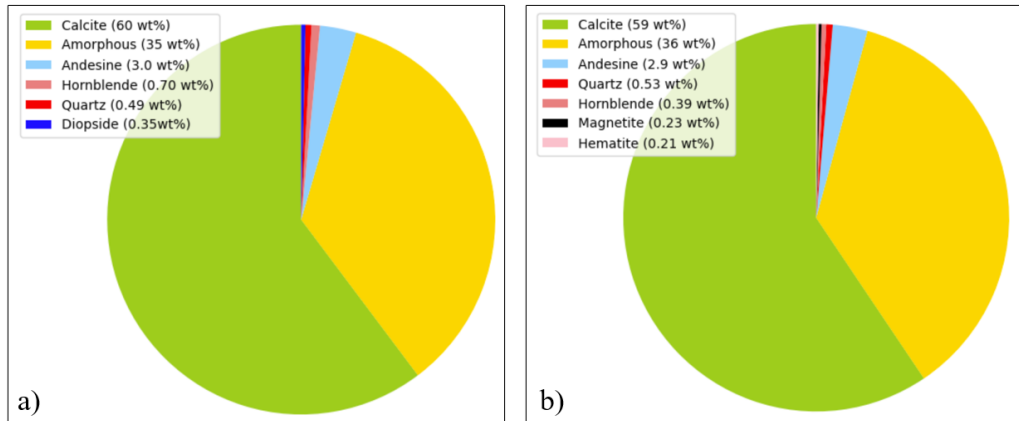


Figure 25: Quantitative results of samples a) 2I and b) 8I.

As can be seen in Figure 25, the *intonaco* samples show a high level of consistency in the proportions of mineral components. Both samples contain approximately 60% calcite, with 2I at 60 wt% and 8I at 59 wt%. The quantity of amorphous component also only differs by one percent between the samples, coming in at 35 and 36 wt% for 2I and 8I respectively. As discussed, the *intonaco* layer at Teotihuacan is known to be a combination of lime-based binder and volcanic glass as aggregate, the latter accounting for the amorphous content. Additional silicate minerals of andesine, hornblende, and quartz again show similar proportions in both samples. Although only two samples are tested here, the precision in ratio of components indicates a strong standardization in production technology. A larger sample size would confirm the breadth of this standardization.

Concerning the base plaster samples, there is slightly more variation in the proportion of components, but overall, the results reveal consistency and standardization of production. Figure 26 shows the quantitative results for samples 2P, 5P, and 8P.

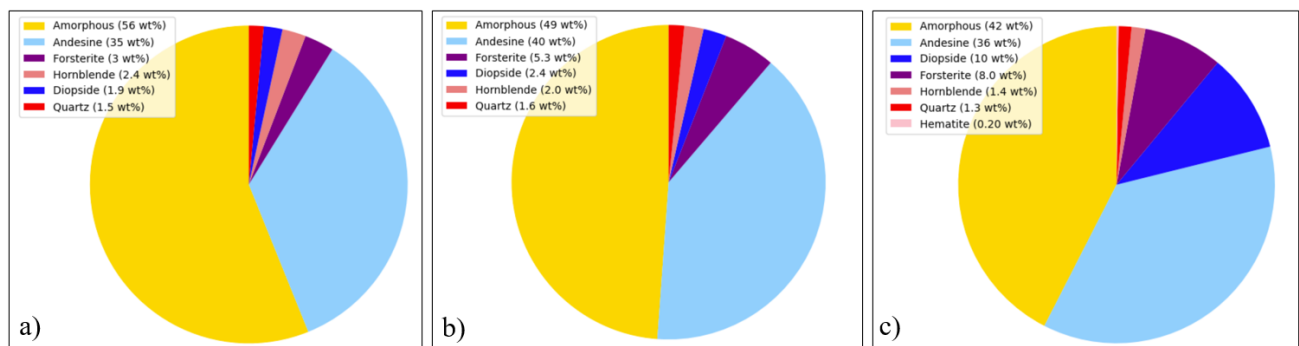


Figure 26: Quantitative results of samples a) 2P, b) 5P, and c) 8P.

The amorphous content ranges between 42-56 wt%, while the content of andesine is approximately 35-40 wt% across all samples. The remaining minerals show relatively small variation, with 8P showing elevated levels of diopside and forsterite.

4.2 Fourier Transform Infrared Spectroscopy (FTIR)

Following the identification of mineral phases via XRD, FTIR spectroscopy was employed to determine information about the possible addition of organic material to the pigment matrices, as well as to potentially characterize the black pigment surfaces of samples 6Pi2 and 7Pi2. The pigment surfaces of samples 2Pi (pink), 6Pi2 (black and red), 7Pi2 (black), and 8Pi (red) were selected for analysis. Challenges arose in the acquisition of data due to experimental limitations – to obtain a usable signal using the Alpha-P compact FTIR spectrometer, as good contact is required between the ATR crystal and the sample surface. Given the small area of the arm of the spectrophotometer and the fragility of some samples, some segmentation of samples occurred under the pressure of the arm. This limited the ability to obtain results from several samples. Of the samples tested, only two meaningful signals were recorded; that of 2Pi and 8Pi, seen in Figure 27.

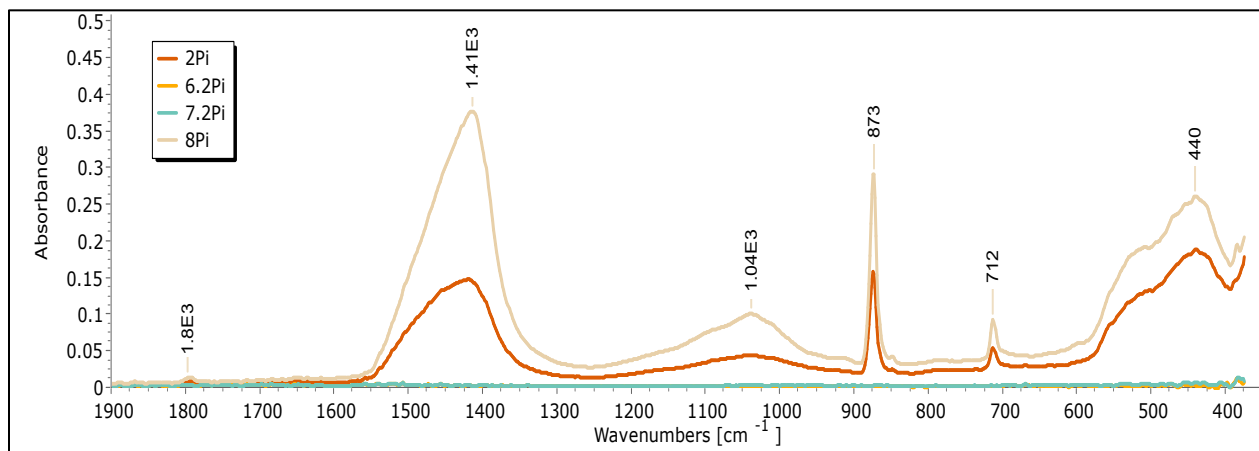


Figure 27: FTIR spectra for samples 2Pi, 6Pi2, 7Pi2, and 8Pi. Samples 6Pi2 and 7Pi2 did not produce meaningful signals, where both 2Pi and 8Pi demonstrate signals corresponding to wood ash.

Through analysis using the Kimmel Center IR Spectra Library, the signals in the spectra of 2Pi and 8Pi were found to correspond that of wood ash. Characteristic peaks at approximately 1410 cm^{-1} , 873 cm^{-1} and 712 cm^{-1} confirm this, with the peak at 1410 cm^{-1} indicative of C-O-C stretching of carbonate group in wood ash (Catauro et al, 2023).

Carbon has previously been identified as a filler in several studies of Teotihuacan pigments, its purpose being to intentionally to create variations in color shades (López-Puértolas et al., 2023; Magaloni, 1996). A 2023 study of pigments from the Quetzalpapalotl Palace, Amanalco neighborhood, and the Tlajinga district in Teotihuacan, found carbon as additive in virtually all samples analyzed, across a pictorial palette of red, pink, orange, yellow and green, and as a primary source of chroma in the blue-grey pigment (López-Puértolas et al., 2023). From this it can be assumed that the presence of wood ash in 2Pi and 8Pi due to its function as a filler in these samples.

Furthermore, carbon was identified in the pigment layer of all samples through micro-Raman and SEM-EDS, suggesting its use as a filler in throughout the samples in this dataset.

Somewhat interestingly, samples 6Pi2 and 7Pi2 are the only two samples of this set with black pigment surfaces, and no discernable FTIR was generated from either sample. As stated, this could be an issue of experimental error given the difficulties of ensuring contact between pigment surfaces and the probe. However, a 2021 study of Teotihuacan pigments was also inconclusive as to the characterization of black pictorial samples, citing that Fiber Optics Reflectance Spectroscopy (FORS) produced no meaningful results for these pigments (Ruvalcaba-Sil et al, 2021).

4.3 Optical microscopy – Polarized light microscopy (PLM)

To discern information about the microstratigraphy of plaster and painted layers of samples 2P, 5P, 2Pi, 6Pi1, 6Pi2, 7Pi1, 7Pi2, and 8Pi, imaging via optical microscopy, or polarized microscopy (PLM) in reflected light was performed. This technique allows for the determination of *secco* versus *fresco* application of *intonaco* and painted layers, as well as the method of preparation of plasters and aggregate. A summary of the features of the stratified samples can be seen in Table 6.

Table 6: Stratified samples and determined features.

| Sample | Layer number | Painting technique | <i>Intonaco</i> thickness (mm) | Pigment layer thickness (μm) |
|--------|--------------|--------------------|--------------------------------|---|
| 2Pi | 3 | secco | 1.3 | 260 |
| 6Pi1 | 3 | fresco | 2.2 | 120 |
| 6Pi2 | 3 | fresco | 2.9 | 63 |
| 7Pi1 | 3 | fresco | 0.91 | 85 |
| 7Pi2 | 3 | fresco | 0.78 | 170 |
| 8Pi | 2 | fresco | 1.2 | 83 |

The *intonaco*, or *enlucido*, layer of mortars used at Teotihuacan is known to be combination of lime-based plaster and rhyolitic volcanic glass shards, where the lower base plaster or *firme* layer is a mixture of mud-based binder and volcanic scoria, called tezontle (Miriello et al, 2021). Figure 28 displays these layers on a reflected light micrograph of the stratigraphy of sample 6Pi1.



Figure 28: Darkfield micrograph in reflected light of sample 6Pi1 in cross-section, indicating the pigment, intonaco, and base plaster layers.

The wall paintings of Teotihuacan were painted using *fresco*, *secco*, and mixed techniques (Argote et al, 2020). *Fresco* is a technique in which pigment suspended in a carbonate binder is applied to wet lime-based mortar, whereas in *secco* applications the painted layer is applied to dry mortar. Mixed techniques have for example been identified in the use of cinnabar pigment, as mercury sulfide is incompatible with *fresco* application, blackening upon interaction with water (Argote et al, 2020).

All samples analyzed except for 2Pi were found to be painted using the *fresco* technique. The identification of *fresco* application can be seen in the intermixing of pigment and *intonaco* layers at their interface, implying application of pigment on wet lime-based mortar, seen in samples 6Pi1, 6Pi2, and 8Pi in Figure 29. Conversely, the interface between pigment and *intonaco* in sample 2Pi shows no mixing of layers but rather a harsh and straight line, indicating *secco* application.

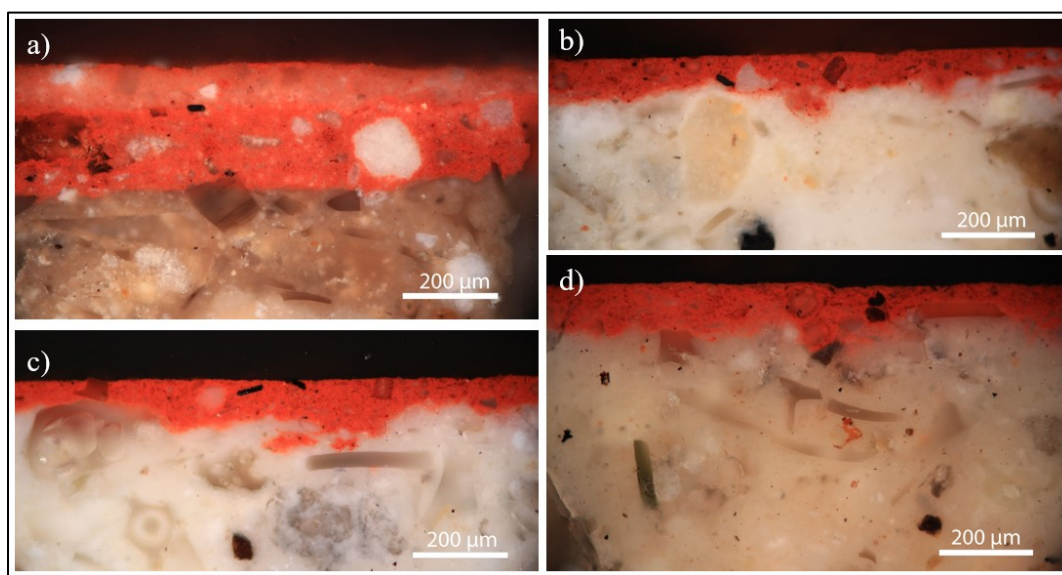


Figure 29: Micrographs of the interface between pigment and intonaco of a) sample 2Pi (*secco* technique) b) sample 6Pi2 (*fresco*) c) sample 6Pi1 (*fresco*) d) sample 8Pi (*fresco*).

Sample 2Pi is also unique of those tested in that there appears to be a distinction between the uppermost section of pigment and the lowermost. Additionally, the painted layer of this sample appears to be significantly thicker than those of the other samples at approximately 260 μm (170 μm for the lowermost layer, 90 μm for the uppermost) compared to 63-170 μm for the other samples. These features can be seen in Figure 30.

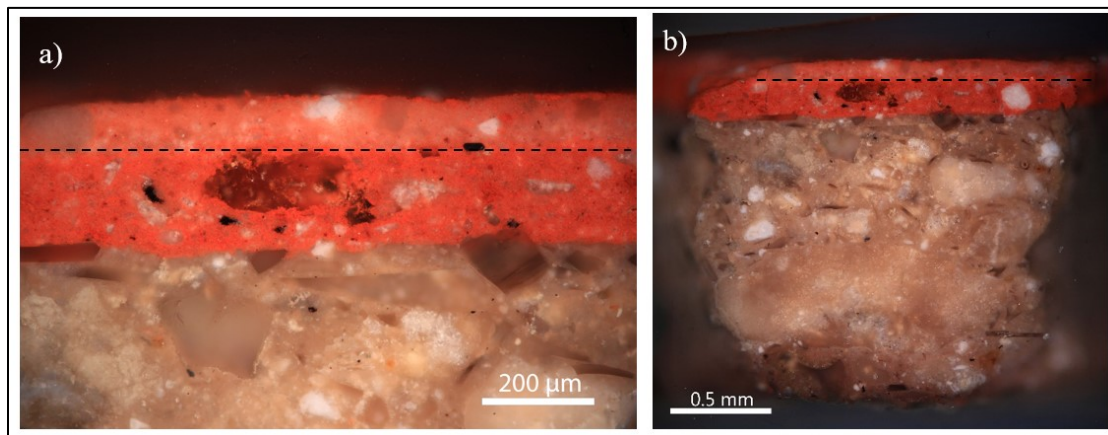


Figure 30: a) Micrograph of sample 2Pi with dotted line indicating the distinction in pigment layer, b) micrograph of sample 2Pi displaying entire cross-section view.

This could be the result of two layers of paint application; a base layer of red and a superficial layer of pink. Micro-Raman analyses also revealed a higher presence of calcite in the upper layer compared to the lower, supporting this hypothesis.

An interesting technological aspect of the wall paintings of Teotihuacan is the artisans' use of additives to produce a sparkling, iridescent effect in the final murals once polished (Ruvalcaba-Sil et al, 2021). Specular hematite is the material most frequently identified in Teotihuacan red pigments for this purpose, and is found in wall paintings throughout the site (López-Puértolas et al, 2023). It is recognized in the pigment layer as black, lamellar inclusions that are larger than the grain size of the matrix; these features indicate a preparation process separate from that of the rest of the pigment material. Figure 31 displays an example of specular hematite particles in the pigment matrix of sample 6Pi1. Other materials that have been identified to be used for this purpose are mica and quartz (López-Puértolas et al, 2023). As mentioned in section 4.1, XRD results revealed the presence of muscovite in samples 6Pi1 and 6Pi2, and quartz in all samples, however these are also accessory components of red ochre. Magnetite was also identified by XRD in the pigment surfaces of samples 2Pi and 8Pi, possibly pointing to the intentional addition of this mineral to again produce a sparkling result.

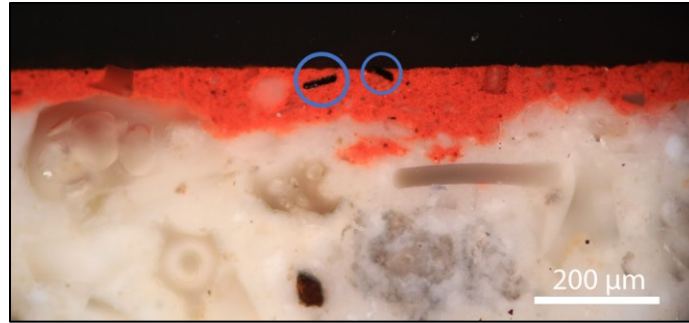


Figure 31: Micrograph of sample 6Pi1 indicating specular hematite and/or magnetite particles in blue circles.

The thickness of the *intonaco* layer varies throughout the tested samples. Sample 6Pi2 was found to have the thickest layer, measuring approximately 2.9 mm, and the thinnest layers were those of 7Pi1 and 7Pi2 measuring about 0.91 mm and 0.78 mm, respectively. Figure 32 displays the micrographs of these sample cross sections, in which the thickness of this layer can be observed.

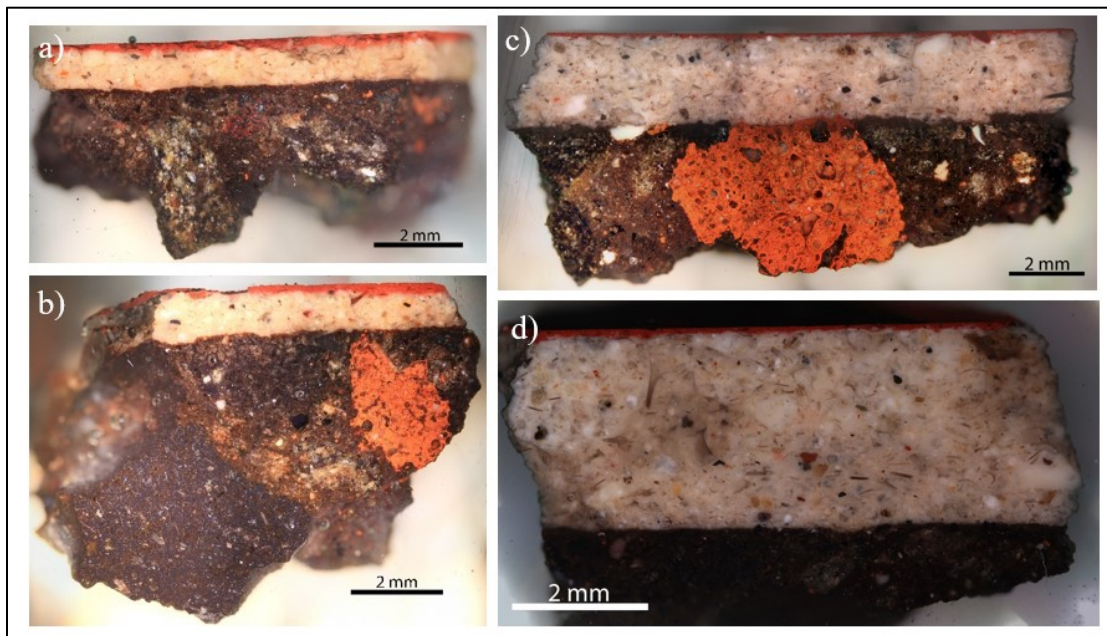


Figure 32: a) Micrograph of sample 7Pi2, b) micrograph of sample 7Pi1, c) micrograph of sample 6Pi1, and d) micrograph of sample 6Pi2.

As mentioned, the *intonaco* layer of Teotihuacan plaster is known to be composed of lime-based mortar and crushed volcanic glass, however the reason for the specific choice of volcanic glass as the aggregate remains unknown.

One hypothesis is that Teotihuacan artisans selected volcanic glass shards to facilitate pozzolanic reactions in the *intonaco* layer, contributing to hydraulicity of the mortars (Secco et al, 2022). As volcanic glass has high silicate and aluminosilicate content, it has the potential to generate pozzolanic reactions when combined with plaster. However, a 2021 study investigating the hydraulicity of lime mortars from the Techinantitla and Plaza de las Columnas compounds in Teotihuacan concluded that the mortars analyzed were in fact hydraulic, but the hydraulicity was

attributed to pozzolanic reactivity of the tezontle in the base plaster, or *firme*, layer and not from the volcanic glass in the *intonaco*, or *enlucido*, layer as originally theorized (Miriello et al, 2021).

It is speculated that Teotihuacan artisans intentionally used a thin *intonaco* layer not only to save lime, as limestone was sourced from the Tula region about 60 km from Teotihuacan, but also to facilitate the migration of chemical elements that enable pozzolanic reactions (Si, Al, Fe) from the tezontle in the lower layer to the upper *intonaco* (Barba et al, 2009; Miriello et al, 2021).

Research on the provenance of glass shards used in this layer have shown that they originate from the Altotonga magmatic system, approximately 120 km from the site of Teotihuacan (Pecci, et al, 2018). Given the lack of relativity of the volcanic shards, theories remain about the reason for their intentional addition to the mortar. The distant place of origin points to a potential ritual or symbolic use of the shards in the *intonaco* layer, however further research is required to confirm any speculation. A depiction of volcanic shards in the *intonaco* and pigment layers of sample 7Pi1 can be seen in Figure 33.

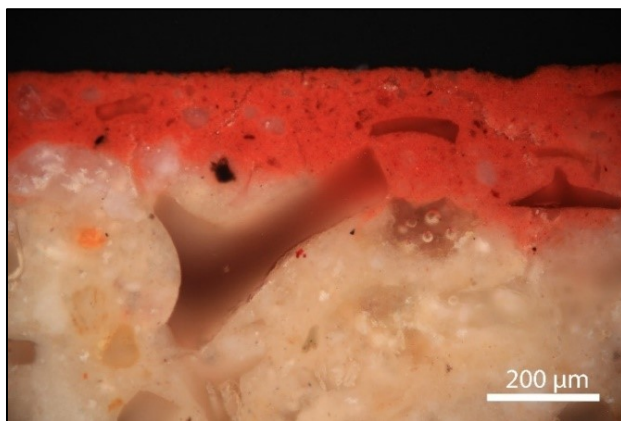


Figure 33: Volcanic glass fragments in the *intonaco* and pigment layers of sample 7Pi1.

Aside from uncertain reactivity or ritual functions of the aggregate, there are features of the volcanic glass shards that may have made them preferable in this application. Favourable properties such as their white color allow them to be added to the plaster without altering color, and the variable grain size, about 20 μm to 1.8 mm, allows for the production of thin mortars using minimal lime (Pecci et al, 2016).

From the Tlamimilolpa (200-350 CE) or perhaps Early Xolalpan (350-450 CE), volcanic glass shards were recognized as the aggregate in lime-based plasters, which continued throughout all technical phases (Magaloni, 1996; Murakami 2010). Of the samples in this dataset, some variations can be observed in the nature and density of volcanic glass aggregate. For example, sample 2Pi seen in Figure 34a) shows rectangular glass fragments characteristic of the third and fourth technical phases outlined by Magaloni (Magaloni, 1996). There is also preferred orientation of the fragments parallel to the pictorial plane, an indication of a smoothed or burnished surface (Pecci et al, 2018).

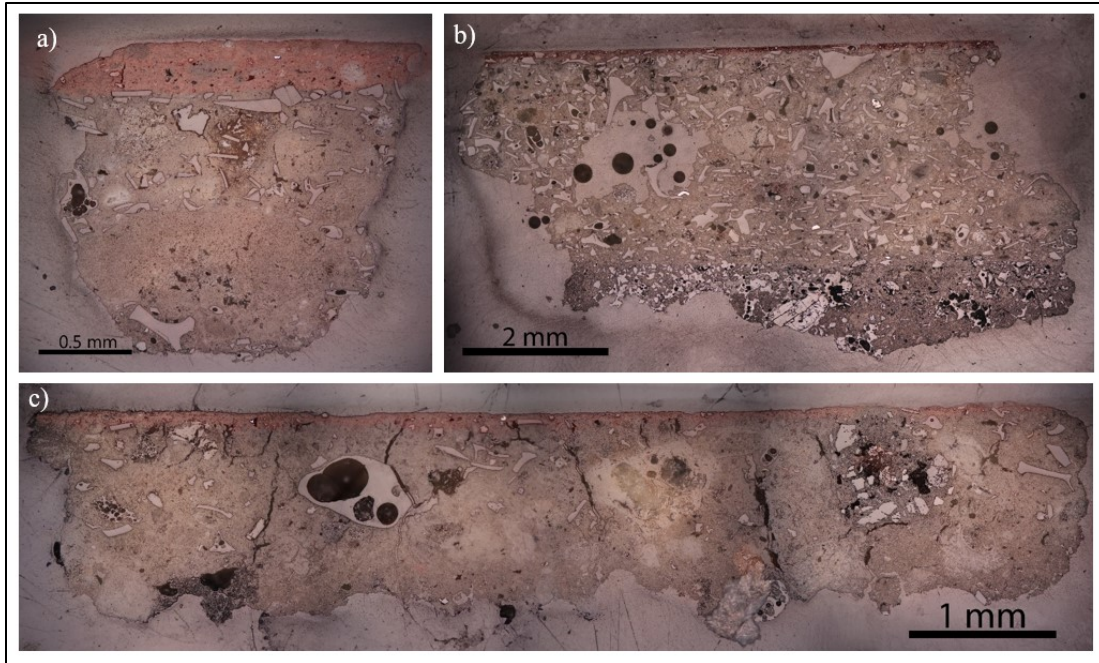


Figure 34: a) Brightfield micrograph in reflected light of sample 2Pi, b) sample 6Pi2, and c) sample 8Pi.

Sample 6Pi2 seen in Figure 34b) shows a varied granulometric size distribution of volcanic shreds in its *intonaco* layer. There is a consistent presence of both curved and rectangular pieces throughout the layer, indicating grinding of the aggregate. A similar style is found in samples 6Pi1, 7Pi1, and 7Pi2.

Conversely, *intonaco* layer of sample 8Pi reveals a different result. There is a minimal presence of glass shreds compared to the other samples studied. There also appears to be diagonal cracking which is not present in other samples, likely a consequence of shrinkage phenomena. Other features of the layer include a large calcite lump and a rock fragment, potentially from the lower base plaster layer or added intentionally to the lime mortar.

The base plaster layer, or *firme*, used in Teotihuacan is known to be a mixture of clayish soil and tezontle. Tezontle is a porous, highly oxidized volcanic rock used in throughout Mexico's construction history. Figure 35 depicts plaster sample 2P, with tezontle fragments indicated in red.

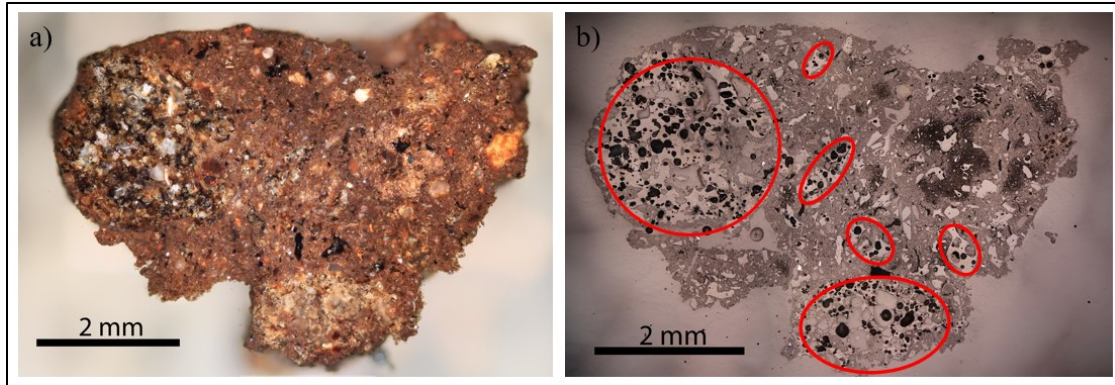


Figure 35: a) Darkfield micrograph of sample 2P, b) brightfield micrograph of sample 2P with tezontle fragments indicated in red.

The combination of clayey soil and tezontle produced a solid base layer upon which the *intonaco* could be applied. This allowed Teotihuacan artisans again to reduce the amount of allochthonous limestone necessary, and make use of abundant, locally available tezontle. As mentioned, the hydraulicity of the *intonaco* could perhaps be attributed to pozzolanic reactions of the tezontle. This theory is further investigated with SEM-EDS and micro-FTIR analyses.

4.4 micro-Raman

To gain insights into the nature of inorganic and organic phases present in the pigment, *intonaco*, and base plaster layers of samples 2Pi, 6Pi1, 6Pi2, 7Pi1, 7Pi2, and 8Pi, analysis using micro-Raman spectroscopy was executed. For sample 2Pi, data points from the pigment layer were collected, for sample 8Pi the majority of data points were collected from the pigment layer with selected points taken in the *intonaco* layer, and for samples 6Pi1, 6Pi2, 7Pi1 and 7Pi2 data points were taken representatively throughout the plaster, *intonaco*, and pigment layers. As samples 2Pi and 8Pi are comprised of only pigment and *intonaco* layers, the remaining samples were selected for data point collection over the entire stratigraphy. The location of data point collection for each sample is summarized in Table 7.

Table 7: Samples analyzed by micro-Raman, with the layers of sampling locations indicated.

| Sample | Pigment | <i>Intonaco</i> | Plaster |
|--------|---------|-----------------|---------|
| 2Pi | x | | |
| 6Pi1 | x | x | x |
| 6Pi2 | x | x | x |
| 7Pi1 | x | x | x |
| 7Pi2 | x | x | x |
| 8Pi | x | x | |

The phases identified are displayed in table 8.

Table 8: Summary of minerals identified using micro-Raman.

| Sample | Cal | Car | Hem | Mag | Diop | Fld | Forst | Qtz | Horn | Apa | Ana |
|--------|-----|-----|-----|-----|------|-----|-------|-----|------|-----|-----|
| 2Pi | x | x | x | | | | | | | | |
| 6Pi1 | x | x | x | x | x | | | | x | | |
| 6Pi2 | x | x | x | x | x | x | x | x | | | |
| 7Pi1 | x | x | x | x | x | x | x | | x | | |
| 7Pi2 | x | x | x | x | | x | | | | x | x |
| 8Pi | x | x | x | x | | x | | x | | | |

*Where Cal: calcite, Car: carbon, Hem: hematite, Mag: magnetite, Diop: diopside, Fld: feldspar, Forst: forsterite, Qtz: quartz, Horn: hornblende, Apa: apatite, Ana: anatase

4.4.1 Pigment layer

First, the results concerning the matrix and additives to the pigment layer across all samples are considered. The pigment matrix mixture remained relatively consistent among all samples, with carbon, calcite, and red ochre detected consistently. Figure 36 displays the results for sample 7Pi2, sampled at three representative points in the pigment layer.

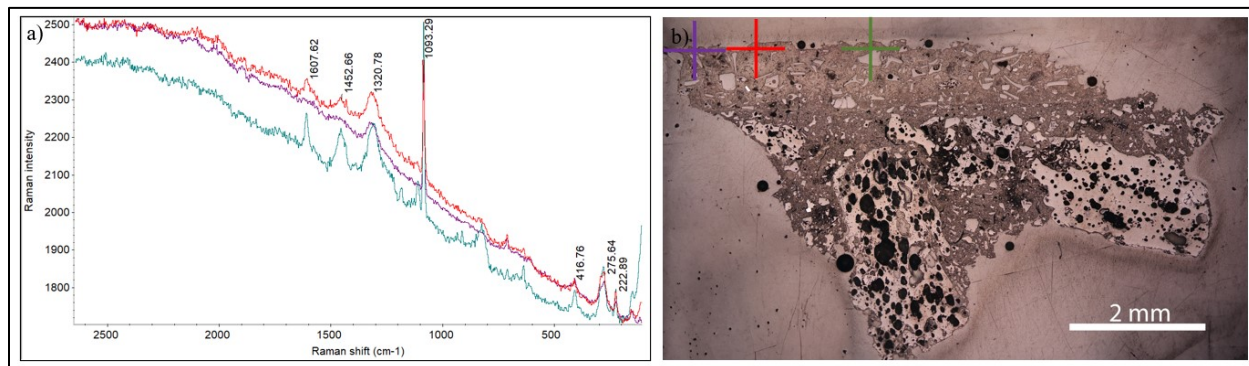


Figure 36: a) Raman spectra of three sampled points in the pigment layer of sample 7Pi2, b) micrograph of samples 7Pi2 indicating sampling locations.

Peaks at approximately 1607 cm⁻¹, 1452 cm⁻¹, and 1320 cm⁻¹ are characteristic of amorphous carbon, with the peak around 1607 cm⁻¹ and representing C=C stretching, and the peak at 1320 cm⁻¹ representing the D band or disorder band of carbon (Casadio et al, 2018; Secco et al, 2021). The peak at 1450 cm⁻¹ is related to trapped hydrocarbons, again indicating the occurrence of organics (Puech et al, 2019; Romero-Sarmiento et al, 2014).

The strong peak at approximately 1090 cm⁻¹ is indicative of calcite, and the smaller wavenumber peaks at 416 cm⁻¹, 275 cm⁻¹, and 220 cm⁻¹ show the presence of red ochre (Marucci et al, 2018; Burgio et al, 2000).

The pigment surface of sample 7Pi2 appears black, but a red underpainting is visible with the naked eye. From previous studies, Teotihuacan black is known to be most commonly charcoal based, and it was anticipated to confirm the presence of carbon particles in the most superficial pigment layer of this sample (López-Puértolas et al, 2023). However, the black layer was unfortunately not observable in this sample cross-section.

Sample 2Pi presents with a light pink pictorial surface, differing from the red (and black) samples studied. As discussed in section 4.3, there appears to be a visual distinction between the upper and lower portions of this pigment layer, perhaps implying separate pigment applications. Figure 37 displays the results of the pigment matrix in the lower and upper regions of the pigment layer, possibly contributing further to this hypothesis.

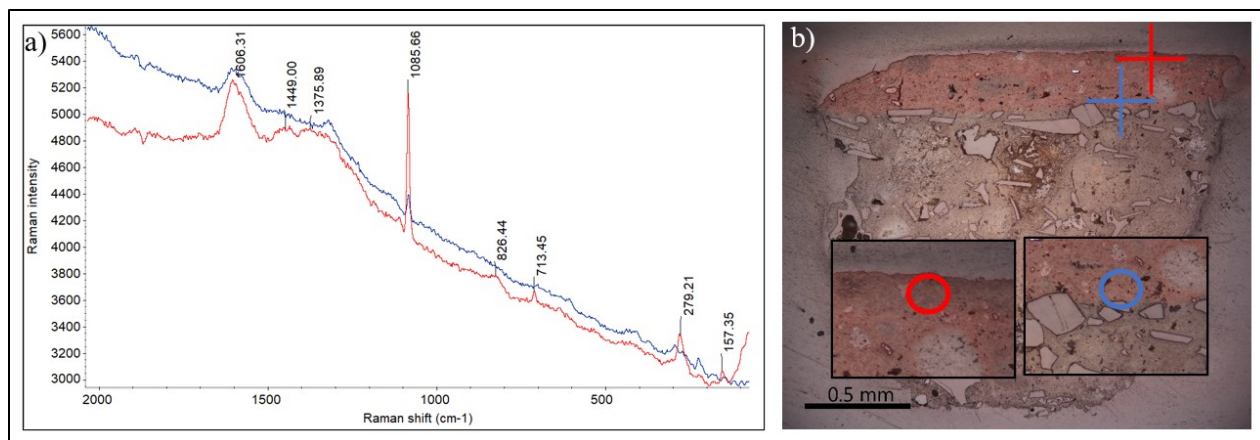


Figure 37: a) Raman spectra of sampled points in the pigment layers of sample 2Pi, indicating the presence of calcite, hematite, and carbon, b) micrograph indicating sampling locations.

A significantly stronger peak of calcite is observed in the upper pigment layer compared to that of the lower pigment layer. As has been previously studied, additional calcite was added to red ochre to produce pink shades in the wall paintings of Teotihuacan.

The presence of specular hematite was confirmed in the pigment layer of this sample (2Pi), as well as in samples 6Pi1, 6Pi2, and 8Pi. Figure 38 depicts the spectra for 2Pi, 6Pi1, and 6Pi2.

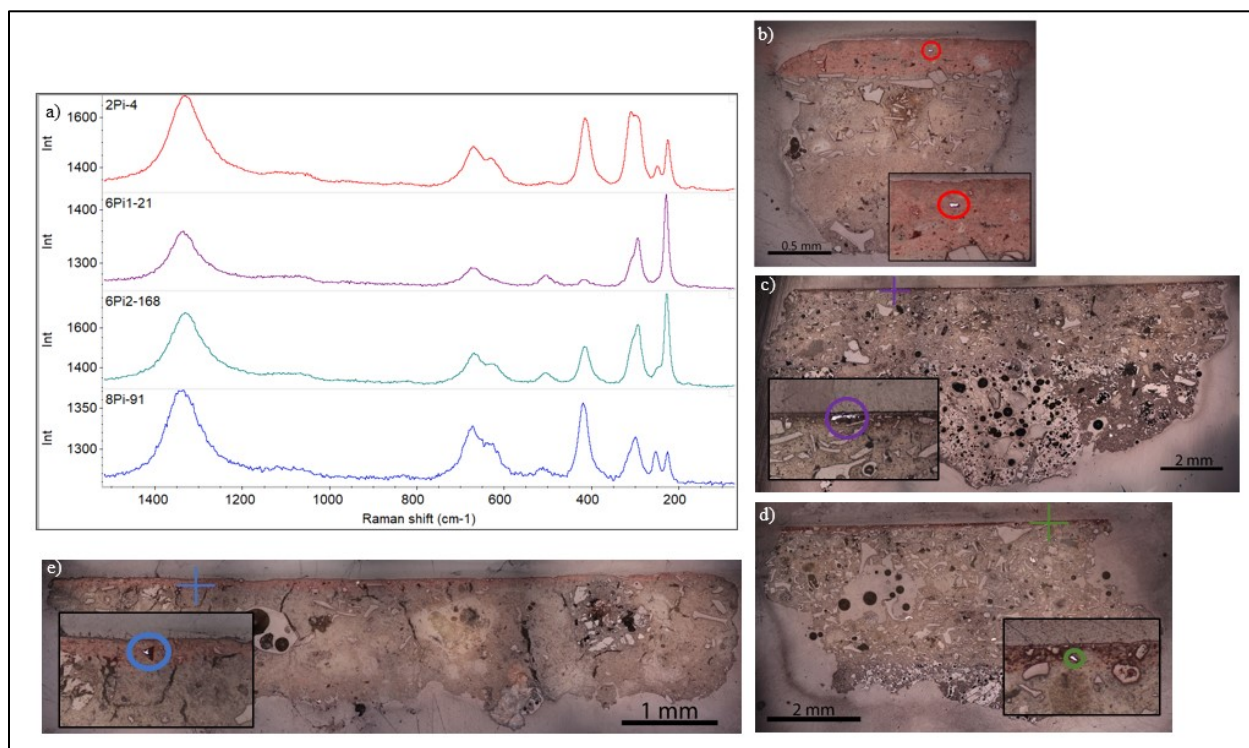


Figure 38: a) Raman spectra of sampled points in samples 2Pi, 6Pi1, 6Pi2, and 8Pi showing signals of hematite, b) micrograph indicating sampled location in sample 2Pi, c) in sample 6Pi1, d) in sample 6Pi, and e) in sample 8Pi.

Through closer examination of the spectrum of sample 8Pi seen in Figure 39, the characteristic bands of hematite can clearly be identified. The strong peak at 1337 cm^{-1} corresponds to the peak of hematite at 1320 cm^{-1} , attributed to the two-magnon scattering that occurs in hematite, but is not observed in other iron oxides such as magnetite (Fe_3O_4) and maghemite ($\gamma\text{-Fe}_2\text{O}_3$) (De Faria et al, 1997). The appearance of low wavenumber peaks, related to Fe-O stretching and bending modes, further confirm the presence of hematite (Secco et al, 2021; Marucci et al, 2018).

It should be noted that the peak at 672 cm^{-1} is an indication of the partial phase transition to magnetite under the power of the laser (Ferreira et al, 2020; Buzgar et al, 2013).

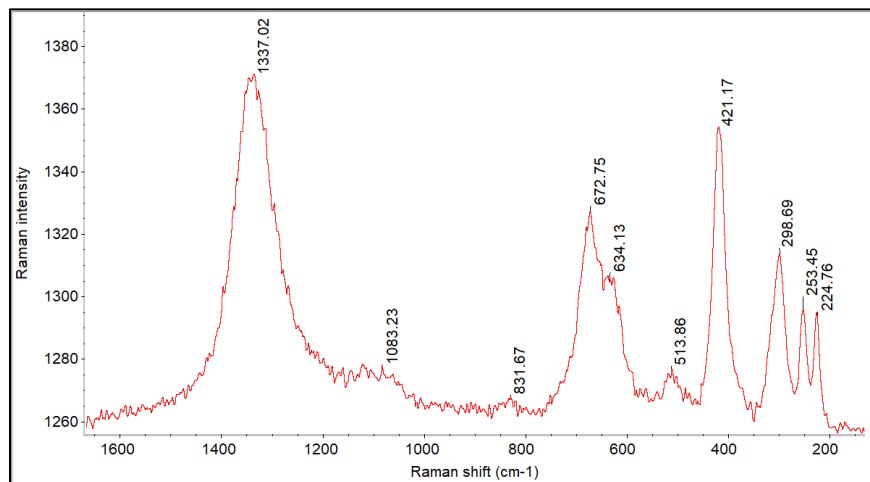


Figure 39: Raman spectrum of sampled point in 8Pi showing peaks of hematite.

As mentioned in section 4.1, quartz is another common additive to pigment compositions in Teotihuacan, used to produce sparkling effect in pink and green colors (López-Puértolas et al, 2023). Its presence was confirmed by micro-Raman in the pigment layers of samples 6Pi2 and 8Pi. Figure 40 displays the spectrum of sample 6Pi2, with clear peaks of quartz at 464 cm^{-1} , 206 cm^{-1} , and 128 cm^{-1} (Lin et al, 2021).

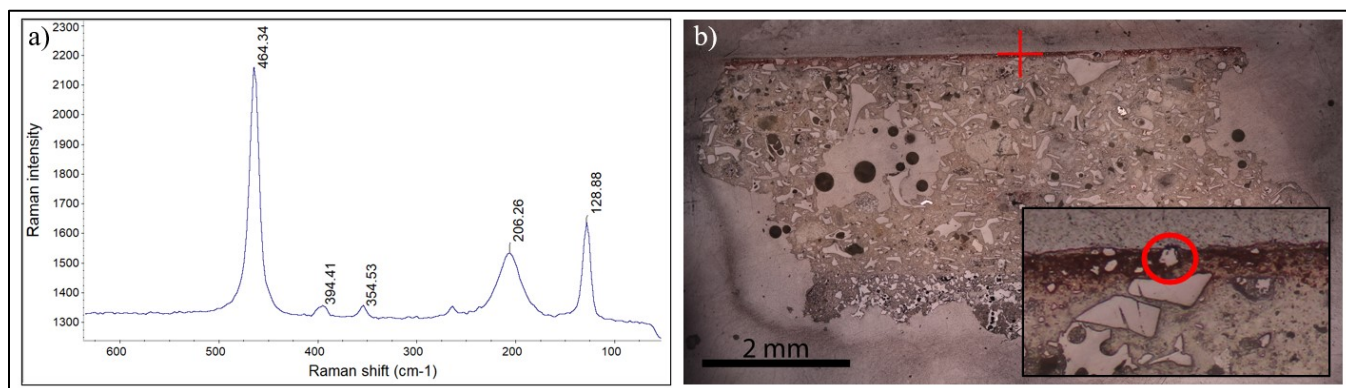


Figure 40: a) Raman spectrum of sampled point in 6Pi2 showing peaks of quartz, b) micrograph of sample 6Pi2 indicating sampled location.

4.4.2 Intonaco layer

The composition of the matrix of *intonaco* layer was found unsurprisingly be composed mainly of calcite. Figure 41 displays the spectra at three representative points for sample 6Pi1, and Figure 42 displays the spectra at two representative points for sample 7Pi1.

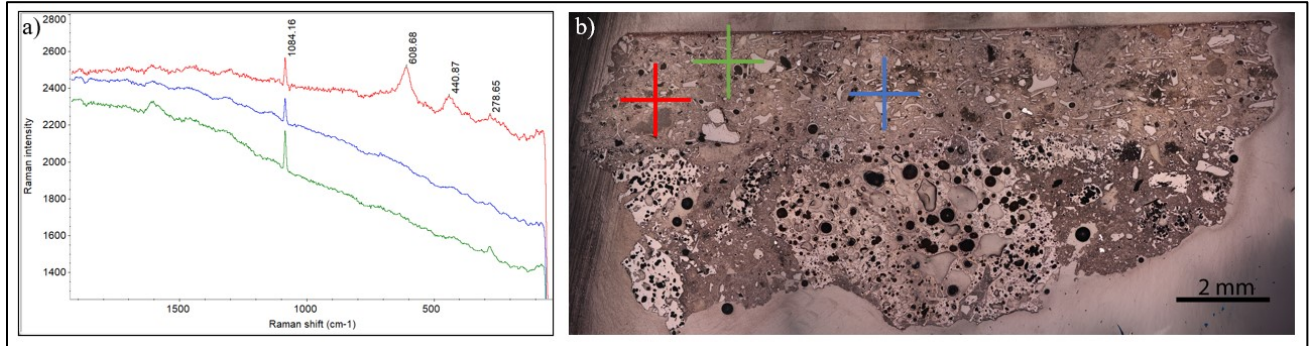


Figure 41: a) Raman spectra of three sampled points in the intonaco layer of 6Pi1, b) micrograph of sample 6Pi1 showing sampled locations.

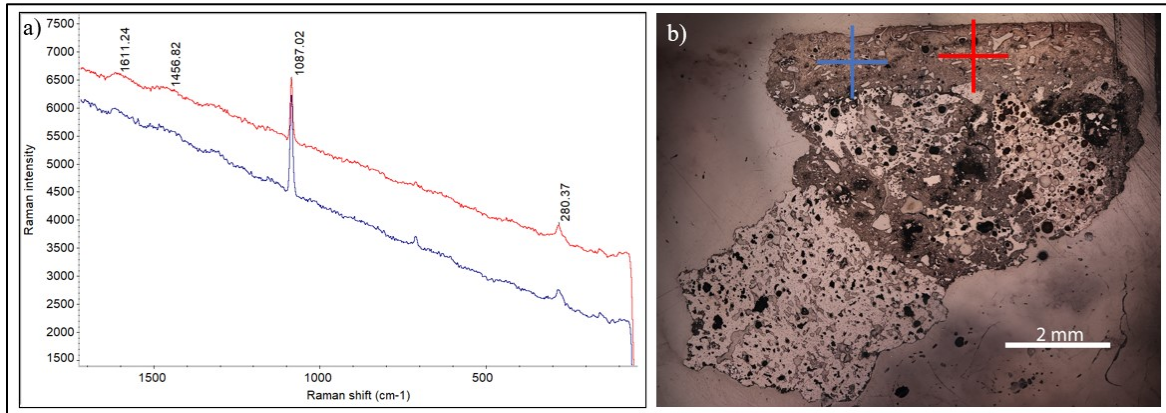


Figure 42: a) Raman spectra of two sampled points in the intonaco layer of 7Pi1, b) micrograph of sample 7Pi1 indicating sampled locations.

The strong peak of calcite at approximately 1085 cm⁻¹ can be seen in all points sampled. There is minimal variation among sampled points, save the presence of peaks at 606 cm⁻¹, 440 cm⁻¹, and 278 cm⁻¹ identified in one sample location of 6Pi2, representing the contribution of an iron oxide. All samples also show small peaks at approximately 1600 cm⁻¹, 1450 cm⁻¹, and 1300 cm⁻¹ indicating the presence of carbon. This is possibly remnant from the firing of limestone in the production process, as has been previously studied in Mesoamerican mortars, or alternatively is a sign of the addition of organic material to the *intonaco* (Ruvalcaba-Sil et al, 2021).

A data point from the *intonaco* layer of sample 7Pi2 reveals the presence of apatite with a strong peak at 961 cm⁻¹, and secondary peaks at 666 cm⁻¹, 533 cm⁻¹, 429 cm⁻¹, 308 cm⁻¹ and 142 cm⁻¹, as well as strong signals of carbon with characteristic peaks at 1605 cm⁻¹ and 1330 cm⁻¹ (Penel et al, 1998).

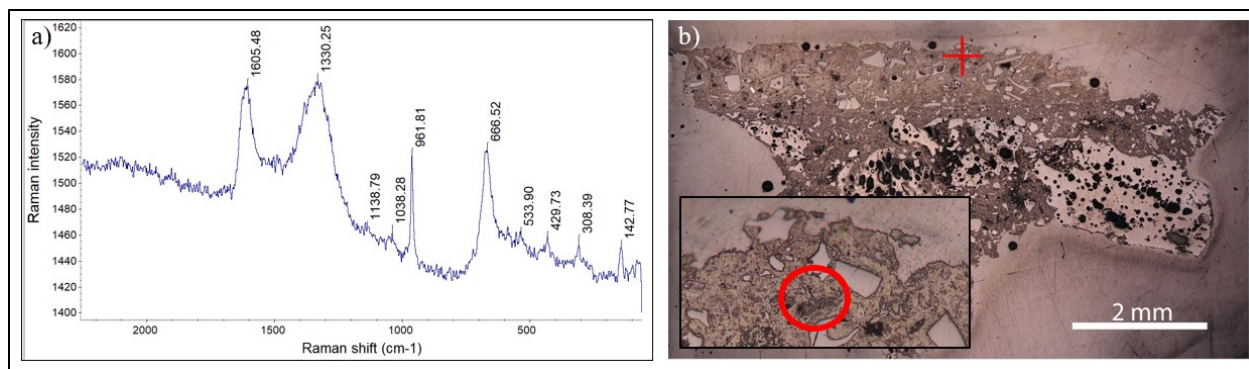


Figure 43: a) Raman spectrum of sampled point in the intonaco layer of sample 7Pi2, showing peaks of carbon and apatite, b) micrograph of sample 7Pi2 indicating sampled location.

The apatite signal detected here is possibly indicative of biological apatite, a calcium phosphate mineral produced in the bone and teeth of vertebrates. The combination of carbon and apatite may point to the use of burnt bone as an additive in this *intonaco* layer. This is the only confirmed identification of apatite in the *intonaco* layer across all samples.

Figure 44 displays three sampled points of *intonaco* aggregate material in sample 6Pi2. Results are comparable, with two data points sharing peaks at approximately 674 cm^{-1} , 578 cm^{-1} , 275 cm^{-1} , 214 cm^{-1} , and 151 cm^{-1} . The other spectrum is similar, with peaks at approximately 674 cm^{-1} , 214 cm^{-1} , and 151 cm^{-1} . As mentioned in the case of hematite, other iron oxides can undergo phase transitions subjected to the power of the laser (Shebanova and Lazor, 2003). The weak and broad peak at 674 cm^{-1} possibly indicates a diminishing signal of magnetite, where the appearance of peaks at 275 cm^{-1} and 214 cm^{-1} represents an increasing hematite signal (Shebanova and Lazor, 2003).

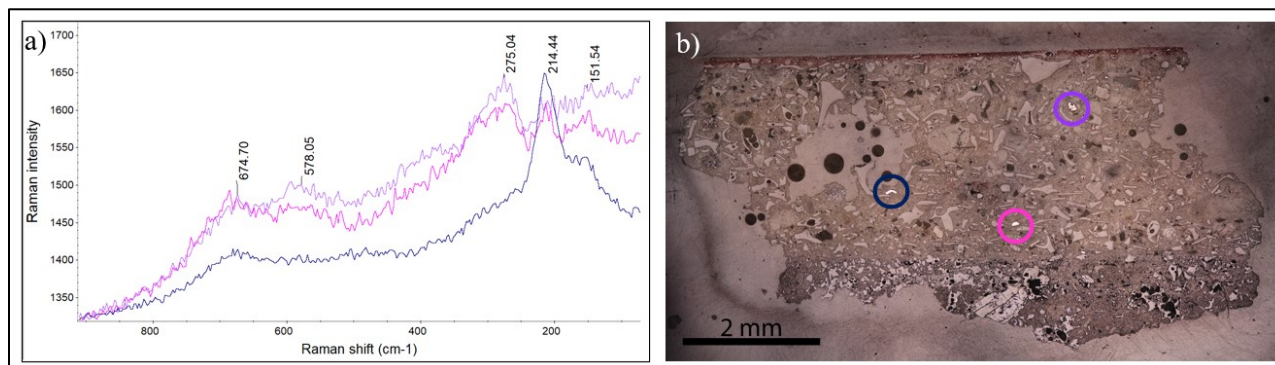


Figure 44: a) Raman spectra of three sampled points in the intonaco layer of sample 6Pi2, b) micrograph of sample 6Pi2 indicating sampled locations.

Two sampled points in the aggregate of sample 8Pi reveal indicative signals of hematite and another iron oxide. Hematite is clearly identified with characteristic peaks at 1318 cm^{-1} , 507 cm^{-1} , 409 cm^{-1} , 293 cm^{-1} , and 226 cm^{-1} , where the other iron oxide, possibly magnetite, is distinguished by peaks at 667 cm^{-1} and 461 cm^{-1} . Both hematite and magnetite were identified by XRPD in the *intonaco* layer of this sample, aligning with the results seen here via micro-Raman.

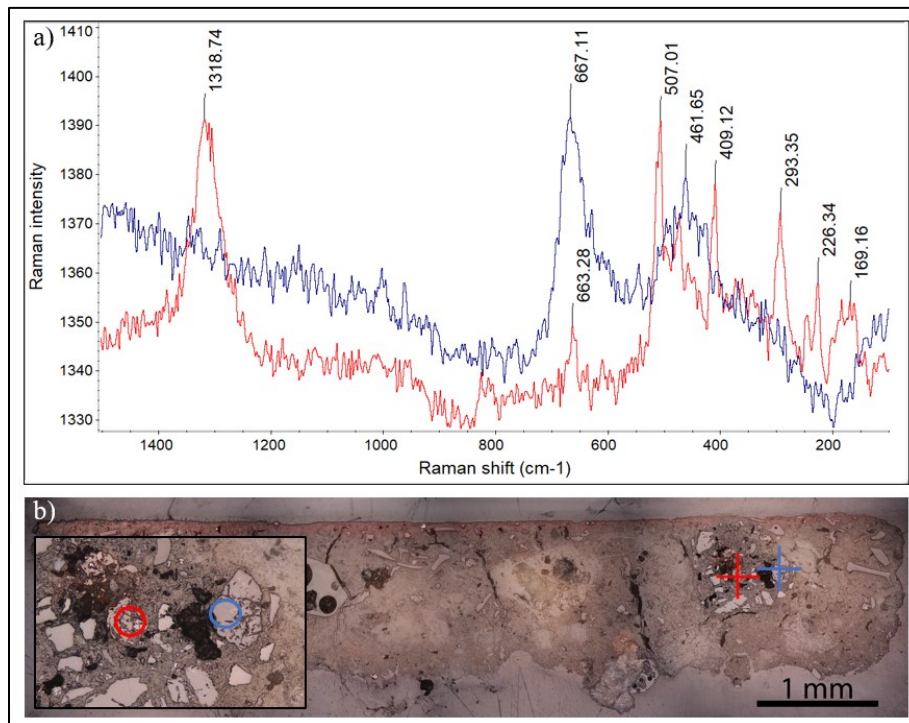


Figure 45: a) Raman spectra of two sampled points in the aggregate of the intonaco layer of sample 8Pi, b) micrograph sample 8Pi indicating sampled locations.

4.4.3 Base plaster layer

The matrix of the base plaster layer of sample 6Pi1 was sampled at four representative points, seen in Figure 46. The spectra show strong similarity, with consistent peaks at 1605 cm^{-1} , representing C=C stretching. Aside from a small peak of calcite that can be observed in one spectrum at 1081 cm^{-1} , the signals are virtually identical. This result may point to the utilization of some kind of organic binder intermixed with the mud-based one to enhance the cohesive properties of the plaster.

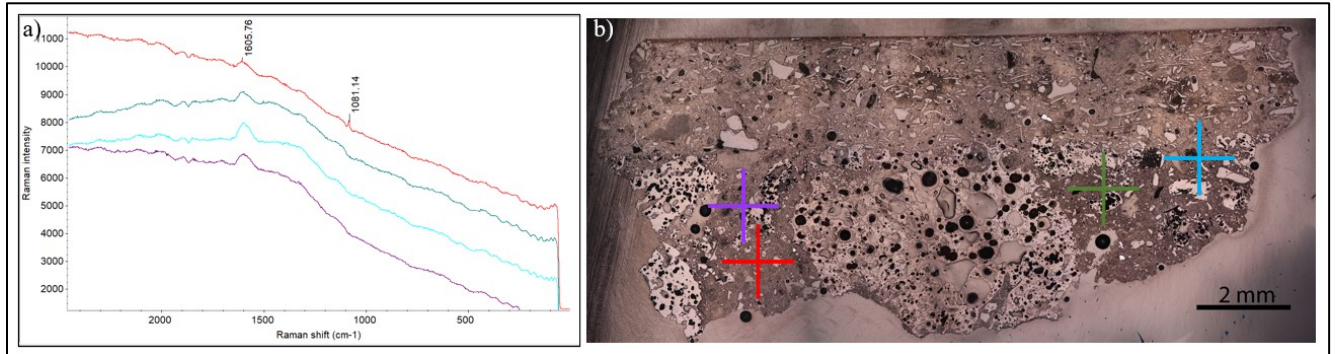


Figure 46: a) Raman spectra of four sampled points in the matrix of the base plaster layer of sample 6Pi1, b) micrograph of sample 6Pi1 showing sampled locations.

A sampled point from the base plaster matrix of 7Pi2 reveals signals of carbon (1552 cm^{-1} , 1453 cm^{-1} , and 1303 cm^{-1}), as well as anatase (TiO_2), with peaks at 638 cm^{-1} , 512 cm^{-1} , 396 cm^{-1} and a strong peak at 145 cm^{-1} (El-Deen et al, 2018). The presence of anatase here is likely related to its association with iron ores.

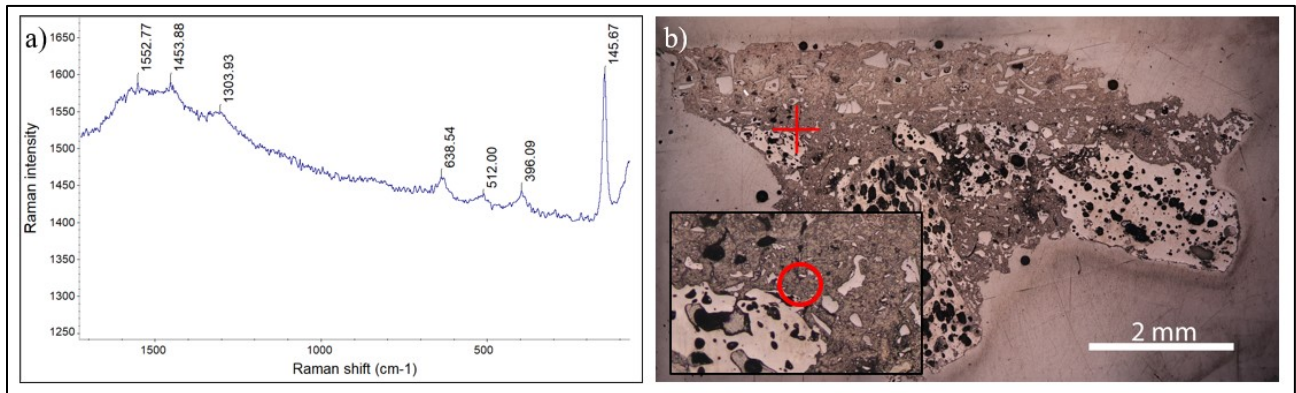


Figure 47: a) Raman spectrum of sampled point in the base plaster layer of sample 7Pi2 showing peaks of carbon and anatase, b) micrograph of sample 7Pi2 showing sampled location.

Representative points taken in the aggregate of sample 6Pi2 and 7Pi1 show the consistent signal of plagioclase feldspar. Characteristic peaks at 506 cm^{-1} and 483 cm^{-1} point to possible identification of labradorite (Buzgar et al, 2013).

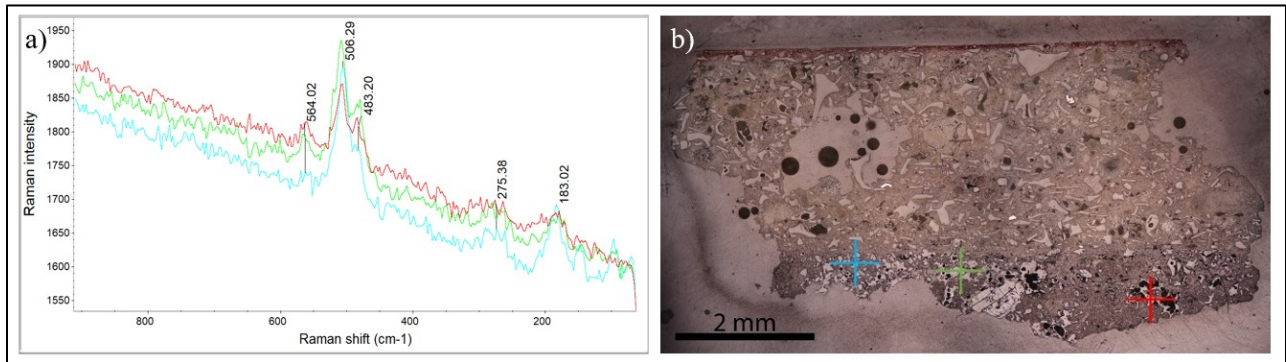


Figure 48: a) Raman spectra of three sampled points in the aggregate of sample 6Pi2 showing peaks of plagioclase feldspar; b) micrograph of sample 6Pi2 indicating sampled locations.

Similarly in sample 7Pi1, the peaks 507 cm^{-1} and 480 cm^{-1} clearly indicate the presence of plagioclase feldspar, possibly labradorite or andesine as concluded by XRPD. Two sampled points also show strong peaks at 664 cm^{-1} , with one showing a weaker peak at this wavelength, perhaps indicating Si-O-Si stretching (Buzgar et al, 2013). These findings confirm the identifications determined by XRPD.

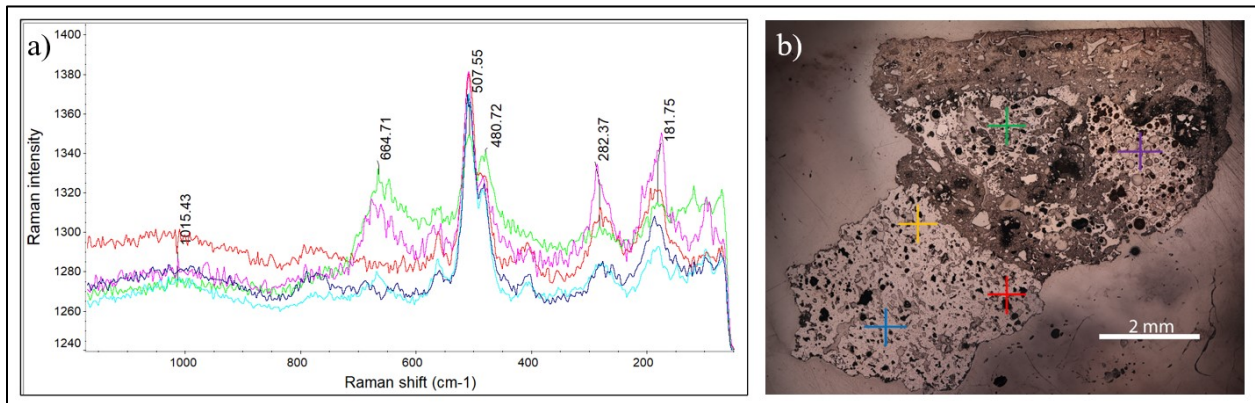


Figure 49: a) Raman spectra of five sampled points in the aggregate of sample 7Pi1 showing peaks of plagioclase feldspar; b) micrograph of sample 7Pi1 indicating sampled locations.

Continuing with the analysis of aggregate of samples 6Pi2 and 7Pi1, the identification of forsterite and hornblende minerals in the base plaster layer are confirmed with micro-Raman. Figure 50 displays the spectrum of a sampled point in the aggregate of sample 6Pi2, clearly displaying peaks of forsterite with strong peaks at 854 cm^{-1} and 823 cm^{-1} due to symmetric and asymmetric vibrations of SiO_4 (Kuebler et al, 2005).

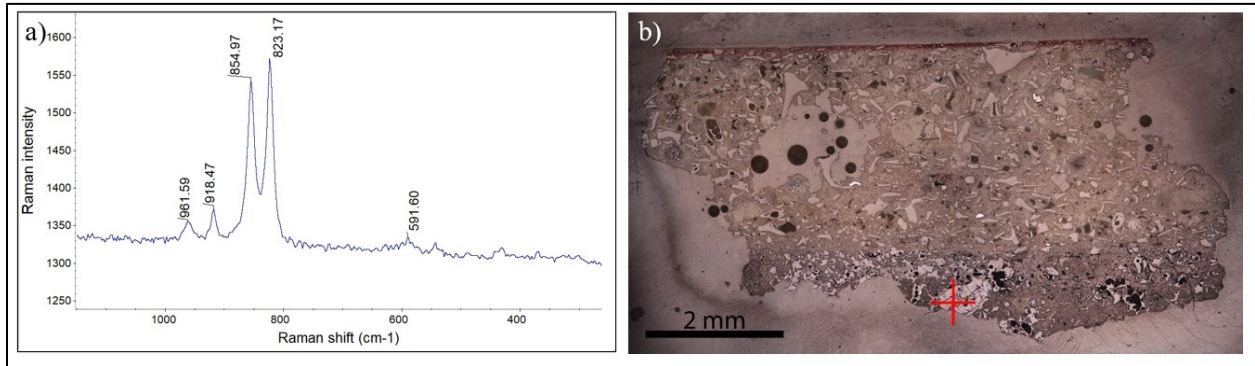


Figure 50: Raman spectrum of sampled point in the aggregate of the base plaster layer of sample 6Pi2 showing peaks of forsterite, b) micrograph of sample 6Pi2 indicating sampled location.

Similarly, the signals of hornblende minerals are identified in both the aggregate of the base plaster and in the *intonaco* layer of sample 7Pi1, pictured in Figure 51. Characteristic peaks at approximately 673 cm^{-1} (symmetric stretching of Si-O-Si) and 1056 cm^{-1} (asymmetric stretching of Si-O-Si) confirm this (Buzgar et al, 2013). There is slight discrepancy between the two spectra, with one displaying additional peaks at 747 cm^{-1} and 544 cm^{-1} . This suggests the presence of two different hornblende minerals, possibly actinolite and tremolite.

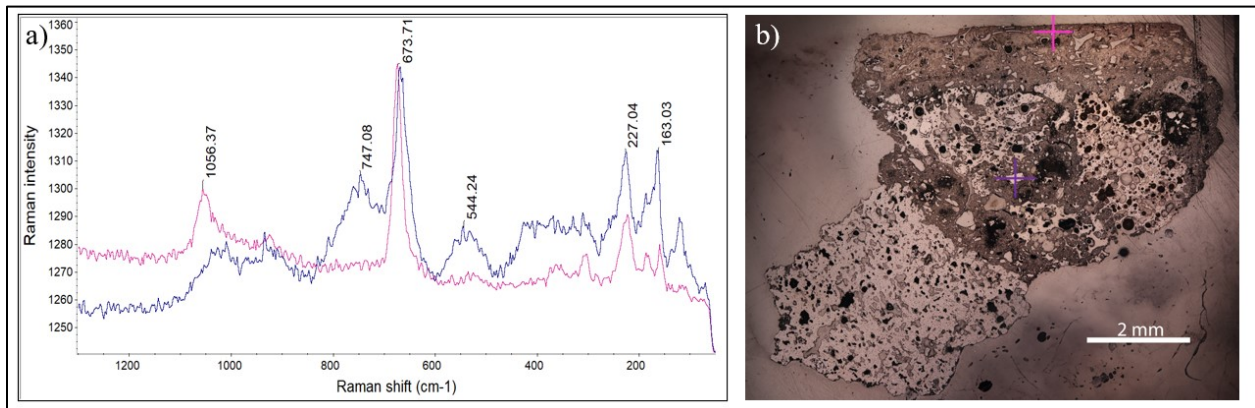


Figure 51: a) Raman spectra of two sampled points sample 7Pi1 showing peaks of hornblende, b) micrograph of sample 7Pi1 indicating sampled locations.

4.5 Scanning Electron Microscopy – Energy Dispersive X-Ray Spectroscopy (SEM-EDS)

SEM-EDS microchemical mapping was performed for samples 2Pi, 6Pi1, 6Pi2, 7Pi1, and 7Pi2 to investigate the nature of the interaction between matrices and aggregates, as well as to gain information about the interfaces of layers. EDS point analyses were executed for these samples as well as sample 8Pi to determine the elemental composition of selected areas of interest, such as inclusions in the pigment layers, the volcanic glass, tezontle, and matrices.

Figure 52 displays the microchemical maps taken at the interfaces between pigment layer and *intonaco* for samples 2Pi, 6Pi1, 6Pi2, and 7Pi1. The *intonaco* layer unsurprisingly is dominated by calcium due to the lime binder, where the volcanic glass aggregate is composed primarily of aluminosilicates.

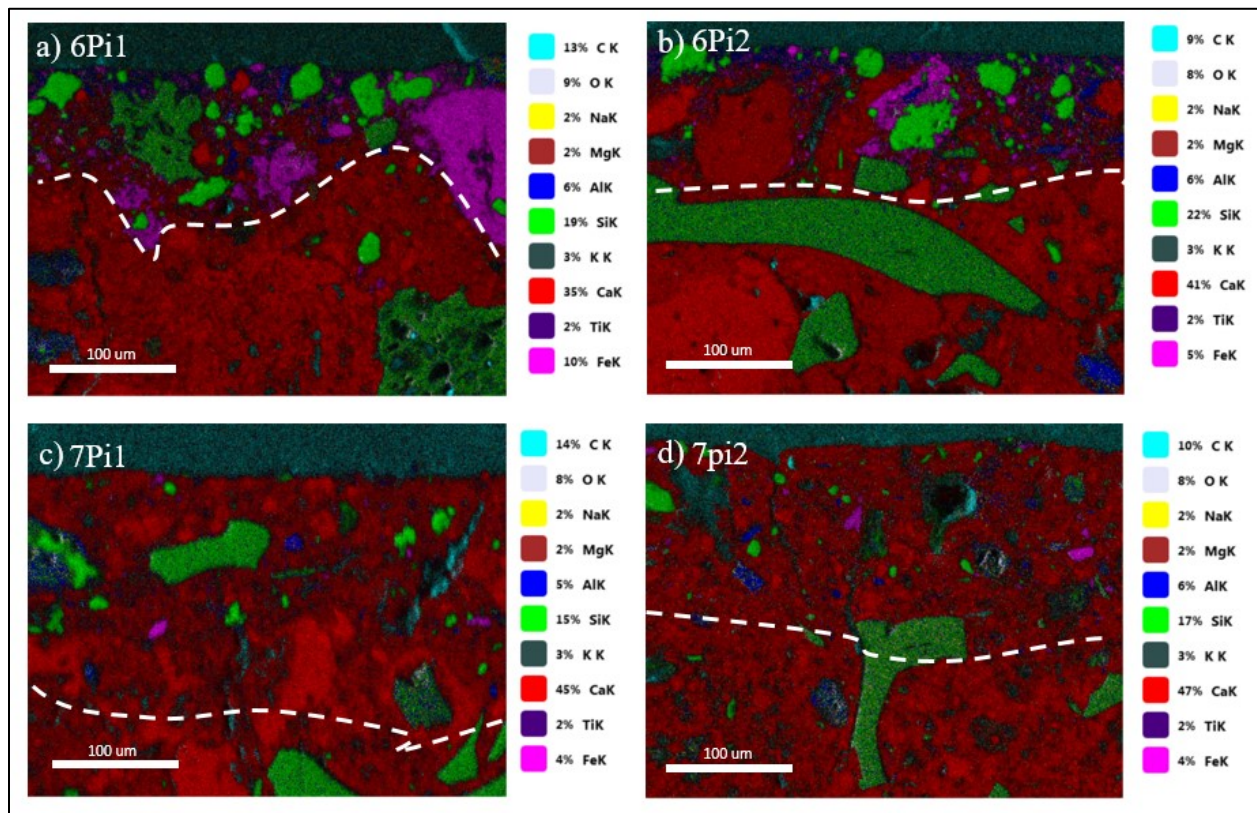


Figure 52: Microchemical maps of the interface between pigment and intonaco layers of a) sample 6Pi1 b) sample 6Pi2, c) sample 7Pi1, and d) sample 7Pi2. White dotted line marks the approximate interface boundary.

In the areas analyzed, samples 6Pi1 and 6Pi2 reveal an elevated presence of silicate components of similar shape and size, as well as elevated iron and aluminum in their pigment layers compared to the other samples. The mapping of sample 2Pi, pictured in Figure 53, reveals a dominance of calcium throughout the pictorial and *intonaco* layers, and a limited amount of iron in the uppermost pigment layer. As this sample presents with a pink uppermost pigment layer and a red underpainting, these results confirm that the color difference is due to higher levels of iron oxides in the lower pigment layer.

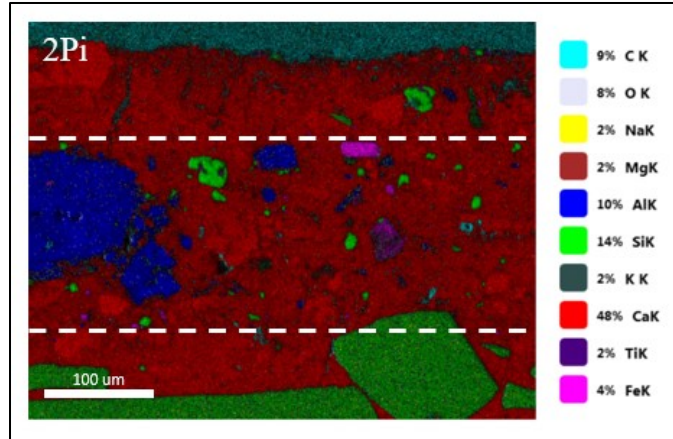


Figure 53: Microchemical map of sample 2Pi pigment and intonaco interface. White dotted lines display interface boundaries.

Figure 54 displays microchemical maps of samples 6Pi2, 7Pi1, and 7Pi2 at the interfaces between the *intonaco* and base plaster layers, with 6Pi1 displaying an area entirely of base plaster.

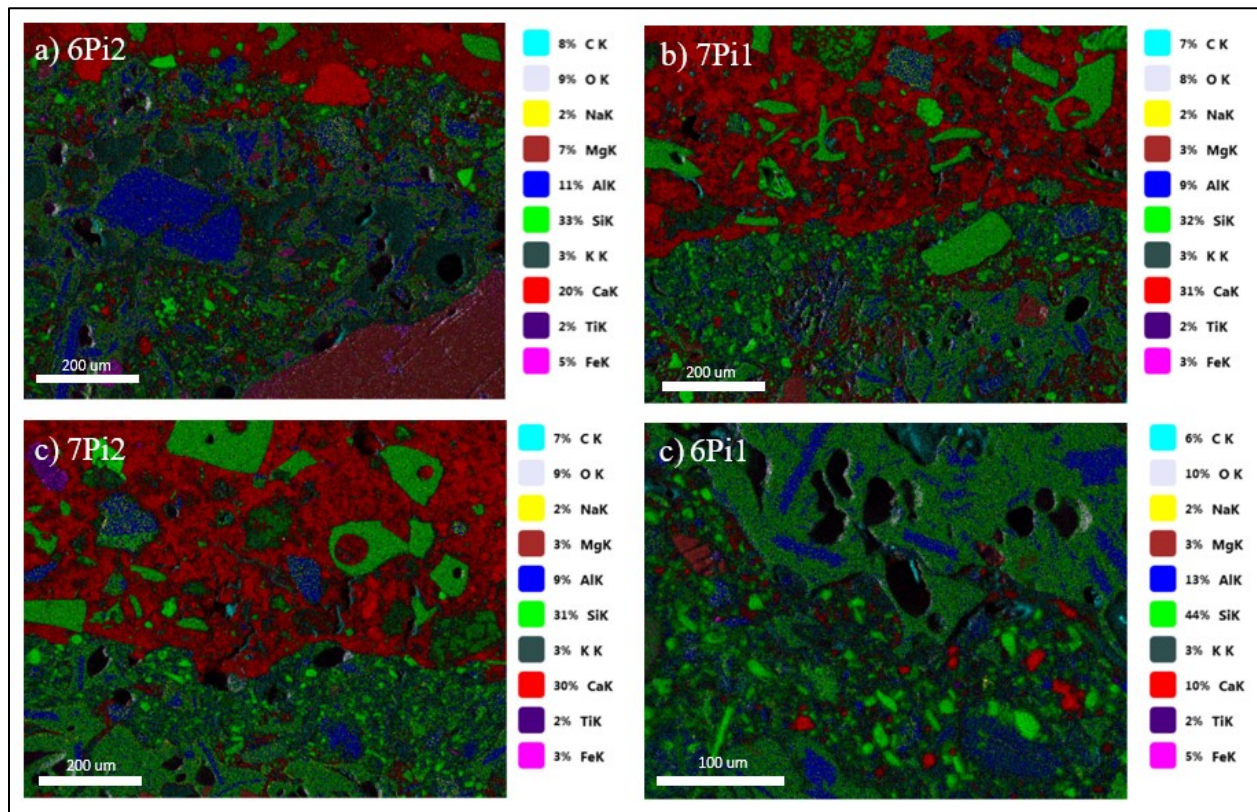


Figure 54: a) Microchemical maps of the interface between intonaco and plaster layer of a) sample 6Pi2, b) sample 7Pi1, c) sample 7Pi2, and d) microchemical map of base plaster layer of sample 6Pi1 featuring tezontle and matrix.

Interestingly, reaction rims are not observed on either the volcanic glass aggregate in the *intonaco* layer, or the tezontle in the base plaster layer. The potential hydraulicity of mortars produced in Teotihuacan is uncertain, however there has been some evidence of pozzolanic activity. In the 2021 paper by Miriello et al, a reaction rim was observed on a tezontle fragment present in the base

plaster layer of a wall painting sample, evidenced by an increase in silicon at the border of a tezontle fragment (Miriello et al, 2021). The results of the microchemical maps produced in this study do not reveal an increase in silicon around volcanic aggregates, suggesting little if any pozzolanic activity of the plaster layers.

In the absence of these reactions, questions about the strength and durability of these mortars remain. As previously postulated and studied, organic additives may play a significant role in contributing to the quality of Mesoamerican mortars. Through the results of micro-Raman analyses, amorphous carbon was identified in the matrices of the *intonaco* layer across all samples; SEM-EDS microchemical maps also reveal the presence of carbon in the *intonaco* layers, seen in Figure 55.

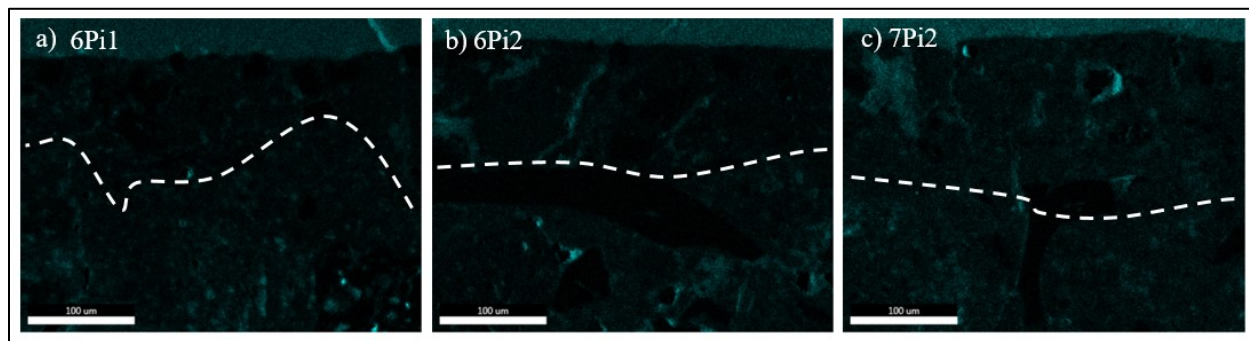


Figure 55: Microchemical maps displaying the presence of carbon (teal) in the *intonaco* and pigment layers of a) sample 6Pi1, b) sample 6Pi2, and c) sample 7Pi2.

The area percentage of carbon at the pigment/*intonaco* interface ranges between 9-14 % for the samples tested. These combined results suggest either a contribution of charcoal from the firing process of the limestone, or the intentional addition of organic additives in the *intonaco* mortar layer. In the case of sample 7Pi2 the combined presence of carbon and apatite was also identified in the *intonaco* layer, perhaps signaling the addition of burnt bone. Further study is required to confirm and characterize the nature of organics in this layer.

Additional investigation using EDS point analysis was used to reveal the elemental composition of matrix and aggregate components of the pigment layers. Figure 56 displays a backscattered electron (BSE) image of sample 6Pi1 and the resulting spectra at three sampled points. These results show a superficial component with a strong signal of carbon and silicon, as well as an iron oxide inclusion, likely specular hematite, or magnetite. The matrix is composed primarily of iron, silicon, aluminum, oxygen, and carbon, indicating red ochre. The presence of these elements is unsurprisingly relatively consistent across the pictorial layers of all samples. There is a low amount of calcium detected in this matrix region, indicating possibly a small contribution of lime binder.

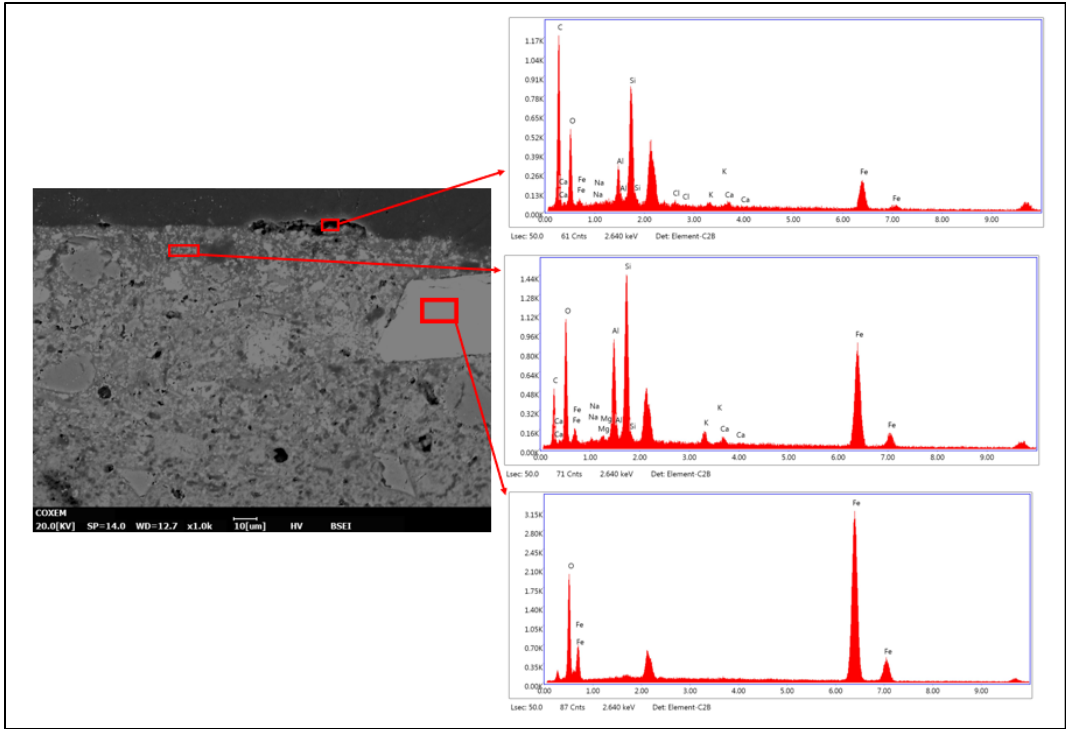


Figure 56: BSE image of sample 6Pi1 indicating three points sampled with EDS, and the resulting spectra.

On the superficial pictorial layer of sample 2Pi, there is the identification of an aluminosilicate mineral, seen in Figure 57. A sampled point in the matrix at the base of the pigment layer again reveals the presence of red ochre, with an elevated signal of aluminum. The aluminum detected here may be due to the presence of aluminum-containing minerals present in red ochre, such as muscovite or kaolinite.

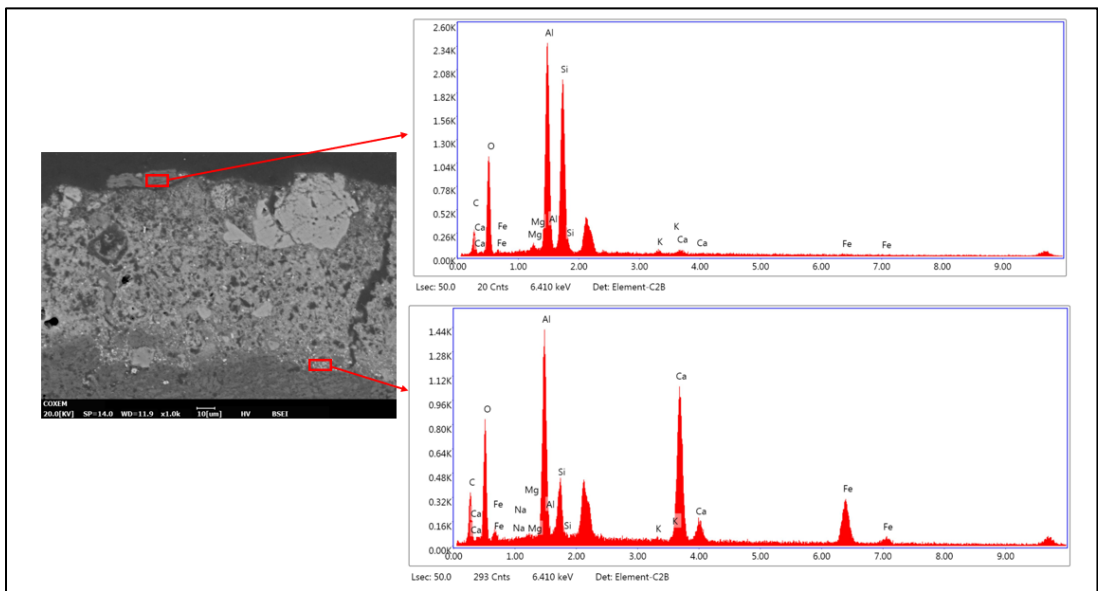


Figure 57: BSE image of sample 2Pi indicating two points sampled with EDS, and the resulting spectra.

Figure 58 displays two sampled areas in the pigment layer of 8Pi. The spectrum of one of the particles distributed in the matrix reveals its identity as an iron oxide, again likely hematite. The matrix again shows elements relating to red ochre, with a strong presence of aluminum, similar to that identified in 2Pi, with a more intense peak of iron.

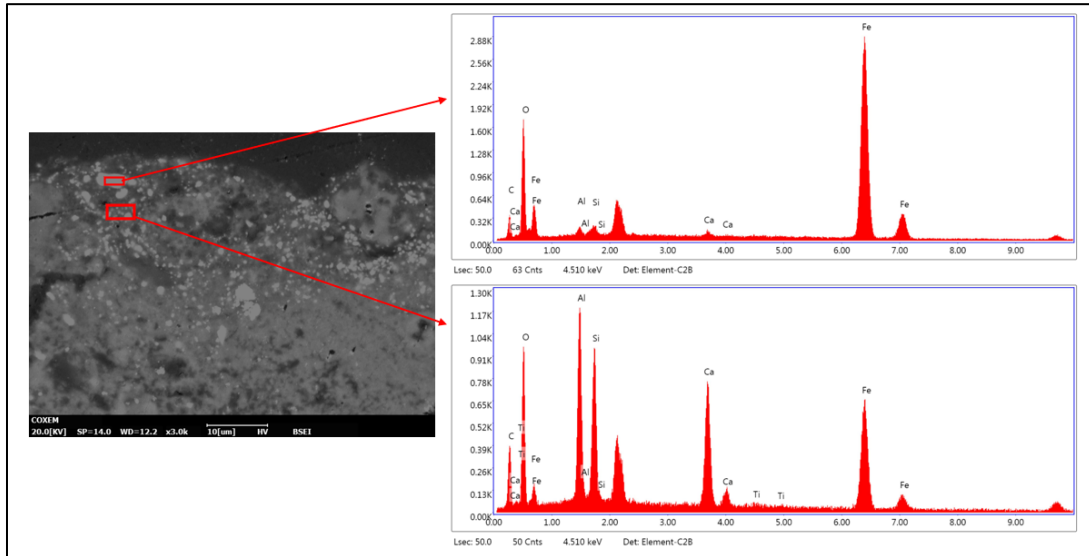


Figure 58: BSE image of sample 8Pi indicating two points sampled with EDS, and the resulting spectra .

A particle of charcoal is identified by a strong signal of carbon and smaller peak of oxygen in the pigment layer of sample 7Pi1, seen in Figure 59. This confirms the use of carbon as an additive in the pigment layer of this sample, as also identified in micro-Raman. An iron oxide inclusion is again identified here, as is consistently detected in all samples.

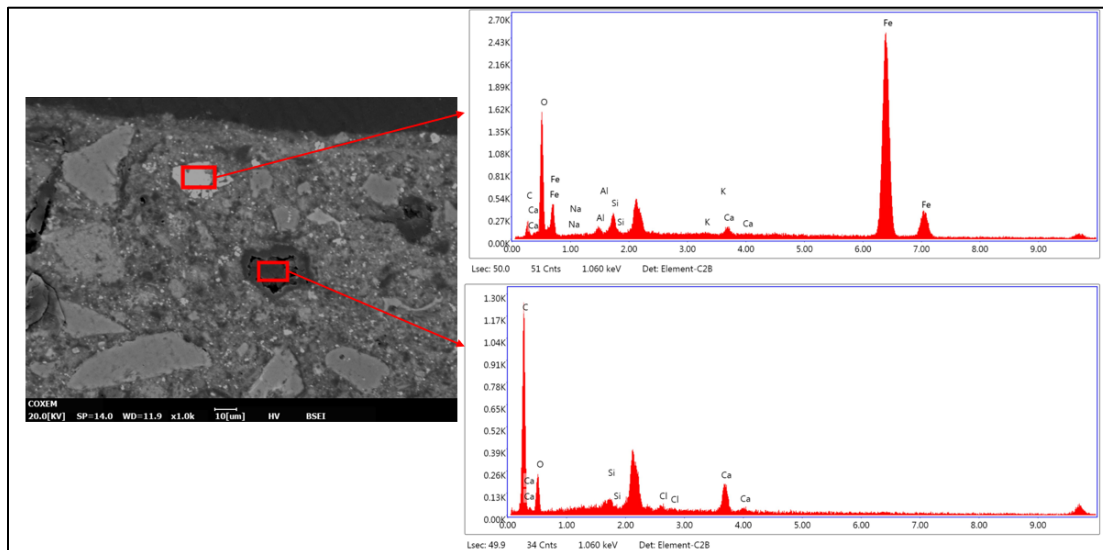


Figure 59: BSE image of sample 7Pi1 indicating two points sampled with EDS, and the resulting spectra.

A strong peak of carbon is identified in the superficial pigment layers of all samples; examples of spectra from samples 8Pi and 7Pi2 can be seen in Figure 60. This demonstrates the prevalence of carbon in the matrix of the pigment layers, specifically in the most superficial portion of the layer.

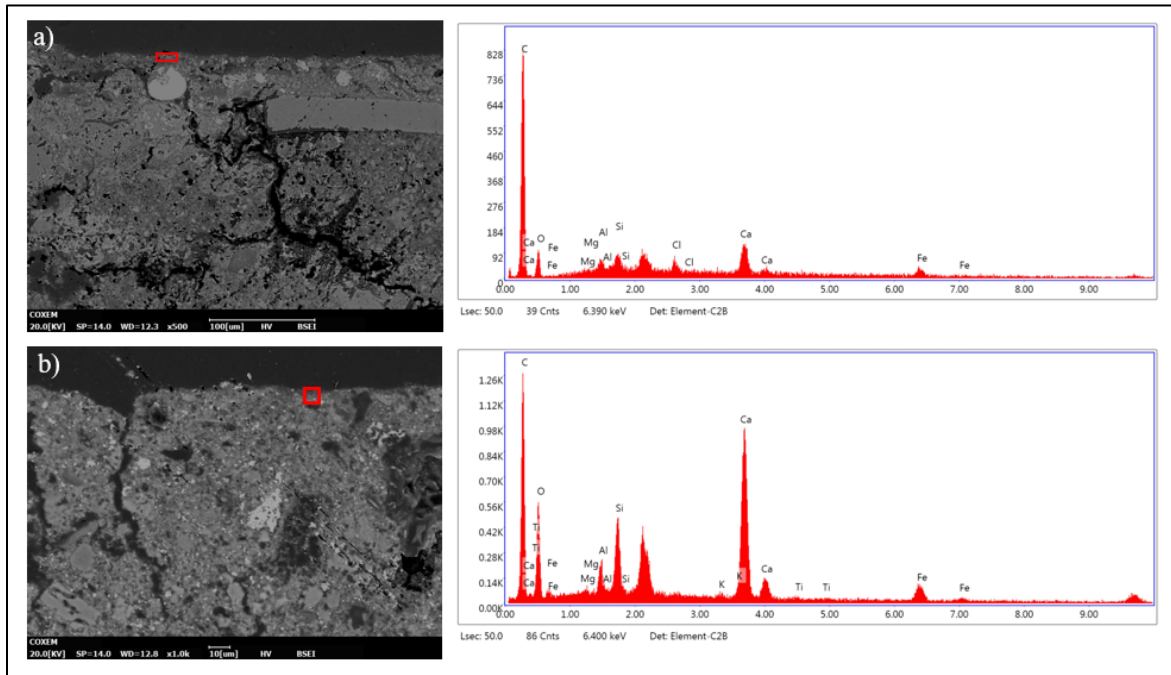


Figure 60: a) BSE image of sample 8Pi indicating point sampled with EDS, and the resulting spectrum, b) BSE image of sample 7Pi2 indicating point sampled with EDS, and the resulting spectrum.

Figure 61 displays the results of two sampled points in the *intonaco* and base plaster of sample 6Pi2. Strong peaks of titanium, iron, and oxygen suggest the presence of ilmenite (FeTiO_3), also identified in sample 6Pi1, and 7Pi2. Ilmenite was identified in a group of red pigment samples from the Xalla palatial complex at Teotihuacan; however, in this study ilmenite was only identified in the plaster layers, and absent in the pigment layers (López-Puértolas et al, 2020).

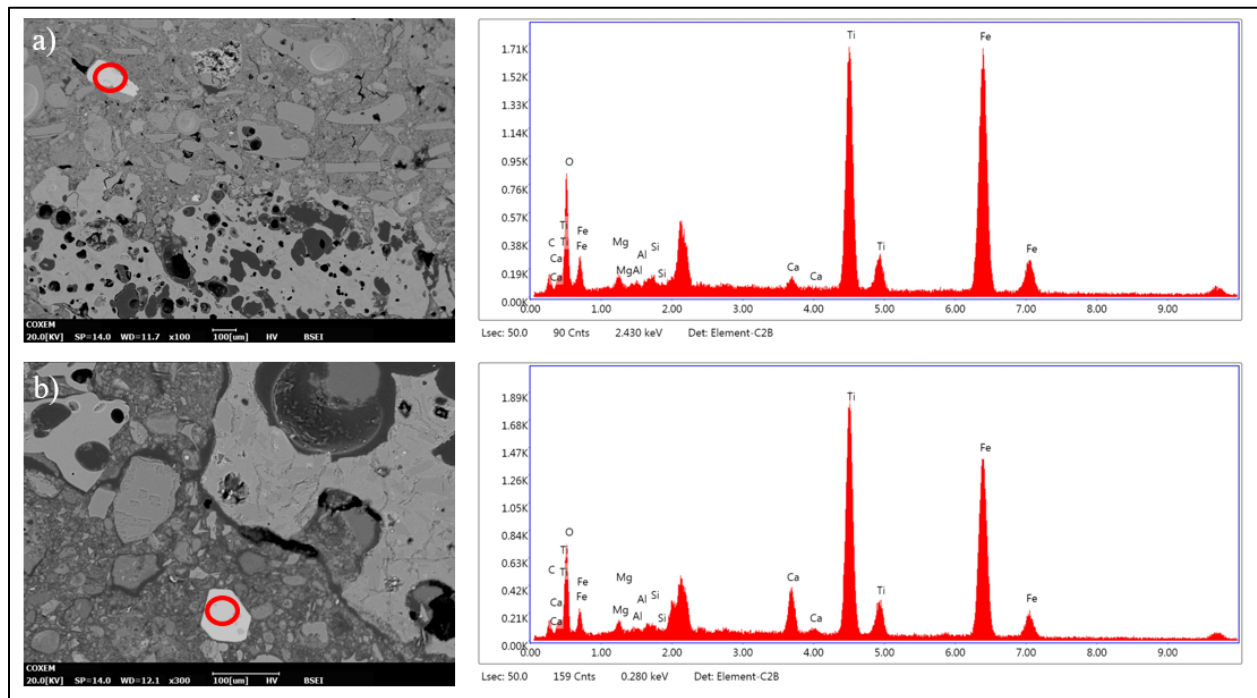


Figure 61: a) BSE image of intonaco /tezonite in sample 6Pi1 indicating point sampled with EDS, and the resulting spectrum showing elements consistent with ilmenite, b) BSE image of base plaster layer in sample 6Pi1 indicating point sampled with EDS, and the resulting spectrum showing elements consistent with ilmenite.

Figure 62 displays the EDS spectrum and sampled location of a point in the base plaster layer of sample 7Pi2. The combined presence of phosphorous, calcium, and oxygen point to the identification of apatite, the sole case of discovery via SEM-EDS among all samples. This result, combined with the detection of apatite in the *intonaco* layer of this sample via micro-Raman, provides further evidence of the intentional addition of burnt bone to the plaster layers of this sample.

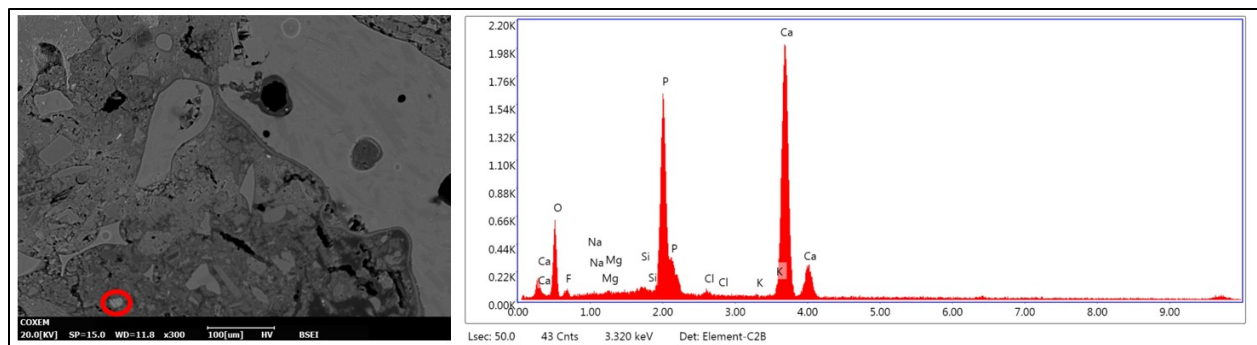


Figure 62: BSE image of sample 7Pi2 indicating point sampled with EDS, and the resulting spectrum showing elements consistent with apatite.

Overall, the results of EDS point analyses confirm the presence of red ochre in the pigment layer of all samples studied, while also providing BSE imaging of this layer at a higher magnitude than seen in the optical microscopy micrographs, seen for example in Figure 58. Additives such as specular hematite and carbon were also confirmed and visualized via BSE imaging. Concerning the base plaster layer, ilmenite was discovered in three samples, which had not previously been identified by other methods. Identification of an apatite mineral in the base plaster of 7Pi2 provides additional evidence for the use of burnt bone in the plaster and *intonaco* layers of this sample.

4.6 micro-FTIR

Micro-FTIR analyses were performed on samples 6Pi2 and 7Pi2, courtesy of Giulia Ricci. Mapping was completed for an area 1000 x 1600 μm covering the *intonaco* and base plaster layers of sample 6Pi2, and an area of 600 x 6400 μm spanning the pigment layer of sample 7Pi2.

Figure 63 displays the integration map of peaks pertaining to silicates, along with the micro-FTIR spectra of three sampled points in the matrix and aggregate of the *intonaco* and base plaster. The peaks used for integration are highlighted in orange.

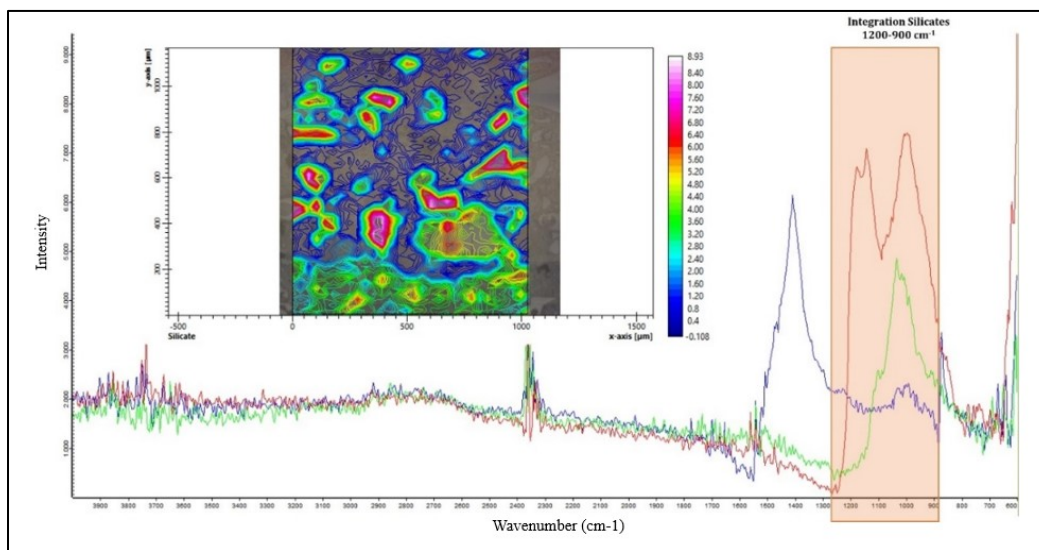


Figure 63: FTIR spectra of three representative points in the matrix and aggregate of the *intonaco* and base plaster, and integration map of the main peaks related to silicates, sample 7Pi2 (provided by Giulia Ricci).

The band between 1080 and 800 cm^{-1} is attributed to stretching vibrations of the Si-O-Al bond, denoting the presence of aluminosilicates (Ellerbrock et al, 2022). Referring to results obtained from XRPD and micro-Raman, these could correspond to plagioclase feldspars such as labradorite or andesine, or perhaps hornblende minerals in the volcanic glass. Peaks in the range 1300-1080 cm^{-1} are due to asymmetric Si-O-Si stretching, indicating amorphous silica (Ellerbrock et al, 2022).

Silicate minerals unsurprisingly represent a high concentration in the aggregate of the *intonaco*, and the distribution of aggregate pieces in the matrix can be clearly observed. When performing separate integrations over each of the peak relating to silicates, differences in the distributions of

these minerals can be observed. Figure 64 displays the results of the integration maps for the peaks in the range 1300-1080 cm^{-1} , and 1080-800 cm^{-1} , highlighted in red and green respectively.

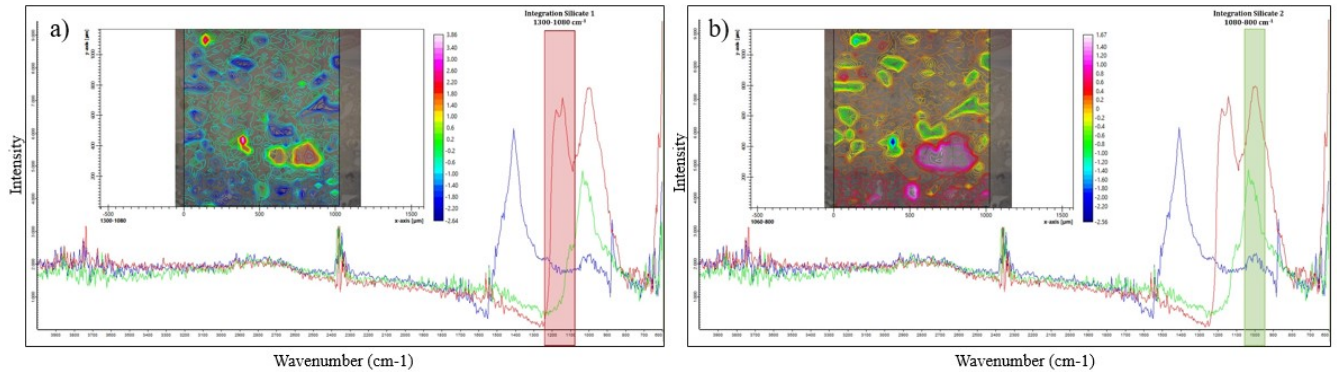


Figure 64: a) FTIR spectra of three sampled points, and integration map of peak of silicates in the range 1300-1080 cm^{-1} , (“silicate 1”), sample 7Pi2. b) FTIR spectra of three sampled points and integration map of peak of silicates in the range 1080-800 cm^{-1} , (“silicate 2”), sample 7Pi2 (provided by Giulia Ricci).

The integration of “silicate 1”, corresponding to asymmetric Si-O-Si stretching, reveals limited presence in the aggregate fragments corresponding to volcanic glass, with a few pieces of aggregate revealing a strong concentration. Conversely, the integration of “silicate 2”, corresponding to Si-O-Al bond vibrations, shows higher presence in the volcanic glass fragments. There also appears to be a relatively high concentration of this band in the matrix of the base plaster layer of this sample.

Figure 65 displays the integration map of the main peak of calcite, along with the micro-FTIR spectra of three sampled points in the matrix and aggregate of the *intonaco* and base plaster. Integrated peaks are highlighted in blue.

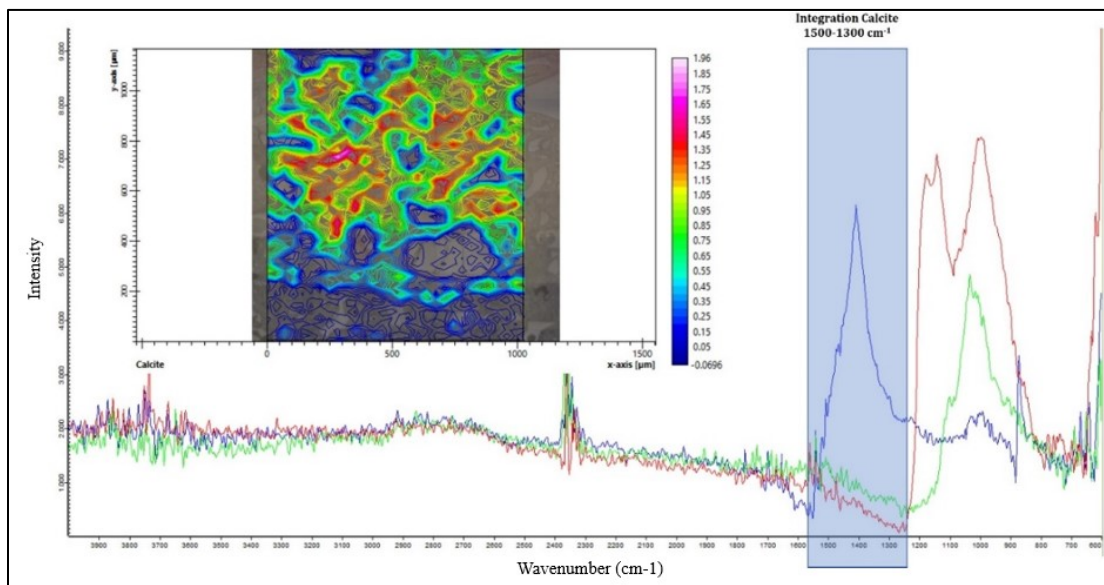


Figure 65: FTIR spectra of three sampled points and integration map of the main peak related to calcite, sample 7Pi2 (provided by Giulia Ricci).

The presence of calcite is dominant in the *intonaco* layer, seen in Figure 65, of course due to the lime binder. Areas of low concentration in the *intonaco* represent the aggregate, and a clear delineation between *intonaco* and base plaster layers is observed through the difference in concentration of calcite.

Continuing to sample 6Pi2, integration maps of the peaks of calcite and silicates reveal their distribution in the pigment layer and pigment/*intonaco* interface. Figure 66 displays the spectra of four representative points in the matrix of the upper *intonaco* and pigment layer, along with the integration map for the peaks relating to calcite in the range of 1500-1300 cm^{-1} , highlighted in blue.

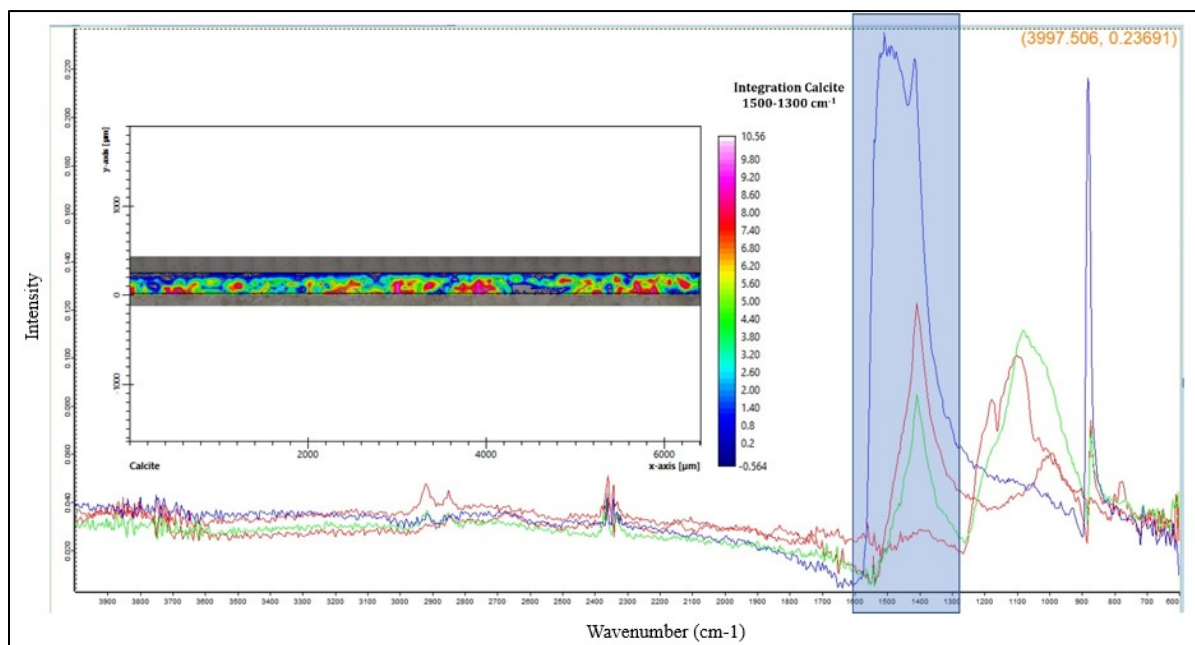


Figure 66: FTIR spectra of four sampled points, and integration map of the main peak related to calcite, sample 6Pi2 (provided by Giulia Ricci).

As can be seen in the map, calcite is present most abundantly in the upper *intonaco* layer of this sample, with continued presence in the matrix of the pigment layer. This unsurprisingly correlates to the use of lime binder to execute the painting in a *fresco* application.

Figure 67 shows the FTIR spectra of the sample's four sampled points, as well as the integration map of all peaks relating to silicates in the range 1200-900 cm^{-1} , highlighted in orange.

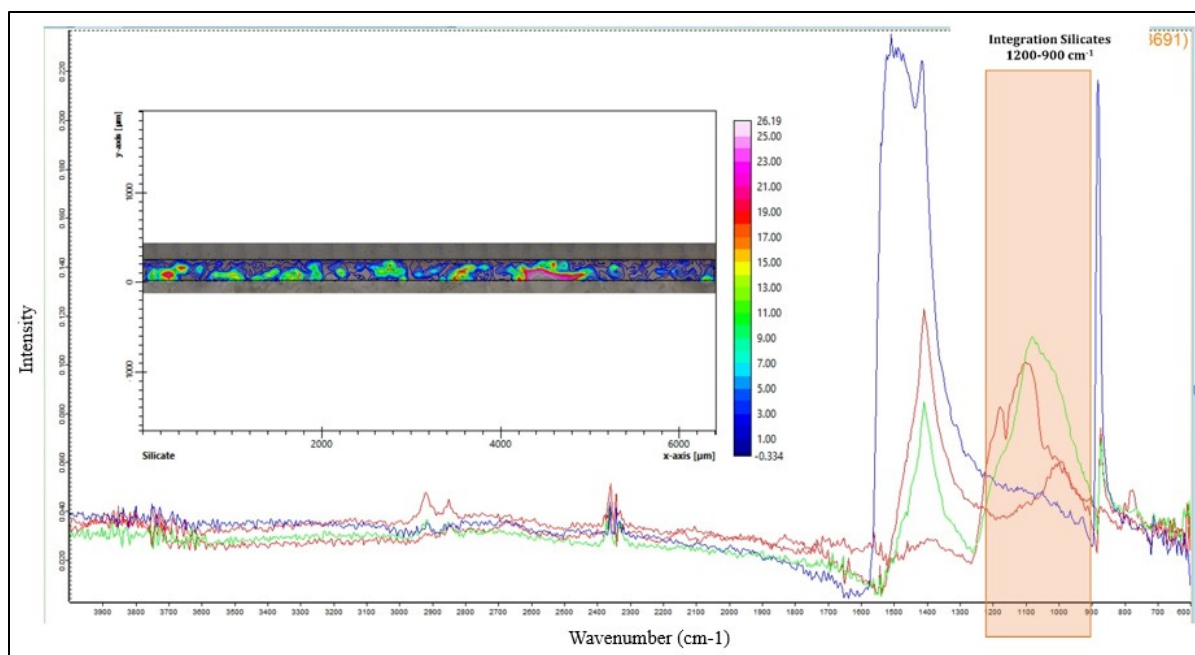


Figure 67: FTIR spectra of four sampled points, and integration map of the main peak related to silicates, sample 6Pi2 (provided by Giulia Ricci).

As expected, silicates correspond to the volcanic glass aggregate of the *intonaco*. Their presence can be seen evenly distributed throughout the upper *intonaco*, at times also in the pigment layer.

The resulting micro-FTIR integration maps of calcite and silicates of two samples in this dataset reveal a representative distribution of binder and aggregate. Differences in the maps displaying the concentration of silicates and aluminosilicates in the *intonaco* and base plaster layers show variation in the composition of volcanic aggregate used. As this work was geared towards experimenting with the capabilities and potential of micro-FTIR in this application, only peaks relating to calcite and silicates were analyzed. Further studies using micro-FTIR integration mapping could also focus on investigating the presence of organics in the *intonaco* and base plaster layer matrices.

5. Discussion

The complementary analytical methods employed in this study uncover novel aspects of the materiality and production methodology of wall paintings from the Techinantitla building complex of Teotihuacan, providing insights into the technical knowledge of these ancient artisans.

Considering the samples collectively, the pigment compositions show strong similarity. A combination of red ochre, carbon, and calcite is used consistently across all samples to produce varying shades of red, as previously identified in Teotihuacan wall painting tradition. The use of specular hematite as an additive to produce sparkling effects in the final murals was identified in almost all samples, as well as quartz crystals in some samples to obtain the same effect in lighter pigment shades. Other iron oxides, namely magnetite and ilmenite were identified in the *intonaco* and base plaster layers of several samples using micro-Raman and SEM-EDS, but interestingly not in the pigment layers. Magnetite was identified by XRD in the pigment layers of samples 2Pi and 8Pi, however this is possibly due to its association with red ochre. This points to a specific and intentional use of specular hematite in this layer.

Characterization of the black pigment surfaces visible in samples 6Pi2 and 7Pi2 proved to be difficult, as FTIR analyses of these surfaces did not produce meaningful results, and subsequent analyses via micro-Raman and SEM-EDS also did not provide conclusive findings in this area. It is hypothesized that the black pigments are charcoal based, as is consistent in previous studies of black pigment at Teotihuacan, however additional investigation would be required to confirm.

Sample 2Pi is unique among the fragments tested in that it is the lone sample painted *a secco*, and it is the only sample with two clearly identifiable red ochre pigment layers. There also appears to be strong orientation of the volcanic glass aggregate in the upper *intonaco* of this sample, possibly indicating smoothing or burnishing of the *intonaco* surface prior to application of pigment. This sample originates from a different area of the complex than the other fragments, possibly providing context for the variation in execution of this mural.

Samples 6Pi1 and 6Pi2 share comparable properties and composition. Similar combinations of mineral phases were identified by XRD in the pigment layers of the two samples, notably providing the only instances of detection of both muscovite and bassanite. They are painted *a fresco*, with comparable *intonaco* thicknesses that are significantly greater than the other samples analyzed.

Samples 7Pi1 and 7Pi2, obtained near the area identified as a temple within the Techinantitla complex, also show similarities in their material composition and production processes. Through XRD analyses they were found to have nearly identical mineral compositions, with the only discrepancy being the presence of diasporite in sample 7Pi2. They were also both painted *a fresco* with comparable *intonaco* thicknesses. Sample 7Pi2 presents a unique feature in that apatite was identified by micro-Raman and EDS microchemical analysis in its base plaster and *intonaco* layers. These findings contribute to the hypothesis that burnt bone was incorporated in the production process of these plasters, which has not been previously identified in the study of plasters from Teotihuacan.

Sample 8Pi, also found near the temple of the site, is interesting in that its *intonaco* layer shows a somewhat sparse and inconsistent distribution of aggregate compared to the other samples studied. This feature coupled with the presence of cracks and a large calcite clump in the plaster possibly indicates a lower quality *intonaco* compared to the other samples, although the proportion of mineral components was consistent with other *intonaco* sample tested, 2I, showing a standardized formula.

Concerning the *intonaco* and plaster samples 2I, 8I, 2P, 5P, and 8P, both XRPD and optical microscopy analyses reveal consistent and standardized production methods. The ratio of mineral phases in the *intonaco* samples is strikingly similar, revealing standardized proportions of binder to aggregate. Comparable proportions were also evident in the three base plaster samples analyzed. Optical microscopy provided additional information on the interaction between binder and aggregate in these layers, allowing for the visualization of glass fragments, tezontle, and matrices. SEM-EDS microchemical mapping did not reveal the presence of reaction rims on the tezontle of the base plaster layers, as was observed by Miriello et al. (2021), leaving questions about the potential hydraulicity of the plasters studied. However, the role that organics play in contributing to the strength and durability of these plasters requires further investigation.

Apart from a few key works, there is scarce scientific study of the development of hydraulic mortars throughout Mesoamerican societies. The 2021 study by Miriello et al. was the first to provide evidence of pozzolanic reactions in the plasters of Teotihuacan, where a 2010 study was one of the first to demonstrate possible hydraulicity in Maya mortars from Calakmul and Lamanai by proving the intentional addition of volcanic ash and resulting reaction rims (Miriello et al, 2021; Villaseñor and Graham, 2010). It is clear that additional research is required to determine the intended purpose and potential reactivity volcanic material additions.

As the development of hydraulic plaster in the Roman and Mediterranean world is well-documented, it provides a useful reference point for comparison with the significantly less researched origins of lime plaster in pre-Columbian Mesoamerica. The height of Roman construction and architectural achievements, approximately 100 BCE to 200 CE, corresponds to the Late Preclassic or Formative period of Mesoamerica (Winter, 1979). This period aligns with the rise of large Maya cities such as Kaminaljuyu and El Mirador, and the beginnings of Teotihuacan society and monumental architecture; for example, the Pyramid of the Sun was constructed approximately 170 CE (Arroyo, 2022; Sugiyama et al, 2017).

Key markers of Roman plaster technology include the addition of pozzolana (volcanic ash) and crushed ceramics to facilitate pozzolanic reactions and produce hydraulic mortars, and the advent of *opus caementicium*, or Roman concrete, enabling the construction of exceptionally stable and enduring monuments and public works.

The Maya independently developed lime plaster in the Middle Preclassic period, approximately 1100 BCE (Rodríguez-Navarro et al, 2023). Refinement of the technology continued throughout their civilization, as well as in contemporary and succeeding societies such as the Teotihuacanos, Zapotecs, and Aztecs. This technological advancement provided the foundation for the major architectural and artistic achievements of ancient Mesoamerica, serving as the ground layer for

wall paintings, floors, and as a durable structural material used to construct temples, palaces, residential compounds, and water management systems.

A defining element of Maya and Mesoamerican plasters is the addition of organic materials such as bark extract or plant fibers to enhance their mechanical properties. The 2023 paper by Rodríguez-Navarro et al. demonstrated that the inclusion of polysaccharide-rich bark extract improved the toughness and weathering resistance of lime plasters tested; and it was evidenced that the Maya created bio-mimetic mortars, with the presence of inter- and intracrystalline organics mimicking the properties of biominerals (Rodríguez-Navarro et al, 2023). In Teotihuacan, nopal juice, or prickly pear extract, was found to be an additive to the plaster of the floor of the Pyramid of Quetzalcoatl (Montes et al, 2005). The addition of nopal juice to lime mortars has been shown to contribute favorable properties such as increased compressive strength and resistance to water penetration (Martinez-Molina et al, 2015).

The significant, yet understudied, role of organic additions in Mesoamerican plaster technology distinguishes it from that of the Roman tradition, whose strength centered on the contribution of pozzolanic materials. However, this is not to discount development of hydraulic mortars in Teotihuacan and other Mesoamerican societies; as previously mentioned the intended purpose of the addition of materials such as volcanic glass, ash, and tezontle, also requires additional research. Increased study of the interplay between organics and pozzolanic materials is essential to understanding how the Maya, Teotihuacanos, and other Mesoamerican civilizations were able to create some of the most resistant and durable plasters of the ancient world.

In the realm of organics-derived additives, an interesting area of further research is the potential addition of burnt bone to the base plaster and *intonaco* layers of plaster at Teotihuacan. This study showed the discovery of apatite in the plaster layers of sample 7Pi2, forming a hypothesis that burnt bone was intentionally added to the ground layers of the wall of this painted fragment. The nature, intentionality, and technical and/or ritualistic function of this additive requires further attention. The importance of other organic material additions of course also requires additional study as there is very little existing research on this topic, particularly concerning the plasters of Teotihuacan. Implementing analytical methods suited for characterizing organics, for example targeted micro-FTIR or thermo-gravimetric/differential scanning calorimetry (TG/DSC) analyses of the base plaster and *intonaco*, could provide a deeper understanding in this area.

As it has been discussed, an increase in research concerning the potential pozzolanic reactions occurring with the tezontle of the base plaster, as well as the volcanic glass shards of the *intonaco* would be valuable. A wider sample set, including samples from different areas and from different chronological periods throughout Teotihuacan would paint a more comprehensive picture of the development of plaster technology, and specifically the role of volcanic aggregates, throughout the site.

This study was inconclusive in characterizing the black pigment surfaces of this sample set; further concerted efforts could be taken in this area, for example using gas chromatography coupled with mass spectrometry (GC-MS) to intentionally target organic pigment identification. Another potential area of further investigation is the use of specular hematite in the red pigment layer; in

this study, hematite particles were identified via micro-Raman in the pigment layer of almost all samples, but magnetite and other iron oxides were only detected in the plaster layers. Research focused on the resource acquisition and intentionality of the use of specular hematite could provide information on the Teotihuacanos' connection and understanding of this material.

6. Conclusions

The findings of this study contribute novel information to our understanding of the materials and methods used by Teotihuacano artisans in the creation of the wall paintings of Techinantitla. Through the application of a range of complementary analytical techniques, namely, XRD-XRPD, FTIR, optical microscopy, micro-Raman, SEM-EDS, and micro-FTIR, this research has revealed insights into the composition and preparation methods of pigment, *intonaco*, and base plaster layers used in the execution of these mural paintings.

Initial XRD results of the pigment surfaces of samples 2Pi, 6Pi1, 6Pi2, 7Pi1, 7Pi2, and 8Pi identified the common use of red ochre, with minerals hematite, kaolinite, and quartz identified in the pigment layer of all samples. The prevalence of red ochre is unsurprising, as it is the most frequently used pigment to produce Teotihuacan red. Accessory minerals, such as andesine, muscovite, diaspore, and magnetite were also discovered, as well as alteration products like gypsum, bassanite, weddellite, vaterite, and tridymite.

XRPD qualitative and quantitative analyses of the *intonaco* and base plaster samples 2I, 8I, 2P, 5P, and 8P showed strong consistency, suggesting standardisation of manufacturing practices. This is evidenced in the similarity of mineral phases detected in these layers, indicating that material acquisition of aggregate is likely from the same source. The quantitative results showed exceptionally similar ratios of binder to aggregate, thereby showing a standardized formula for production.

As for the black pigment layers of samples 6Pi2 and 7Pi2, FTIR measurements did not produce meaningful signals, likely due to limitations of the experimental setup. The other two samples analyzed via FTIR, 2Pi and 8Pi, did show signals of wood ash, indicating its presence as an additive or filler material, as was an established practice in Teotihuacan wall paintings.

Optical microscopy mapping and imaging of all samples provided a more detailed picture of the preparation process of the wall painting fragments. All stratified samples except for 2Pi were found to be painted *a fresco* with two preparatory layers – an *intonaco* layer consisting of a lime-based binder with volcanic glass aggregate, and a base plaster layer consisting of a mud-based matrix and tezontle aggregate. Sample 2Pi is unique in that it was painted *a secco*, and possessed two distinct red pigment layers. Visualization of the interaction between binder and aggregate of both plaster layers also allowed for a better understanding of technology involved in the creation of these elements.

Extensive micro-Raman sampling across the pigment, *intonaco*, and base plaster layers of the stratified samples confirmed the identification of mineral phases recognized by XRD-XRPD, while also providing new discoveries. The matrices of the pigment layers consistently showed peaks of carbon, calcite, and hematite, further confirming the combination of red ochre and calcite, as was shown by XRPD results, while also demonstrating the consistent use of carbon in the pigment layers as was suggested by FTIR. The use of specular hematite in the pigment layers was confirmed, as was suspected via optical microscopy imaging and previous studies. Interestingly, pieces of magnetite were detected in the *intonaco* layer of samples with micro-Raman, but not in

the pigment layers. This suggests an intentional use of specular hematite for the purpose of producing a sparkling effect in the final murals.

Micro-Raman results of aggregate and binder in the *intonaco* and base plaster layers again confirmed results of XRD measurements. Characteristic peaks of minerals such as diopside, hornblende, plagioclase feldspars, and forsterite were identified, consistent with previous results, corresponding to volcanic glass and tezontle aggregate. An interesting finding in the *intonaco* layer of sample 7Pi2 was the identification of apatite. The combined presence of carbon and apatite in this location could be an indication of biological apatite, suggesting the use of burnt bone as a component in the plaster; the detection of apatite via EDS point analysis in the base plaster layer of this sample provides further evidence for this theory. The possible ritualistic or technical purpose of this addition merits future study.

Concerning the plaster matrices, strong signals of calcite were unsurprisingly observed in the *intonaco* layers. More interestingly, weak peaks of amorphous carbon were also detected in both the *intonaco* and base plaster matrices, pointing to the potential presence of an organic additive in these plaster layers.

The tradition of the inclusion of volcanic glass and scoria in the plaster layers raises questions about the potential for pozzolanic activity of these materials. Recent research has demonstrated pozzolanic reactions in plasters from Teotihuacan through the identification of reaction rims formed on tezontle aggregate (Miriello et al, 2021). The present study employed SEM-EDS microchemical mapping to investigate this phenomenon, however no reaction rims on the tezontle or volcanic glass were observed. This is not to say that the plasters studied here are not hydraulic, only that this area requires further research.

With uncertain hydraulicity, the role of potential organic additions in contributing to the mechanical properties of the plaster layers begs increased investigation. There has been evidence for the use of nopal juice as an addition to plaster at Teotihuacan, as well as studies concerning organic components imparting strength and durability to Maya mortars. In this work, micro-Raman results identified carbon the *intonaco* and base plaster layers, and SEM-EDS microchemical mapping revealed the presence of carbon throughout the plaster layers. These preliminary results may imply the presence of an organic additive, but additional research is necessary of characterize this potential component, as well as to investigate the role it may play in the strength and durability of these plasters.

Finally, results of micro-FTIR revealed the distribution of calcite and silicates in the pigment and plaster layers of samples 6Pi2 and 7Pi2. The strong presence of calcite was unsurprisingly seen in the *intonaco* and pigment layers, where volcanic glass fragments showed a high concentration of aluminosilicates. Additional work using micro-FTIR mapping could possibly focus on identifying organic additives in the *intonaco* and base plaster layers.

In closing, this research highlights both the sophistication and consistency of Teotihuacan wall painting and plaster production. Through the analytical methods employed, it was possible to uncover information about pigment base formulas and additives, the composition and application of plaster layers, and the interaction of these elements. These findings deepen our understanding

of Teotihuacano artisans' technological expertise and knowledge of material properties – particularly their ability to harness these properties to create intended effects, both technically and visually. Areas discussed in this study that warrant additional attention include the characterization of black pigment surfaces, and the possibility and purpose of burnt bone as a component of Teotihuacan plaster. One of the most significant unanswered questions of this work is root of the strength and durability of these plasters. Further research focused on identifying organic additives and investigating possible pozzolanic reactions of the volcanic material will be essential to unveil the intricacies and lasting impact of the wall paintings of Teotihuacan.

References

- Argote, et al. 2020. "Cinnabar, hematite and gypsum presence in mural paintings in Teotihuacan, Mexico." *Journal of Archaeological Science Reports* 32, 102375.
- Argote, et al. 2020. "Designing the underworld in Teotihuacan: Cave detection beneath the moon pyramid by ERT and ANT surveys." *Journal of Archaeological Science Reports*. Vol 118, 105141.
- Arroyo. 2022. "The city over the city: Kaminaljuyu and urbanism." In *Early Mesoamerican Cities: Urbanism and Urbanization in the Formative Period*, edited by Michael Love and Julia Guernsey, pp 121-141. Cambridge University Press, 2022.
- Artioli. 2012. "Science for the cultural heritage: the contribution of X-ray diffraction." *Rend. Fis. Acc. Lincei* 24 (Suppl 1), 55–62 (2013).
- Barba, et al. 2009. "Provenance of the limestone used in Teotihuacan (Mexico): a methodological approach." *Archaeometry* 51, 4 (2009) 525–545. doi: 10.1111/j.1475-4754.2008.00430.x
- Barca, et al. 2019. "Geochemical and petrographic characterization of pyroclastic deposits of Los Humeros Volcanic Complex used as aggregates in the plasters from Teotihuacan (Mexico)." *Microchemical Journal* 145 (2019) 852-863.
- Barrios de Senisterra. 2019. *Mesoamerican Open Spaces and Mural Paintings as Statements of Cultural Identity*. Cambridge Scholars Publishing.
- Bell et al. 1997. "Raman spectroscopic library of natural and synthetic pigments (P re- N 1850 AD)". *Spectrochimica Acta Part A* 53 (1997) 2159-2179.
- Burgio, et al. 2000. "Library of FT-Raman spectra of pigments, minerals, pigment media and varnishes, and supplement to existing." *Spectrochimica Acta Part A* 57 (2001) 1491–1521.
- Buzgar, et al. 2013. "The composition and source of the raw material of two stone axes of Late Bronze Age from Neamț County (Romania) - A Raman study." *Analele Stiintifice ale Universitatii "Al. I. Cuza" din Iasi Seria Geologie* 59 (1) (2013) 5–22.
- Casadio, et al. 2018. "Raman spectroscopy of Cultural Heritage materials: overview of applications and new frontiers in Instrumentation, sampling modalities, and data processing." *Topics in current chemistry, 2016, Analytical Chemistry for cultural heritage*, 374, pp.62. ff10.1007/s41061-016-0061-zff. fhal-01455522.
- Catauro et al. 2023. "Mosses on Geopolymers: Preliminary Durability Study and Chemical Characterization of Metakaolin-Based Geopolymers Filled with Wood Ash." *Polymers* 15(7):1639.
- Clayton, Sarah. 2015. "Part III Early Urban Landscapes: 13 Teotihuacan: an early urban center in its regional context." In *The Cambridge World History*, edited by Norman Yoffee, pp. 227 - 316. Cambridge University Press.

Cowgill. 2015. *Ancient Teotihuacan: Early Urbanism in Central Mexico*. Cambridge University Press, New York.

De Faria. 1997. "Raman microspectroscopy of some iron oxides and oxyhydroxides." *Journal of Raman Spectroscopy*, vol. 28, issue 11, pp. 873-878.10.1002/(SICI)1097-4555(199711)28:11<873::AID-JRS177>3.0.CO;2-B

Domingo, et al. 2021. "Characterizing the pigments and paints of prehistoric artists." *Archaeological and Anthropological Sciences* Vol 13, article 196.

El-Deen, et al. 2018 "Anatase TiO₂ nanoparticles for lithium-ion batteries." *Ionics* 24(3). Available: 10.1007/s11581-017-2425-y.

Encyclopedia Britannica. 2024. "Teotihuacan." Available <https://www.britannica.com/place/Teotihuacan#/media/1/587661/139062>. Accessed August 23, 2024.

Ferreira, et al. 2020. "Laser-Induced Hematite/Magnetite Phase Transformation. *J. Electron. Mater.* 49, 7187–7193 (2020). <https://doi.org/10.1007/s11664-020-08535-7>

Fiori et al. 2009. "Vaterite in the mortars of a mosaic in the Saint Peter basilica, Vatican (Rome)." *Journal of Cultural Heritage* 10(2):248-257.

Goguitchaichvili, et al. 2004. "Pre-Columbian mural paintings from Mesoamerica as geomagnetic field recorders." *Geophysical Research Letters*, Vol. 31, L12607.

González-Gómez, et al. 2018. "Calcium oxalates in biofilms on limestone walls of Maya buildings in Chichén Itzá, Mexico." *Environmental Earth Sciences* 77, 230 (2018).

Grove. 1970. *The Olmec Paintings of Oxtotitlan Cave, Guerrero, Mexico*. Dumbarton Oaks, Trustees for Harvard University. Washington, D.C.

Hansen, et al. 2000. "Ancient Maya Burnt-Lime Technology: Cultural Implications of Technological Styles." University of California, Los Angeles.

Hirth, et al. 2020. *Teotihuacan, the World Beyond the City*. Dumbarton Oaks Research Library and Collection. Washington, D.C.

Kingery, et al. 1988. "The Beginnings of Pyrotechnology, Part II: Production and Use of Lime and Gypsum Plaster in the Pre-Pottery Neolithic Near East." *Journal of Field Archaeology*. 15 (2):219–244.

Kubler. 1967. *The Iconography of the Art of Teotihuacán*. Dumbarton Oaks, Trustees for Harvard University. Washington D.C.

Kuebler, et al. 2005. "Extracting Olivine (Fo-Fa) Compositions from Raman Spectral Peak Positions." *Lunar and Planetary Science XXXVI* (2005).

Lin, et al. 2021. "Comparison and characterization of pigments and dyes by Raman spectroscopy." *Analytical Sciences* (2022) 38:483–495.

- López-Puértolas, et al. 2023. “New insights on Teotihuacan color technology: a proposal of a technological style for mural painting.” *Archaeological and Anthropological Sciences*
- López-Puértolas, et al. 2020. “Characterization of color production in Xalla's palace complex, Teotihuacan.” *STAR: Science & Technology of Archaeological Research*, 5(2), 221–233.
- Magaloni, et al. 2011. “An Analysis of Mayan Painting Techniques at Bonampak, Chiapas, Mexico.” Materials Research Society symposia proceedings. *Materials Research Society* 352.
- Magaloni. 1996. *El espacio pictórico teotihuacano, tradición y técnica*. In *De la Fuente, B. (Coord.)*, La pintura mural prehispánica en México, volumen I: Teotihuacán, tomo II: Estudios. IIE-UNAM, Mexico, pp. 187–226.
- Martinez-Molina, et al. 2015. “Physical properties of cement-based paste and mortar with dehydrated cacti additions.” *International Journal of Architectural Heritage*, 9(4), 443-452. <https://doi.org/10.1080/15583058.2013.800919>
- Marucci, et al. 2018. “Raman spectroscopic library of medieval pigments collected with five different wavelengths for investigation of illuminated manuscripts.” *Analytical Methods* Issue 10, 2018.
- Manzanilla. 2009. *Domestic Life in Prehispanic Capitals: A Study of Specialization, Hierarchy, and Ethnicity*. University of Michigan Press.
- Miriello, et al. 2021. “Hydraulicity of lime plasters from Teotihuacan, Mexico: a microchemical and microphysical approach.” *Journal of Archaeological Science* 133 (2021) 105453.
- Millon. 1973. *Urbanization at Teotihuacan, Mexico*. University of Utah Press.
- Miller. 2012. *The art of Mesoamerica: from Olmec to Aztec*. Thames and Hudson Ltd. London.
- Montes, et al. 2005. “Analysis of stucco floors from the Citadel of the archaeological zone of Teotihuacan, Mexico.” *Materials Research Society*. Vol 852.
- Murakami. 2010. *Power relations and urban landscape formation: a study of construction labor and resources at Teotihuacan*. Unpublished PhD thesis, Arizona State University.
- Paszatory. 1997. *Teotihuacan: an experiment in living*. University of Oklahoma Press.
- Pecci, et al. 2018. “Identifying a technological style in the making of lime plasters at Teopancazco (Teotihuacan, México).” *Archaeological and Anthropological Sciences* Volume 10, pages 315–335, (2018).
- Penel, et al. 1998. “MicroRaman Spectral Study of the PO₄ and CO₃ Vibrational Modes in Synthetic and Biological Apatites.” *Calcif Tissue Int* **63**, 475–481 (1998). Available: <https://doi.org/10.1007/s002239900561>
- Poliszuk, Andrea. 2014. “Analysis of Cultural Heritage Materials by Infrared Spectroscopy.” In *Infrared Spectroscopy: Theory, Developments and Applications*, edited by Daniel Cozzolino, pp.519-536. Nova Science Publishers.

Puech et al. 2019. “Analyzing the Raman Spectra of Graphenic Carbon Materials from Kerogens to Nanotubes: What Type of Information Can Be Extracted from Defect Bands?” *Journal of Carbon Research*. 2019; 5(4):69. <https://doi.org/10.3390/c5040069>

Rodríguez-Navarro. 2012. “Binders in historical buildings: Traditional lime in conservation.” Dpto. Mineralogía y Petrología, Universidad de Granada, Fuentenueva s/n, 18002 Granada.

Rodríguez-Navarro, et al. 2023. “Carbonation mechanisms and kinetics of lime-based binders: An overview.” *Cement and concrete research*, Vol 173 November 2023, 10730.

Rodríguez-Navarro, et al. 2023. “Unveiling the secret of ancient Maya masons: Biomimetic lime plasters with plant extracts.” *Science Advances*. Vol 9, Issue 16. Available DOI: 10.1126/sciadv.adf6138

Romero-Sarmiento et al. 2014. “Evolution of Barnett Shale organic carbon structure and nanostructure with increasing maturation.” *Organic Geochemistry*. Volume 71, pages 7-16. ISSN 0146-6380. <https://doi.org/10.1016/j.orggeochem.2014.03.008>

Ruvalcaba-Sil, et al. 2021. “Analytical Approach for the Study of Teotihuacan Mural Paintings from the Techinantitla Complex.” *Minerals* 2021, 11(5), 508.

Secco, et al. 2022. “Cementation processes of Roman pozzolanic binders from Caesarea Maritima (Israel).” *Construction and Building Materials* 355 (2022) 129128.

Secco, et al. 2021. “Ochre-Based Pigments in the Tablinum of the House of the Bicentenary (Herculaneum, Italy) between Decorative Technology and Natural Disasters” *Minerals* 2021, 11, 67.

Shebanova and Lazor, 2003. “Raman study of magnetite (Fe₃ O 4): laser-induced thermal effects and oxidation.” *J. Raman Spectrosc.* 2003; 34: 845–852 Published online in Wiley InterScience (www.interscience.wiley.com). DOI: 10.1002/jrs.1056

Sugiyama, et al. 2017. “Inside the Sun Pyramid at Teotihuacan, Mexico: 2008—2011 Excavations and Preliminary Results.” *Latin American Antiquity*. 2013;24(4):403-432. doi:10.7183/1045-6635.24.4.403

Thirumalini, et al. 2018. “Experimental investigation on physical and mechanical properties of lime mortar: Effect of organic addition.” *Journal of Cultural Heritage* 31 (2018) 97–104.

Tomasini, et al. 2012. “Micro-Raman spectroscopy of carbon-based black pigments.” *J Raman Spectroscopy* 43:1671–1675.

The Met. 2024. “Wall painting: Teotihuacan.” Available <https://www.metmuseum.org/art/collection/search/321291>. Accessed August 23, 2024.

Villaseñor and Graham. 2010. “The use of volcanic materials for the manufacture of pozzolanic plasters in the Maya lowlands: a preliminary report.” *Journal of Archaeological Science*, Volume 37, Issue 6, 2010, Pages 1339-1347. Available <https://doi.org/10.1016/j.jas.2009.12.038>.

Winter. 1979. "Roman Concrete: the Ascent, Summit, and Decline of an Art." *Transactions of the Nebraska Academy of Sciences*. Volume VII, 1979.